

Radiation conditions in an Antarctic environment

Von dem Fachbereich Physik
der Universität Hannover
zur Erlangung des Grades
Doktorin der Naturwissenschaften
Dr. rer. nat.
genehmigte Dissertation
von
Dipl.-Met. Sigrid Wuttke
geboren am 22. Januar 1976 in Hannover

2005

Referent: Prof. Dr. Gunther Seckmeyer, Universität Hannover
Korreferent: Prof. Dr. Alkiviadis Bais, Aristotele University of Thessaloniki,
Griechenland
Tag der Promotion: 13. Dezember 2004

Diese Arbeit wird auch in den Berichten zur Polarforschung und Meeresforschung erhältlich sein. Die Berichte zur Polar- und Meeresforschung werden vom Alfred-Wegener-Institut für Polar- und Meeresforschung in Bremerhaven in unregelmäßiger Reihenfolge herausgegeben.

Keywords - Schlagworte

Antarctica, Solar Radiation, Spectral Measurements

Antarktis, Solare Strahlung, Spektrale Messungen

Abstract

This thesis aimed at characterising luminance, spectral radiance and albedo in Antarctica for selected situations motivated by surface energy budget and UV effects studies. A new spectroradiometer deployed at Neumayer, Antarctica ($70^{\circ} 39' \text{ S}$, $8^{\circ} 15' \text{ W}$), during the austral summer 2003/04 fulfils the stringent requirements set up by the Network for the Detection of Stratospheric Change (NDSC) as well as those of the World Meteorological Organisation. A recent intercomparison showed deviations up to 5% for various atmospheric conditions from an operational NDSC and a US National Science Foundation spectroradiometer. At 298 nm the instruments agree within $\pm 8\%$. Considering the low absolute irradiance levels and the strong increase of the solar spectrum in the UVB, such deviations are acceptable and represent state-of-art spectroradiometers.

A dependence of luminance and spectral radiance on solar zenith angle (SZA) and surface albedo has been identified. Antarctic radiance measurements show increasing horizon brightening for increasing wavelengths. For snow and cloudless sky the horizon luminance exceeds the zenith luminance by as much as a factor of 8.2 and 7.6 for a SZA of 86° and 48° , respectively. In contrast, over grass this factor amounts to 4.9 for a SZA of 86° and only a factor of 1.4 for a SZA of 48° . Thus, a snow surface with high albedo can enhance horizon brightening compared to grass by 40% for low sun at a SZA of 86° and by 80% for high sun at a SZA of 48° . For cloudy cases, zenith luminance and radiance exceed the cloudless value by a factor of 10 due to multiple scattering between the cloud base and high albedo surface.

At 500 nm the spectral albedo nearly reaches unity with slightly lower values below and above 500 nm. Above 800 nm the spectral albedo decreases to values between 0.45 and 0.75 at 1000 nm. For one cloudless case an albedo up to 1.02 at 500 nm could be determined. This can be explained by the larger directional component of the snow reflectivity for direct incidence combined with a slightly mislevelled sensor. A decline of albedo for increasing snow grain size has been found. The theoretically predicted increase in albedo with increasing SZA could not be observed. This is explained by the small range of SZA during albedo measurements combined with the effect of changing snow conditions outweighing the effect of changing SZA. The measured spectral albedo serves as input for radiative transfer models describing radiation conditions in Antarctica.

Zusammenfassung

In dieser Arbeit wurde für ausgewählte Situationen in der Antarktis Leuchtdichte mit einem Skyscanner sowie spektrale Strahldichte und Albedo mit einem neuen Spektralradiometer charakterisiert. Dieses Gerät erfüllt die strengen Richtlinien des *Network for the Detection of Stratospheric Change* (NDSC) und der *World Meteorological Organisation*. Bei einem NDSC Messgerätevergleich im Vorfeld der Antarktismessungen hat sich eine geringe Abweichung um 5% im Vergleich zu einem NDSC Gerät und einem Spektralradiometer der US National Science Foundation für verschiedene atmosphärische Bedingungen gezeigt. Bei 298 nm wichen diese Geräte um $\pm 8\%$ voneinander ab. Das ist angesichts der geringen Absolutbestrahlungsstärken und des steilen Anstiegs des solaren Spektrums im UVB sehr gut und zeichnet qualitativ hochwertige Geräte aus.

Eine Abhängigkeit der Leuchtdichte und spektralen Strahldichte vom Sonnenzenitwinkel (SZA) und der Albedo wurde identifiziert. Strahldichtemessungen in der Antarktis zeigten eine zunehmende Horizontüberhöhung für wachsende Wellenlängen. Für Schnee und wolkenlosen Himmel ist die Leuchtdichte am Horizont bei einem SZA von 86° 8.2 mal so groß wie die Zenitleuchtdichte. Für einen SZA von 48° übersteigt die Leuchtdichte am Horizont die im Zenit um das 7.6-fache. Im Gegensatz dazu beträgt dieser Faktor über Gras 4.9 für einen SZA von 86° und nur 1.4 für einen SZA von 48° . Also kann eine Schneedecke mit hoher Albedo im Gegensatz zu Gras die Horizontüberhöhung um 40% bei niedrigem (SZA = 86°) und 80% bei hohem Sonnenstand (SZA = 48°) verstärken. Sowohl Leucht- als auch Strahldichte sind bei bewölktem Himmel im Vergleich zum wolkenlosen um ein 10-faches größer.

Die gemessene Albedo erreicht bei 500 nm fast den Wert 1 und nimmt mit zunehmender Wellenlänge leicht ab. Über 800 nm ist die Abnahme der Albedo stärker, so dass bei 1000 nm Werte zwischen 0.45 und 0.75 erreicht werden. Für wolkenlosen Himmel wurde bei 500 nm eine Albedo von 1.02 bestimmt. Die Erklärung liegt in der ausgeprägten Vorwärtskomponente des Reflexionsverhaltens des Schnees in Verbindung mit einem leicht schief ausgerichteten Meßkopf. Eine Abnahme der Albedo für zunehmende Korngrößen des Schnees wurde beobachtet. Der in der Theorie vorhergesagte Anstieg der Albedo mit zunehmendem SZA konnte nicht festgestellt werden. Das liegt an der geringen Spanne an Sonnenständen bei den Albedomessungen in Kombination mit dem Effekt der veränderlichen Schneebedingungen, der den SZA-Effekt überwiegt. Die gemessene spektrale Albedo wird als Eingabe in Strahlungstransfermodelle benutzt, die die Strahlungsbedingungen in der Antarktis simulieren.

Contents

Keywords	3
Abstract	4
Zusammenfassung	5
1 Introduction	9
1.1 Aims	12
1.2 Synopsis	13
2 State of the Art	14
2.1 Basic Radiometric Quantities	14
2.2 Measuring Solar Radiation	17
2.2.1 Broadband Instruments	17
2.2.2 Spectroradiometers	18
2.3 Monitoring Spectral Irradiance in Antarctica	19
2.4 Review of Previous Results	20
2.4.1 Albedo and its Effect on Irradiance	20
2.4.2 Radiance Measurements	21
3 Development of a NDSC Spectroradiometer	24
3.1 Technical Details	24
3.2 Instrument Characterisation	27
3.2.1 Cosine Error of Irradiance Input Optics	27
3.2.2 Field of View of Radiance Input Optics	29
3.2.3 Slit Function	31
3.2.4 Wavelength Shift	32
3.2.5 Detection Threshold	33
3.2.6 Absolute Calibration	33
3.3 Quality Control	35
3.4 Quality Assurance	37
3.4.1 Ispra Intercomparison	37
3.4.2 Ruthe Intercomparison	40

Contents

3.4.3	5 th North American Intercomparison for UV Spectroradiometers	41
3.5	Compliance with NDSC Standards	47
3.5.1	Assessment of Complying with NDSC Specifications	49
3.5.2	Assessment of NDSC Intercomparison	50
4	Antarctic Campaign - Methods	51
4.1	Measurements at Neumayer	51
4.2	Spectral Irradiance	55
4.2.1	Radiometric Stability during Irradiance Measurements	55
4.2.2	Wavelength Stability during Irradiance Measurements	57
4.3	Albedo	60
4.3.1	Measuring Spectral Albedo	60
4.3.2	Measuring Broadband UV Albedo	63
4.4	Luminance	64
4.5	Spectral Radiance	66
4.5.1	Radiometric Stability during Radiance Measurements	67
4.5.2	Absolute Radiance Calibration	67
4.6	Ancillary Measurements	69
4.6.1	Total Ozone Column	69
4.6.2	Cloud Base Height and Sunshine Duration	70
5	Antarctic Results	71
5.1	Albedo	71
5.1.1	Spectral Behaviour of Albedo	72
5.1.2	Effect of SZA and Snow Grain Size on Albedo	74
5.2	Luminance	77
5.2.1	Zenithal Scans of Luminance	78
5.2.2	Diurnal Cycle of Luminance	79
5.3	Spectral Radiance	80
5.3.1	Cloudless Zenith Radiance	80
5.3.2	Cloudless vs. Overcast Zenith Radiance	81
5.3.3	Zenithal Scans of Radiance	84
5.3.4	Model vs. Measurement	84
5.4	Spectral Irradiance	90
5.5	Ancillary Measurements	93
5.5.1	Ozone	93
5.5.2	Cloud Base Height and Sunshine Duration	93
6	Discussion	96
6.1	Albedo	96
6.1.1	Methodical Uncertainties	96
6.1.2	Effect of SZA and Snow Grain Size on Albedo	98

Contents

6.2	Luminance	102
6.2.1	Horizon Brightening	103
6.2.2	Luminance under Overcast Sky	105
6.2.3	Link to Previous Studies	105
6.3	Spectral Radiance	106
6.3.1	Cloudless vs. Overcast Spectral Radiance	106
6.3.2	Horizon Brightening	107
6.3.3	Measured Compared to Modelled Radiance	114
6.4	Spectral Irradiance	118
6.4.1	Measured Compared to Modelled Irradiance	118
6.4.2	Relation to other Measuring Sites	119
7	Conclusions	120
7.1	Assessment of Objectives	120
7.1.1	Characterising Luminance and Spectral Radiance	120
7.1.2	Spectral Behaviour of Snow Albedo	121
7.1.3	Assessing the Effect of Albedo on Incident Radiation	122
7.1.4	Spectral Irradiance connected to UV Monitoring	122
7.1.5	Model Evaluation using Spectral Irradiance	123
7.2	Insights into Possible Future Work	123
7.2.1	Technical Improvements	123
7.2.2	Future Research Needs	124
	List of Symbols	129
	List of Acronyms	131
	List of Figures	133
	List of Tables	135
	Bibliography	136
	Acknowledgements	146
	Danksagungen	147
	Curriculum Vitae	149

1 Introduction

The vast continent of Antarctica has been a major focus of scientific exploration for relatively few decades when compared to most areas on Earth. Yet, what is already known about Antarctica conclusively demonstrates that despite its remote location it plays a significant role in the interaction between the atmosphere, oceans, cryosphere and biosphere. Encircled by the world's most biologically productive oceans, Antarctica is the largest storehouse of fresh water on the planet, a major site for the production of the cold deep water that drives ocean circulation, a major player in Earth's albedo dynamics, and an important driving component for atmospheric circulation (BOROWSKI, 2003; LÜDER, 2003).

The energy budget of the Antarctic continent is mainly controlled by the surface albedo, which is defined as the ratio of reflected to incident radiation. The surface albedo (300 to 3000 nm) of Antarctic Ice shelves is around 0.83 (SCHMIDT and KÖNIG-LANGLO, 1994). A change in prevailing climatic conditions can enhance feedback mechanisms, such as the ice-albedo feedback, which can be triggered by a change in temperature. Depending on the sign of temperature change, the ice-albedo-feedback has contrary effects:

1. A rise in temperature leads to an enhancement in snow and sea ice melt, which in turn causes the surface albedo to decrease. More radiation is absorbed increasing the energy budget and leading to a further rise in temperature.
2. A decrease in temperature leads to a greater production in sea ice, which in turn increases the surface albedo. Less radiation is absorbed decreasing the energy budget and leading to a further cooling.

Even though a rise in overall global temperature has been detected (HOUGHTON et al., 2001), regional trends deviate from the global one (VAUGHAN et al., 2001). For the region around the Antarctic Peninsula an increase in temperature that is larger than the global temperature increase has been observed (JACKA and BUDD, 1998; VAUGHAN et al., 2001). In contrast, a cooling over the interior of Antarctica has been found (COSIMO, 2000; THOMPSON and SOLOMON, 2002).

Due to the detected rise in temperature over the Peninsula and sub-Antarctic, the ice-albedo-feedback mechanism under (1) is induced there. Regional warming

1 Introduction

in the sub-Antarctic region is also linked to higher precipitation in the Antarctic (GIORGI et al., 2001). Depending on the temperature regime, precipitation in the Antarctic will fall in the form of rain (most likely over the Peninsula in summer) or snow (most likely over the Antarctic continent). More freshly fallen snow increases the albedo so that the feedback mechanism (2) is initiated over the Antarctic continent. These two contradictory processes need to be considered when investigating climate related albedo effects in Antarctica.

Difficulties in predicting the extent of climate change exist due to deficiencies in coupling atmospheric, oceanic and cryospheric models into one general model of the global climate system. Especially the improvement of the parameterisation of subgrid processes, such as clouds, radiation, precipitation and turbulence, in global circulation models (GCMs) is a major goal of current climate research (LEFEBRE et al., 2003). KONDRATYEV and CRACKNELL (1998) state the necessary accuracy of the surface albedo as input into GCMs to be 0.02 to 0.04. Small errors or changes in its value represent large fractional changes in absorbed solar radiation in the overall heat budget at the snow covered surface. Correct prescriptions and variability parameterisation of surface albedo are very difficult to achieve, based on a wide range of albedo variations and a limited data base of surface albedo observations (KONDRATYEV and CRACKNELL, 1998).

High quality albedo measurements are vital in order to improve input parameterisations for GCMs and also for validating satellite based albedo retrievals. However, accurate ground based albedo measurements are sparse, especially for the polar regions (HANSEN and NAZARENKO, 2004; ZHOU et al., 2001). LI and ZHOU (2003) also identify the lack of experimental investigations on spectral albedo in the field of snow and sea ice research. The available data cover only a small range of snow and ice types and few solar zenith angles (SZA).

Another aspect that has raised public concern in the context of Antarctic research is the ozone hole occurring in spring each year. It has been first discovered by FARMAN et al. (1985). The Antarctic ozone hole describes a region of depleted stratospheric ozone with total ozone columns of less than 220 Dobson Units (DU; WMO, 2003). One DU is defined as the thickness of a layer in mm, when all the ozone molecules of an atmospheric column would be deposited on the Earth's surface under normal conditions (1013 hPa, 0°C). The mechanisms leading to the generation of the Antarctic ozone hole are, for example, described by FABIAN (1992).

Minimum ozone values around 100 DU have been seen every year since the early 1990s. The estimates of the ozone hole area show an increase in recent years. Therefore, it is not possible to state that the ozone hole has already reached its maximum (NEWMAN et al., 2003). Attention was given to this question especially after the unusually small and short lived ozone hole in 2002. In contrast, the ozone hole in 2003 was one of the largest ever recorded. This year's

1 Introduction

(2004) seems to develop along average values considering the last ten years (<http://www.cpc.ncep.noaa.gov/products/stratosphere/polar/polar.html>).

Due to the stratospheric ozone loss, a negative stratospheric temperature trend has been detected (NEWMAN et al., 2003). This cooling strengthens the Antarctic polar vortex of westerly winds, a stratospheric analogue of the Antarctic Oscillation's (AAO) ring of westerlies in the lower atmosphere (KERR, 2002). THOMPSON and SOLOMON (2002) compared the timing of ozone induced cooling and vortex intensifications in the stratosphere with similar changes in the lower atmosphere and at the surface. They concluded to have found good evidence that ozone is important in driving the AAO and thus climate change, particularly during late spring. KERR (2002) is reluctant to connect Antarctic climate change only to stratospheric ozone depletion driving the AAO, and promotes the consideration of other contributing factors. The discussion about the evidence that anthropogenic emissions of ozone depleting gases have a distinct impact on climate not only at stratospheric levels but also at the Earth's surface is still ongoing (GILLETT and THOMPSON, 2003).

Ozone depletion is not only important with respect to climate change, it also enhances solar ultraviolet (UV; 280 to 400 nm) radiation reaching the Earth's surface (KERR et al., 2003). Especially biological organisms react to changing UV levels. For the photosynthesis, the visible part of the solar spectrum (400 to 780 nm), referred to as photosynthetic active radiation (PAR), plays the most important role (KARSTEN et al., 1999). The biological effectiveness of incident radiation varies for different species, which presents the motivation to conduct spectral measurements of radiation parameters (SECKMEYER, 1997).

Spectral UV irradiance has been monitored in the Antarctic by the National Science Foundation's (NSF) Polar UV Network at three Antarctic sites for more than 12 years. Statistically significant trends in UV irradiance could not be detected due to the large year-to-year variability and the fact that the network was established only after the first occurrence of the ozone hole (BERNHARD et al., 2004). Therefore, the need for longer time series of spectral UV irradiance is conveyed.

Since most biological organisms are not horizontally orientated, the knowledge of spectral radiance would present an advantage over spectral irradiance in order to assess the impact of incoming radiation on biological organisms. Further, the fraction of the diffuse UVB (280 to 315 nm) irradiance from the global irradiance and the presence of many biologically sensitive organisms that are only partially sheltered from the sky hemisphere predicates a further need for sky radiance measurements (GRANT et al., 1997a). However, spectral measurements of sky radiance in the Antarctic have not been reported in scientific literature so far.

1.1 Aims

In order to understand radiation conditions in an Antarctic environment it is vital to gain knowledge about effects specific to Antarctica. The two major differences compared to other parts of the world are:

1. the large glaciated area leading to a high surface albedo affecting the surface energy budget;
2. the ozone hole occurring each spring inside the Antarctic stratospheric vortex leading to enhanced surface UV levels.

Both points motivate radiation measurements with a high spectral resolution from the UV to the near infrared (IR). To account for the influence of the high surface reflection on the radiation parameters, the experimental determination of spectral albedo is crucial. Keeping these points in mind, the aims of this study are:

- To characterise spectral radiance and sky luminance in dependence of viewing angle for selected periods;
- To characterise the spectral behaviour of snow albedo for specific atmospheric conditions;
- To assess the influence of albedo on spectral radiance, luminance and spectral irradiance;
- To sample spectral irradiance in an extended wavelength range (280 to 1050 nm) during one Antarctic summer to provide a connection to ongoing Antarctic monitoring programs of spectral irradiance;
- To evaluate radiative transfer models for both, spectral irradiance and radiance, in an extended wavelength range (280 to 1050 nm) and for high albedo conditions.

Investigations on luminance and spectral radiance have not been reported in scientific literature so far. The wavelength range covered in the spectral measurements exceeds the UV, which is currently monitored at various Antarctic sites. It extends into the near infrared up to 1050 nm presenting a novelty in Antarctic spectral radiation measurements. In addition, spectral albedo is measured for the first time with the same high resolution spectroradiometer deployed to detect spectral irradiance and radiance. Another first is the combination of radiation parameters comprising spectral irradiance, radiance, albedo, and sky luminance

1 Introduction

measured at an Antarctic location. This unique data set will provide a basis for the characterisation of the radiation conditions in an Antarctic environment for specific atmospheric conditions, which will contribute to a further understanding of radiation processes acting as a driving force for atmospheric dynamics.

1.2 Synopsis

The contents of the following chapters are shortly stated to gain an overview of the structure of this thesis.

The second chapter gives background information on radiative properties. Different types of radiation detectors are presented briefly. A short overview of current spectral measurements of irradiance is given.

The third chapter contains the development of the new spectroradiometer owned by the Institute of Meteorology and Climatology (IMUK), University of Hannover. This instrument now complies with the standards of spectral radiation measurements set up by the Network for the Detection of Stratospheric Change (NDSC) and guidelines of the World Meteorological Organisation (WMO).

In the fourth chapter the radiation measurements at the German Antarctic Neumayer Station are described.

Results of the Antarctic campaign with respect to the measured and modelled radiation parameters are summarised in Chapter 5. They are discussed in Chapter 6.

Chapter 7 contains conclusive remarks and recommendations derived from this study. It also delivers suggestions for possible future research.

Due to the separation of presenting the results in Chapter 5 and the discussion on the results in Chapter 6, each radiation parameter is addressed twice. It is also possible to read the discussion on a certain radiation parameter directly following the presentation of its results.

2 State of the Art

2.1 Basic Radiometric Quantities

In this study all radiative quantities are defined according to the German Industry Norm (DIN 5031, 1982). They can be either defined in terms of energy or in terms of photons. $dN_p = dW/(h \cdot \nu)$ links these options, where N_p is the number of photons, W is the radiative energy, h is Planck's constant, and ν is the frequency (DIN 5031, 1982).

The total power emitted or received by a body in the form of radiation is termed **radiant flux** Φ :

$$\Phi := \frac{dW}{dt} \quad , \quad [\Phi] = 1\text{W} \quad . \quad (2.1)$$

In this case W is the emitted or received energy.

The radiant flux Φ of electromagnetic radiation incident on a given surface per unit area A is known as the **irradiance** E :

$$E := \frac{d\Phi}{dA} \quad , \quad [E] = 1\frac{\text{W}}{\text{m}^2} \quad . \quad (2.2)$$

The **radiant exitance** M is the radiant flux Φ of electromagnetic radiation leaving a given surface per unit area dA , and is accordingly defined as

$$M := \frac{d\Phi}{dA} \quad , \quad [M] = 1\frac{\text{W}}{\text{m}^2} \quad . \quad (2.3)$$

The irradiance E and the radiant exitance M are both **radiant flux densities**. The irradiance E describes the receiver and the radiant exitance M is a parameter concerning the sender.

The **radiant exposure** H is a measure of the total energy of the radiation incident on a surface per unit area dA integrated over the irradiation time:

$$H := \frac{dW}{dA} = \int_{\Delta t} E(t)dt \quad , \quad [H] = 1\frac{\text{J}}{\text{m}^2} \quad . \quad (2.4)$$

2 State of the Art

The term dose is also commonly used for the description of radiant exposures.

The radiant flux Φ emitted per unit solid angle Ω by a point source in a given direction is called the **radiant intensity** I :

$$I := \frac{d\Phi}{d\Omega} \quad , \quad [I] = 1 \frac{\text{W}}{\text{sr}} \quad . \quad (2.5)$$

The **radiance** L is defined as the radiant flux Φ per unit area dA and per unit solid angle $d\Omega$:

$$L := \frac{d\Phi}{dA d\Omega \cos \alpha} \quad , \quad [L] = 1 \frac{\text{W}}{\text{m}^2 \text{sr}} \quad . \quad (2.6)$$

α denotes the angle between the direction of the beam and the direction perpendicular to the surface.

To describe the spectral properties of radiation each parameter is referred to by wavelength. The **spectral radiance** L_λ , for example, is given by:

$$L_\lambda := \frac{dL}{d\lambda} \quad , \quad [L_\lambda] = 1 \frac{\text{W}}{\text{m}^2 \text{sr nm}} \quad . \quad (2.7)$$

By presenting the spectral radiance $L_\lambda(\lambda, \vec{x}, \theta, \phi)$ as a function of wavelength λ , direction \vec{x} , and the spherical coordinates θ (zenith angle) and ϕ (azimuth angle), a nonpolarised radiation field is completely described. The spectral irradiance for a flat receiver can be obtained by integrating the spectral radiance L_λ over all unit solid angles:

$$\begin{aligned} E_\lambda(\lambda, \vec{x}) &= \int_{2\pi} L_\lambda(\lambda, \vec{x}, \theta, \phi) d\Omega \\ &= \int_0^{\pi/2} \sin(\theta) \cos(\theta) \int_0^{2\pi} L_\lambda(\lambda, \vec{x}, \theta, \phi) d\phi d\theta \quad . \end{aligned} \quad (2.8)$$

The factor $\cos(\theta)$ only considers the projection of the receiving plane perpendicular to the direction of the incident radiation.

It is common agreement to measure the solar radiation incident on the Earth's surface on a horizontal plane (BERNHARD and SECKMEYER, 1999). Many types of detectors exist, but the most resourceful instruments are the ones measuring the global spectral irradiance $E_{\lambda, glo}$, i.e., the radiant energy dW arriving per time interval dt , per wavelength $d\lambda$, and per area dA on a horizontal surface from all parts of the sky above the horizontal, including the disc of the sun itself (SECKMEYER et al., 2001):

2 State of the Art

$$E_{\lambda,glo} = \frac{dW}{dt dA d\lambda} = E_{\lambda,dir} \cdot \cos(\theta) + E_{\lambda,dif} \quad . \quad (2.9)$$

The spectral global irradiance $E_{\lambda,glo}$ incident on the Earth's surface is the sum of spectral direct ($E_{\lambda,dir}$), and spectral diffuse ($E_{\lambda,dif}$) irradiances. The spectral direct irradiance $E_{\lambda,dir}$ describes the part, which arrives at the surface directly from the disc of the sun after travelling through the atmosphere. Note that only the projection of the receiver's area perpendicular to the direction of the beam contributes to the incoming irradiance, which is taken into account by the factor $\cos(\theta)$, with θ being the solar zenith angle. The spectral diffuse irradiance $E_{\lambda,dif}$ is the part arriving on an horizontal surface from all parts of the sky above the horizontal, excluding the disc of the sun.

The reflectance of the Earth's surface, irradiated by sun and sky radiation is termed **albedo** a . According to SECKMEYER et al. (2001) it is given by

$$a = \frac{M}{E} \quad . \quad (2.10)$$

In this definition the radiant exitance M is equal to the radiant power Φ reflected from the surface with the area A . In general, the albedo depends strongly on wavelength. In this study, the spectral albedo as well as albedo integrated over various wavelength intervals will be subject to investigation. A definition of the spectral albedo will be given in Section 4.3.1, Equation 4.5. Other definitions of albedo exist in the literature. In IQBAL (1983) the albedo is very generally defined as the ratio of radiation reflected from a surface to the radiation incident on that surface. In other meteorological publications the albedo sometimes includes the radiation that is thermally emitted by the surface, especially with respect to the albedo of the planet Earth (planetary albedo) at the top of the atmosphere (e.g. MEYERS LEXIKON, 1989).

A different way to describe a field of radiation is based on the photometric unit **candela** (cd). The candela is the luminous intensity, in a given direction, of a source that emits monochromatic radiation of frequency $540 \cdot 10^{12}$ Hz and that has a radiant intensity in that direction of $\frac{1}{683}$ Wsr⁻¹. This definition is available at <http://physics.nist.gov/cuu/Units/candela.html>.

The following definitions are based on DIN 5031 (1982):

The unit of the **Luminous intensity** I_{ph} is the candela

$$[I_{ph}] := 1 \text{ cd} \quad , \quad (2.11)$$

which is similar to the radiant intensity I .

Luminance L_{ph} is equivalent to radiance L and is defined as

$$L_{ph} := \frac{dI_{ph}}{dA \cos(\alpha)} \quad , \quad [L_{ph}] = 1 \frac{\text{cd}}{\text{m}^2} \quad , \quad (2.12)$$

where α denotes the angle between the normal of the area element dA and the direction of the luminance L_{ph} .

2.2 Measuring Solar Radiation

Different types of radiation detectors exist to measure solar spectral radiation incident on the Earth's surface. Depending on the application, broadband, filter or spectral radiometers are employed. These types differ with respect to their wavelength resolution. The purpose of broadband and spectral radiometers is briefly described in the following sections as these are the two types of instruments deployed in this study.

2.2.1 Broadband Instruments

Broadband instruments are usually sensitive to a complete wavelength region such as the incoming solar radiation (e.g. Pyranometers; 300 to 3000 nm) or only the UV part of the spectrum (e.g. biometers). Sometimes they are fitted with optical filters to resemble their response to biological effective radiation. Broadband instruments tend to have less operational problems in the field compared with spectroradiometers because of their simpler design. However, quality control (QC) and assurance (QA) have to be followed rigorously in order to obtain high quality data (CEDE et al., 2002a). Various networks of broadband radiation detectors have been formed.

The Baseline Surface Radiation Network (BSRN; <http://bsrn.ethz.ch/>) was established from the needs of both the climate change and satellite validation communities. It is a project of the World Climate Research Programme (WCRP). The goal of this network is to provide continuous, longterm, frequently sampled, state-of-the-art measurements of surface radiation fluxes adhering to the highest achievable standards of measurement procedures, calibration and accuracy. It is aimed at providing data for calibrating satellite-based estimates of the surface radiation budget and radiation transfer through the atmosphere as well as to monitor regional trends in radiation fluxes at the Earth's surface (MCARTHUR, 1998). These are fundamental tasks regarding the understanding of the Earth's climate system, climate variability and climate change resulting from human influence. The German Antarctic Neumayer station is part of the BSRN network since 1992 (KÖNIG-LANGLO and HERBER, 1996).

Regarding the monitoring of changes in ultraviolet radiation, several countries arranged a so-called UV monitoring network (UV net), in which the detectors are strategically distributed to cover the extent of the different regions (CEDE et al., 2002b). Aims of these networks include the provision of information on the geographic and temporal climatology of UVB irradiance to human health effects researchers, ecosystem scientists, model developers, the agricultural research community, and those seeking ground truth for satellite measurement systems (BIGELOW et al., 1998; JOHNSON et al., 2002).

2.2.2 Spectroradiometers

The rationale to carry out spectral radiation measurements is to determine long term trends, to establish UV climatologies, and to perform process studies in order to validate radiative transfer models (SECKMEYER, 1997).

High quality spectral radiation data can only be obtained if stringent quality control and assurance procedures are applied. Standards for spectral radiation measurements have been set up by the NDSC (MCKENZIE et al., 1997) as well as the WMO (SECKMEYER et al., 2001). Currently, there are two major databases where spectral radiation data are available for user communities:

- the World Ozone and Ultraviolet Radiation Data Centre (WOUDC) operated by the Meteorological Service of Canada in Toronto, Canada (<http://www.woudc.org/>), and
- the European ultraviolet database (EUVDB) in Helsinki, Finland (<http://ozone2.fmi.fi/wvdb/>).

In general, two different types of spectroradiometers exist: scanning and array spectroradiometers. Most spectroradiometers used for UV monitoring are scanning instruments meaning that they contain one exit slit and turning reflection gratings to dissolve the incident radiation into its spectral components. By rotating the grating radiation with a selected wavelength is reflected onto the exit slit. Thus the spectrum is scanned wavelength by wavelength and fine spectral resolutions of less than 1 nm are possible. This is the principle of the IMUK spectroradiometer, which will be explained in detail in Chapter 3.

The advantage of the array spectroradiometers is that they are capable of recording solar spectra almost instantaneously. The detectors of these instruments consist of, e.g., microchannel plate photomultipliers (PMT; HANKEN and TÜG, 2002) or diode array detectors. The wavelength range is determined by the size of the detector array. UV instruments with a 1024×256 charge coupled device (CCD) array, for example, span the range from 288 to beyond 360 nm (LANTZ et al.,

2002). Due to the array detector with a fixed number of channels, no movable parts inside the monochromators are necessary. This makes these instruments more robust compared to scanning spectroradiometers. In principle, they are ideal for use in remote regions such as Antarctica, where operational and technical support is limited.

Array spectroradiometers also have disadvantages compared to scanning instruments. Due to the numerous channels of the array detector the middle slit needs to be widened compared to scanning spectroradiometers. This limits or even prevents important stray light rejection. This stray light causes the detection limit of the array spectroradiometer to increase. Thus, they are less suitable to be employed to UVB measurements, where absolute levels of irradiance are very low due to a strong atmospheric ozone absorption. Another disadvantage is the given number of channels and the fixed grating, and consequently a predetermined wavelength resolution. This wavelength resolution may not allow an oversampling, which simplifies the determination of wavelength shifts (SECKMEYER et al., 2001). These deficiencies concerning the data quality need to be improved in array instruments before their data is of the same high quality compared to state-of-the-art scanning spectroradiometers.

2.3 Monitoring Spectral Irradiance in Antarctica

A network to measure solar spectral UV irradiance in Antarctica has been established by the United States (US) National Science Foundation (NSF) Polar Program. This UV monitoring network is operated by Biospherical Instruments Inc. (BSI; <http://www.biospherical.com/nsf/>). Starting in 1989, spectral UV irradiance is measured at Palmer (64° 46' S, 64° 03' W), McMurdo (77° 50' S, 166° 40' E), and Amundsen-Scott Station at the South Pole (90° S). Each site is equipped with a scanning SUV-100 spectroradiometer manufactured by BSI. This instrument measures global spectral irradiance between 280 and 600 nm with a resolution of 1 nm. It is designed for permanent installation and continuous operation in harsh climates. The system is fully automated and needs operator attention only for periodic manual calibrations and operational checks (BERNHARD et al., 2003).

Spectral UV irradiance is also being measured at the Japanese Antarctic station Syowa (69° 00' S, 39° 35' E) with a Brewer single monochromator spectroradiometer. Spectra are recorded from 290 to 325 nm. These measurements have started in 1991 with the objective to investigate irradiance levels under ozone hole conditions (TAKAO et al., 1999). It has been found that maximum irradiance levels have been observed in years when the ozone hole lasted until the beginning of December as in 1995. Thus the effect of low total ozone column in combination with large solar zenith angles lead to the highest UV levels observed

in Antarctica (TAKAO et al., 1999).

At Neumayer (70° 39' S, 8° 15' W), a UV spectroradiometer developed by the Alfred Wegener Institute for Polar and Marine Research (AWI) in collaboration with isiTec GmbH has been in operation for a few years. This instrument is described by HANKEN and TÜG (2002). It measures spectral UV irradiance in a wavelength range from 280 to 400 nm. This instrument is based on a Bentham DM150 double monochromator and multichannel detector from Hamamatsu for the UVB and an Oriel spectrograph with a diode array detector for the UVA (315 to 400 nm). However, this instrument can only be considered a prototype and further modifications are necessary to reach the goal of complying with the standards of the NDSC (HANKEN and TÜG, 2002).

Conducting radiation measurements at Neumayer provides a link between the UV monitoring sites currently in operation on the Antarctic continent. The NSF polar UV net sites comprise a location on the Antarctic Peninsula (Palmer), one near the Ross Shelf Ice (McMurdo) and at Amundsen-Scott (South Pole) on the Antarctic plateau. The Japanese station Syowa is situated on an Island close to the coast (see Figure 4.1). The location of Neumayer is unique, as it is a coastal station built on an Ice Shelf surrounded by ice all year round. There may be only a few weeks in summer, when the sea ice in Atka Bay breaks up. This break up does not occur each summer. Areas of open water remain small. The range of solar zenith angles is larger at Neumayer compared to Amundsen-Scott. The albedo remains high throughout the year, which is not given for the other coastal stations due to rocks in the surroundings reducing the albedo. In addition, summer melting of snow has been reported for these sites (TAKAO et al., 1999; RICCHIAZZI and GAUTIER, 1998).

2.4 Review of Previous Results

2.4.1 Albedo and its Effect on Irradiance

Antarctica is a favourable site for albedo measurements over pure snow, because compared to the northern hemisphere, the Antarctic snow is less contaminated with soot (HANSEN and NAZARENKO, 2004). So far, albedo measurements in the Antarctic have only been performed with broadband or filter spectroradiometers (GRENFELL et al., 1994; SMOLSKAIA et al., 1999; ZHOU et al., 2001), but never with the same type of high-resolution instruments used for measuring spectral irradiance or radiance.

Spectral albedo measurements conducted in Antarctica by GRENFELL et al. (1994) yield a dependence of albedo on wavelength, snow grain size and solar zenith angle. These measurements have been performed with a filter radiometer

2 State of the Art

with a resolution of about 20 nm. A uniform high albedo with 0.96 to 0.98 is reported across the UV and visible, nearly independent of snow grain size and solar zenith angle. The albedo in the near infrared is lower, dropping below 0.15 in the strong absorption bands of ice at 1500 and 2000 nm.

The high albedo of a snow covered surface, especially in the UV and visible, has a large effect on the downwelling radiation due to multiple reflections between the ground and the scattering atmosphere. Model calculations of ultraviolet irradiance for cloudless sky from LENOBLE (1998) show enhancements in irradiance levels of nearly 50% at 320 nm for a snow covered surface in comparison with snow free conditions.

A number of previous studies investigate the combined effect of surface albedo and clouds on UV irradiance:

McKenzie et al. (1998): Experimental studies have shown an increase in UV irradiance of approximately 40% due to a snow albedo of 0.8. The enhancement in UV irradiance levels over a snow covered surface compared to a snow free surface amounts to 70% when a cloud cover is present.

Kylling et al. (2000): Snow cover at Tromsø, Norway, increases the erythemal UV dose by more than 20%. The maximum increase of a daily dose compared to snow free conditions is 63% for a cloudy day.

Nichol et al. (2003): The moderation of cloud reduction on UV irradiance in the Antarctic due to a high surface albedo is investigated. Compared to a cloudless case and a low surface albedo (0.05) a reduction of 40% in UV irradiance for cloudy conditions results. Increasing the surface albedo to 0.8 and 0.96 lead only to an attenuation by 20% and 10%, respectively.

In mid-latitudes vegetation, buildings and rocks prevent a complete snow cover of the surface. The albedo of such inhomogeneous surfaces is not uniform. Thus efforts have been undertaken to estimate the effective albedo representative for such inhomogeneous surfaces (DEGÜNTHER et al., 1998; RICCHIAZZI and GAUTIER, 1998; SCHWANDER et al., 1999; SMOLSKAIA et al., 1999; MAYER and DEGÜNTHER, 2000; WEIHS et al., 2001).

2.4.2 Radiance Measurements

Sky radiance distributions have been measured by GRANT and HEISLER (1997), GRANT et al. (1997a) and (1997b) in West Lafayette, Indiana, USA, with broadband sensors sensitive to three wavelength bands (UVB, UVA, and PAR). They measured sky radiance for

2 State of the Art

- clear sky situations, defined by less than or equal to 10% cloud cover determined by hemispheric sky photographs and aerosol turbidity measurements used as an indicator of the uniformity of sky conditions. Evidence of horizon brightening in the UVA, but not in the UVB, was found. The horizon brightening increased with increasing SZA. Further, a region with reduced radiance opposite the solar disk was found (GRANT et al., 1997a).
- translucent overcast skies, defined by a cloud cover of greater than 90% determined by hemispheric sky photographs and the solar disk visible on the photographs. No region of reduced radiance opposite the sun was evident in the translucent overcast distributions as was perceived in the clear sky radiance distributions. Horizon brightening was observed for high SZA (GRANT et al., 1997b).
- obscured overcast sky, defined by a complete cloud cover determined by hemispheric sky photographs and a PAR transmittance of less than or equal to 0.25. The results showed the highest sky radiance at the zenith and a decline of radiance towards the horizon (GRANT and HEISLER, 1997).

In all three studies the authors remark that the sky radiance distribution under greater surface albedo conditions, such as snow cover, may differ from their results since the albedo strongly influences the radiance distribution under all cloud conditions.

One of the few measurements of spectral sky radiance has been conducted by BLUMTHALER et al. (1996). Measurements at various locations in Europe have been performed to investigate a variety of atmospheric conditions. However, there is a lack of measurements over a snow covered surface. They found a variation in spatial distribution of sky radiance in the UVB of only 2, but in the UVA up to a factor of 10. They further concluded that due to increased scattering sky radiance measurements in the UVB are more sensitive to aerosol particles as well as tropospheric ozone.

WEIHS et al. (2000) have investigated the behaviour of sky radiance distribution under broken cloud conditions. Aim of their work was to quantify the alteration in ground UV radiances, compared with those of cloudless skies, which can occur due to broken cloud conditions. Their results showed that, on average, the maximum enhancement in surface UV was due to reflection of clouds located at 60° to 75° scattering angle and at a viewing zenith angle lower than 30°. Thus their result is also valid for zenith sky radiance. Radiances from cloudy sky locations were either higher by up to a factor of 2.5 or lower with minimum values being only 8% of the cloudless radiances.

A recent study by HUBER et al. (2004) describes spectral sky radiance measurements over a snow covered surface at an Alpine site. Due to the mountainous surroundings, the ground was inhomogeneously covered by snow. They also

2 State of the Art

compared their experimental data with model results from a one-dimensional radiative transfer model. Relative to the modelled situation with homogeneously snow-covered terrain, diffuse sky radiance over snow-free terrain, is reduced by up to 40%, depending on solar zenith angle. They indicate that diffuse sky radiance measurements in a low aerosol environment are especially valuable for the assessment and validation of radiative transfer models. Thus, diffuse sky radiance measurements at an Antarctic site are especially beneficial in this context. HUBER et al. (2004) express the need for additional measurements of spectral diffuse sky radiance to comprehensively validate radiative transfer models.

3 Development of a NDSC Spectroradiometer

In order to develop and maintain an internationally recognised spectroradiometric system it is vital to meet the data requirements set up by international organisations. The WMO as well as the NDSC have assembled a list of data specifications that have to be met in order to submit data to their databases (SECKMEYER et al., 2001; MCKENZIE et al., 1997). Two aims are to monitor long term changes in UV and to make properly calibrated UV data available to the scientific community.

For this study, a new spectroradiometric system has been purchased. The different components have been chosen to cover a wavelength range from 290 to 2500 nm. Before deployment, the spectroradiometer has to be tested with respect to malfunctions. Further, it had to be characterised thoroughly in the radiation laboratory of IMUK. Routines for Quality Control (QC) of the data have been developed. For Quality Assurance (QA) the IMUK instrument has successfully participated in European intercomparisons within the project Quality Assurance of Spectral Ultraviolet Measurements in Europe through the development of a transportable unit (QASUME; GRÖBNER et al., 2004). To comply with the specifications of the NDSC, the IMUK spectroradiometer has taken part in an NDSC intercomparison in Boulder, Colorado. It thus also provides a link between these European instruments and the NDSC instruments.

It is planned to use the IMUK instrument as a mobile NDSC instrument, supporting long term measurements as a travelling standard. Instruments applying for the NDSC status can be compared with this new travelling NDSC instrument in order to achieve the desired status.

This chapter describes the development of the new IMUK NDSC spectroradiometer, starting with the technical details, leading to the characterisation, QC, and last to the QA procedures.

3.1 Technical Details

The IMUK scanning spectroradiometer is designed to measure solar spectral irradiance and radiance in a wavelength range from 250 to 1050 nm. Further extension into the IR up to 2500 nm is possible, but not yet realised. It basically consists

3 Development of a NDSC Spectroradiometer

of four components: the entrance optics, a double monochromator, radiation detectors and devices to control the measurements and store the data.

For spectral irradiance measurements, the entrance optic consists of a shaped Teflon diffuser, which is protected by a quartz dome. This diffuser is optimised for a low cosine error. The entrance optic used at IMUK is commercially available from schreder-cms, Ing. Dr. Schreder, Austria, <http://schreder-cms.com>. It is heated for the temperature never to sink below 30°C to avoid humidity affecting the measurement.

The entrance optic used for spectral radiance measurements is especially designed for this purpose by Czibula & Grundmann GbR (<http://www.photo-meter.com/>). The input optic consists of a 100 mm long tubus. The field of view (FOV) is limited by a quartz glass window which protects the interior of the tubus. A baffle in the middle of the tubus serves for restraining the FOV as well as to reject stray light. At the bottom end, an optical fibre can be attached. When measuring radiance the input tubus is attached to the Skyscanner, which was also designed by Czibula & Grundmann in order to conduct luminance and radiance measurements. With the Skyscanner, it is possible to point the radiance entrance optic towards any desired direction in the sky.

Quartz optical fibres lead from both entrance optics into a multiway entrance. Depending on the active entrance optics, a swing-away-mirror (SAM) inside the multiway entrance is positioned in a way to precisely reflect the incoming light onto the entrance slit of the monochromator.

The central element of the spectroradiometer is a model DTMc300 double monochromator manufactured by Bentham Instruments Ltd. (<http://www.bentham.co.uk>, see Figure 3.1). The double monochromator consists of two identical single Czerney Turner monochromators. The focal length is 300 mm. The light enters the monochromator through a motorised entrance slit, which is set to 0.74 mm for wavelengths between 280 and 500 nm and to 1.48 mm for wavelengths between 500 and 1050 nm. These are also the widths of the exit slits. The middle slit is set to 1.85 mm. For the wavelength ranges of 280 to 500 nm and 501 to 1050 nm holographic reflection gratings with 2400 and 1200 grooves per mm are employed in each monochromator, respectively. Stray light is suppressed by a number of baffles and the middle slit.

A PMT, model DH-10-Te, is employed as a detector for the wavelength range from 280 to 500 nm, whereas a silica diode is used from 500 to 1050 nm. The output current of the PMT is further processed by a decadal current amplifier. This signal is converted to a digital signal, which can be processed by computer.

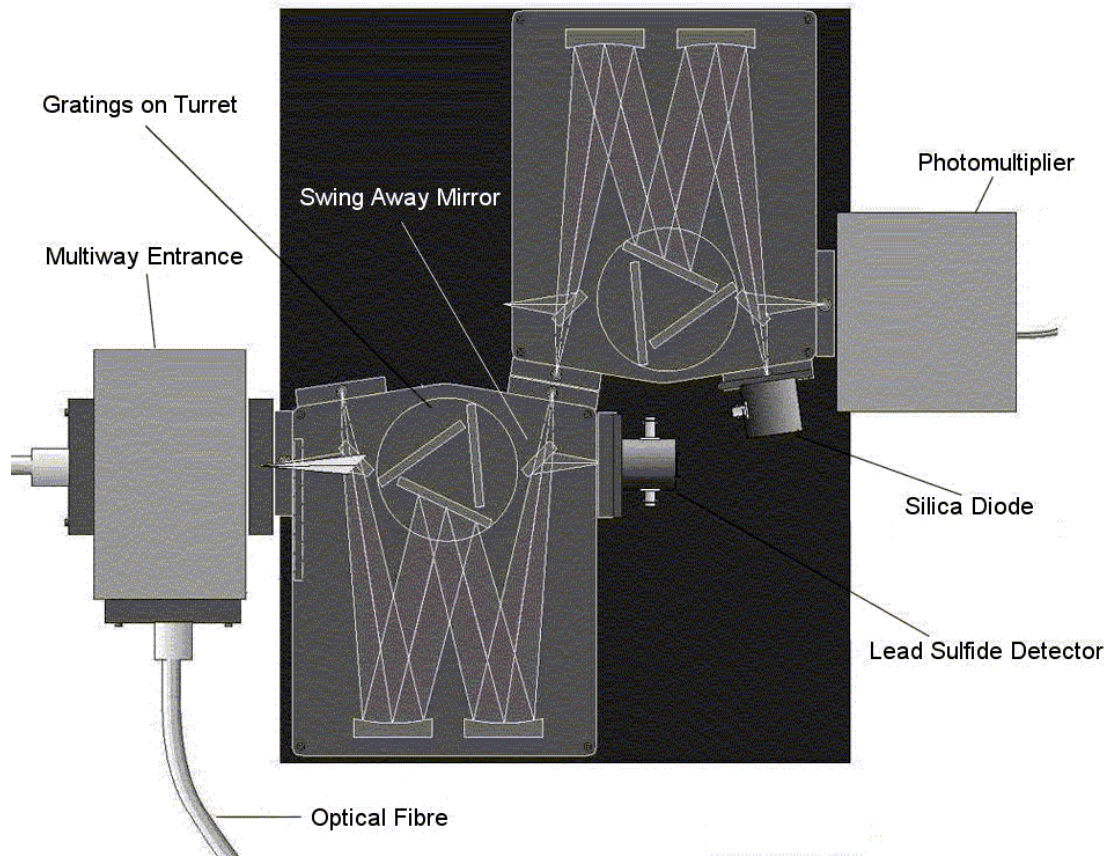


Figure 3.1: Schematic diagram of the Bentham DTM300 double monochromator including the multiway entrance and detectors. The path of light is controlled by mirrors. Separation of the light into its spectral components is achieved by holographic reflection gratings.

3.2 Instrument Characterisation

In order to comply with the NDSC and WMO standards for measuring spectral solar radiation parameters, the spectroradiometer has to be characterised thoroughly. The characterisation consists of several experiments (SECKMEYER et al., 2001; MCKENZIE et al., 1997), which serve to estimate the uncertainty budget of the spectroradiometer.

3.2.1 Cosine Error of Irradiance Input Optics

The radiant power reaching a flat surface is proportional to the cosine of the angle θ between the direction of incidence to the surface normal. Therefore, spectroradiometers for measuring solar spectral irradiance E_λ should have a response as close to $\cos(\theta)$ as possible. This response is called the cosine response of the system. In reality, the response of the entrance optics deviates from this response and depends mainly on SZA, solar azimuth angle (SAA), and wavelength. This deviation can be quantified by

$$f(\theta, \phi) = \frac{S(\theta, \phi)}{S(0^\circ, \phi) \cos(\theta)} \quad , \quad (3.1)$$

with θ being the incidence angle of the radiation and ϕ the azimuth angle (BERNHARD and SECKMEYER, 1997).

The entrance optics used at IMUK has nominally one of the lowest cosine errors. The deviation from the ideal cosine response $f(\theta, 0^\circ)$ of the IMUK entrance optics is shown in Figure 3.2 for 320, 400, and 500 nm and for one azimuth direction. At 320 nm the deviation from the ideal cosine response is lowest with less than 5% for $\theta < 85^\circ$. At 500 nm the deviation exceeds 5% for $\theta > 70^\circ$. The isotropic deviation describes the integral deviation from the ideal cosine response for incident angles between 0° and 85° . The larger deviations from the cosine response for larger incidence angles θ are due to the curvature of the Teflon cap. The area of the projection of the diffuser cap is increased compared to a flat geometry, thus leading to a higher response. To avoid this excessive response for large θ , a shadow ring can be incorporated into the design of the input optic to block the incoming radiation. Such a shadow ring is part of the IMUK input optic, but it is just covering 2° from the horizontal. A larger shadow ring would not lead to erroneous values of detected irradiance, because absolute values of irradiance are very low for large SZA.

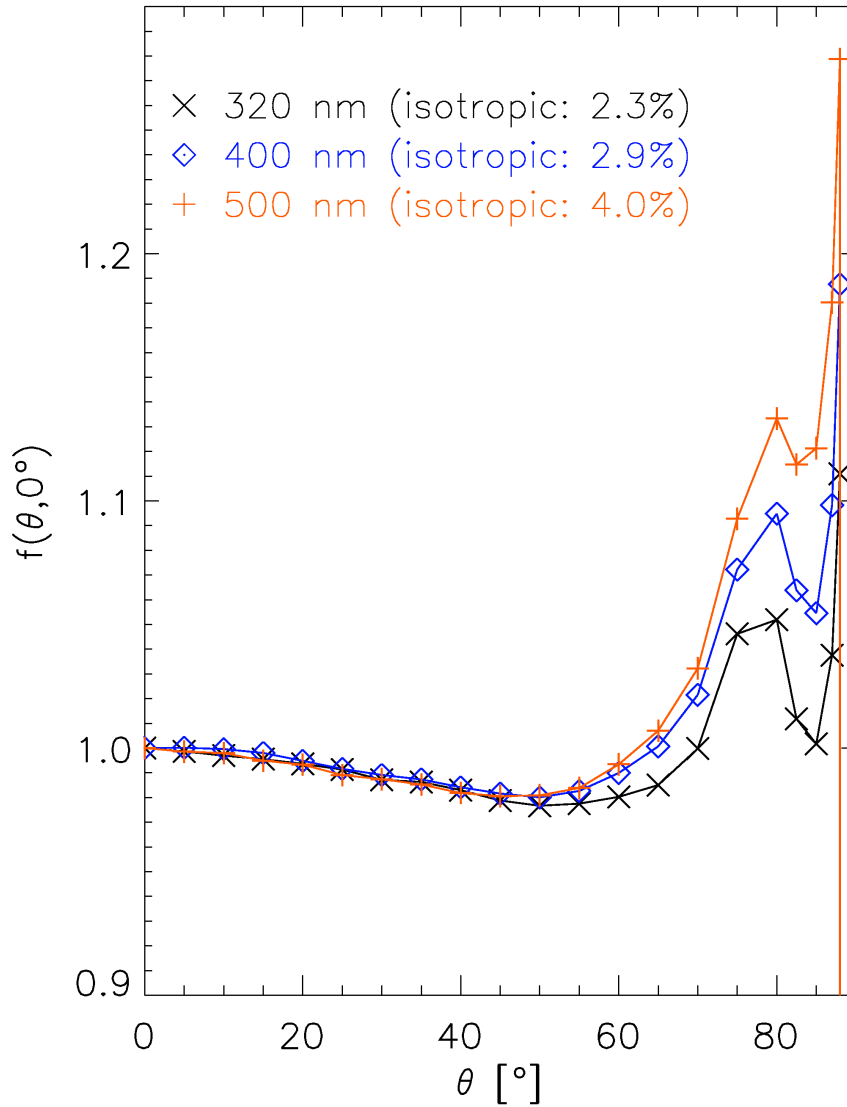


Figure 3.2: The deviation from the ideal cosine response of the IMUK entrance optics for different wavelengths and one azimuth direction. For 320 nm, the cosine error is less than 5% for solar zenith angles below 85°. The cosine error for larger wavelengths is slightly higher. The very large deviations for $\theta > 85^\circ$ are possible because of a low shadow ring. For a closer explanation see text.

3.2.2 Field of View of Radiance Input Optics

It is vital to know the exact size of the field of view of the entrance optics in order to estimate absolute radiance. The distribution of sky radiance is assumed to be constant over the area of the FOV. Thus the smaller the FOV the more accurate the sky radiance measurements (GRÖBNER, 1996).

The determination of the FOV was performed in the IMUK radiation laboratory. A 100 W tungsten halogen lamp was placed in front of the entrance optics. The entrance optics was mounted on a rotation table, which allowed to turn the entrance optics in steps of 0.5° . The scale-reading precision is 0.25° . A laser was used to align the lamp with the entrance optics in order to find the direction where the radiation emitted by the lamp is perpendicular to the plane of the quartz glass window of the entrance optics. This is the position to receive the maximal signal and the direction denoted with 0° . Measurements have been performed from 400 to 490 nm in steps of 10 nm. This wavelength range was chosen because of the high sensitivity of the spectroradiometer in this spectral range. A possible spectral dependency may be observed when measurements at more than one wavelength are conducted.

Two sets of measurements have been performed. Within the first set, the entrance optic was turned in steps of 5° in a range of $\pm 90^\circ$ from the 0° -direction. The measurements have been normalised to the maximum value in the 0° -direction. The results are shown in Figure 3.3. This coarse resolution in rotation angle was chosen to investigate the behaviour at large angles from the centre direction. Figure 3.3 shows a difference of four to five orders of magnitude between the maximum of the FOV and angles between 10° and 60° from the centre. At $\pm 70^\circ$ from the centre a local maximum only being three to four orders of magnitude lower than the centre of the FOV is detected. This indicates a possible reflection inside the input tubus. To remove this reflection its inside may need to be coated black, which can only be done by the manufacturer.

A resolution of 5° is far too low to characterise the FOV. Therefore, measurements from $+7^\circ$ to -7° from the 0° -direction in steps of 0.5° have been performed in addition. The result is displayed in Figures 3.4 and 3.5 on a linear and logarithmic scale, respectively. The sides of the FOV are steep, thus there is no reflection problem within the $\pm 7^\circ$ range. A slight asymmetry can be observed in Figure 3.4. It may be due to the way the optical fibre is fitted into the entrance optics. Another reason may be the uncertainty in aligning the entrance optics and the lamp. The maximum of the FOV is shifted by about 0.25° out of the centre direction. This can be explained by the scale-reading uncertainty.

The full width at half maximum of the FOV is about 4.4° . This translates to a solid angle of $4.63 \cdot 10^{-3}$ sr when integrated. Since the flanks of the FOV have a steep slope (see Figures 3.3 to 3.5), the input tubus is suitable for the detection

3 Development of a NDSC Spectroradiometer

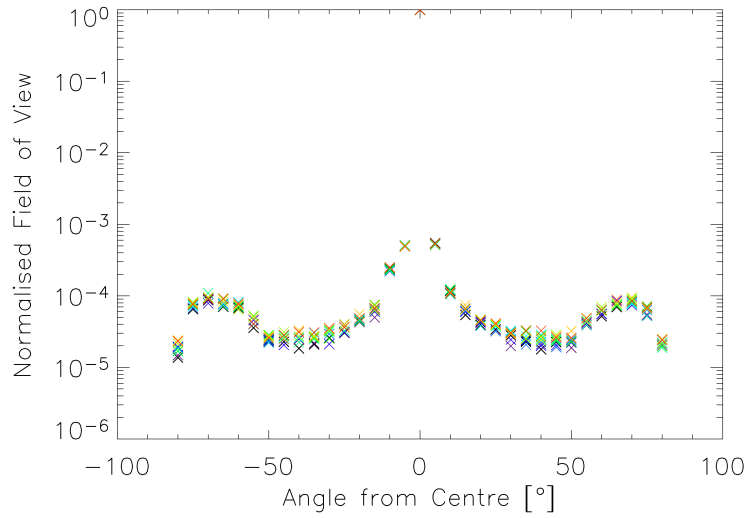


Figure 3.3: Field of view measured in steps of 5° from $\pm 90^\circ$ away from the centre. Outside the FOV the radiation is lower by 4 to 5 orders of magnitude. The local maximum around $\pm 70^\circ$ may be due to reflections inside the tubus. The different colours represent different wavelengths from 400 to 490 nm.

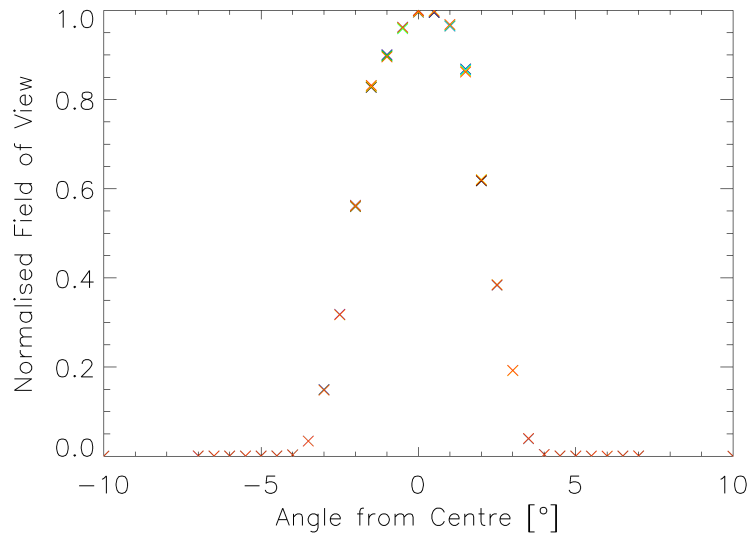


Figure 3.4: Field of view on a linear scale, measured in steps of 0.5° in a range of $\pm 7^\circ$ from the 0° -direction. The sides of the FOV are steep minimising incident radiation from directions outside the FOV. The slight asymmetry may be due to misaligning the sensor and lamp. The different colours represent different wavelengths from 400 to 490 nm.

3 Development of a NDSC Spectroradiometer

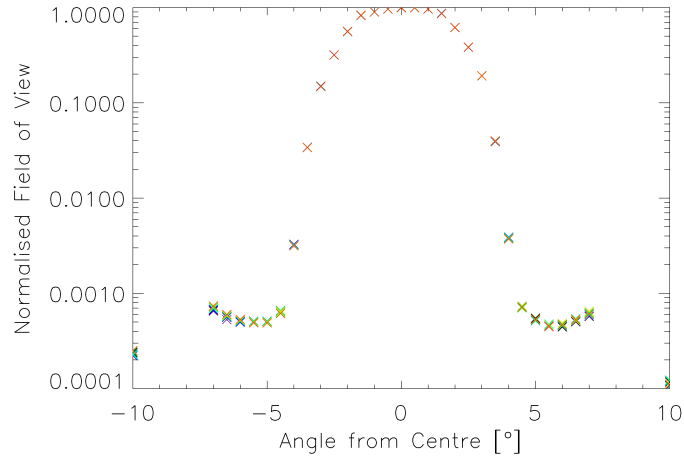


Figure 3.5: Field of view on a logarithmic scale, measured in steps of 0.5° in a range of $\pm 7^\circ$ from the 0° -direction. A slight increase in response at $\pm 7^\circ$ from the centre is observed. The different colours represent different wavelengths from 400 to 490 nm.

of sky radiance.

3.2.3 Slit Function

The entrance and exit apertures of monochromators have finite widths. As a consequence, not only do photons with the desired wavelength λ_0 pass through the monochromator but also those with wavelengths inside a certain interval around λ_0 . When the monochromator is set to a fixed wavelength λ_0 , its transmittance as a function of wavelength is called the slit function. The width of the slit function is usually quantified by the full width of the function of half its maximum (FWHM) and is denoted the bandwidth B of the monochromator. The slit function of a spectroradiometer should be determined by measuring a light source with variable wavelengths. Such a source can be a tuneable laser, which is hardly available. In practice, the slit function is determined by scanning a monochromatic light source, such as a HeCd-laser or selected lines from a low pressure mercury lamp. This is justified because of the assumption that the slit function of the spectroradiometer does not change over the measured wavelength interval when scanning across a monochromatic line.

At IMUK, a low pressure mercury lamp is employed to characterise the slit functions of the spectroradiometer. In the wavelength range from 250 to 500 nm the measured FWHM for the IMUK spectroradiometer is 0.54 nm. Due to the wider entrance and exit slits and the gratings with lower resolution the slit function between 501 and 1050 nm is 1.96 nm (see Figure 3.6).

3 Development of a NDSC Spectroradiometer

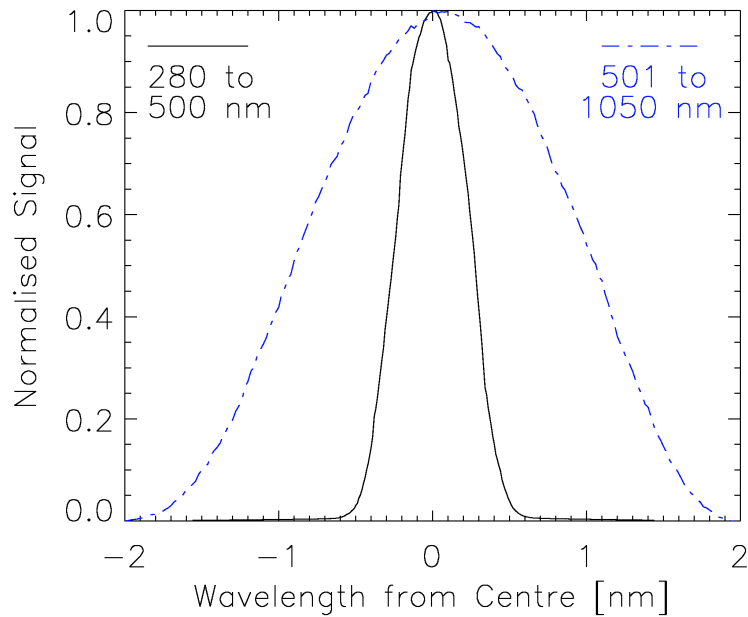


Figure 3.6: Normalised mean slit function of the IMUK spectroradiometer. The FWHM is 0.54 nm and 1.96 nm for the wavelength range between 250 and 500 nm and 501 and 1050 nm, respectively. Both slit functions are based on measurements of emission lines of a low pressure mercury lamp (253.65 nm line between 250 and 500 nm and 546.07 nm line between 501 and 1050 nm).

3.2.4 Wavelength Shift

The wavelength setting of a spectroradiometer is calibrated by measuring the spectrum of a mercury lamp. The line position of this lamp is known to within 0.0001 nm (SANSONETTI et al., 1996). Comparing measured and actual line positions, a wavelength scale is assigned to the monochromators. If the wavelength shift is well defined, the resulting systematic errors can be corrected. An alternative method to determine the wavelength shift is the comparison of measured spectra with the Fraunhofer lines of the sun (SLAPER et al., 1995). A wavelength uncertainty of ± 0.1 nm may lead to an uncertainty in DNA weighted irradiance of up to $\pm 3.5\%$ and of up to $\pm 2\%$ in erythemally weighted irradiance (BERNHARD and SECKMEYER, 1999). This underlines the importance of wavelength stability especially in the UV region of the solar spectrum.

Changes in ambient temperature of the instrument cause wavelength shifts as well as changes in absolute irradiance. The wavelength shifts are the dominant problem due to thermal expansion of the mechanical components, for example the gratings, inside the monochromators. Examinations of the wavelength shift

3 Development of a NDSC Spectroradiometer

at changing ambient temperatures have been performed for three wavelengths. Example results are shown in Figure 3.7.

To minimise the effect of changing ambient temperature on the spectroradiometer, it is placed inside a temperature stabilised box during measurements. This box is equipped with an air conditioning system to hold the inside temperature constant to within ± 0.5 K. The box further protects the instrument from outside weather conditions.

When a new campaign starts and the spectroradiometer is set up at a new location, the wavelength setting of the monochromator is likely to have changed due to transportation. Therefore, a new wavelength calibration has to be performed prior to each campaign. This means, that the initial wavelength shift of the monochromators is not constant for a certain ambient temperature. Therefore, error bars are not included in Figure 3.7, which only provides an example of wavelength shift as a function of ambient temperature.

3.2.5 Detection Threshold

The detection threshold for the IMUK spectroradiometer has been determined by measuring a 100 W lamp through a cut off filter. A WG320 filter by Schott has been placed between the lamp and the entrance optics. The transmission of the filter is available at <http://www.newportglass.com/schott.htm>. To calculate the detection threshold, the measurements have been convoluted with a triangular slit function with an FWHM of 1 nm as suggested by SECKMEYER et al. (2001). For a signal-to-noise ratio (S/N) of 1 at 1 nm FWHM the detection threshold for the IMUK instrument is $9 \cdot 10^{-7} \text{ Wm}^{-2}\text{nm}^{-1}$.

3.2.6 Absolute Calibration

With the radiometric calibrations the spectral responsivity $r(\lambda)$

$$r(\lambda) = \frac{S_L(\lambda)}{E_L(\lambda)} \quad (3.2)$$

of a radiometer is determined. $E_L(\lambda)$ is produced by a calibration source, and $S_L(\lambda)$ is the signal of the spectroradiometer when measuring the source. The measured spectral irradiance E_λ is

$$E_\lambda = \frac{S_M(\lambda)}{r(\lambda)}, \quad (3.3)$$

3 Development of a NDSC Spectroradiometer

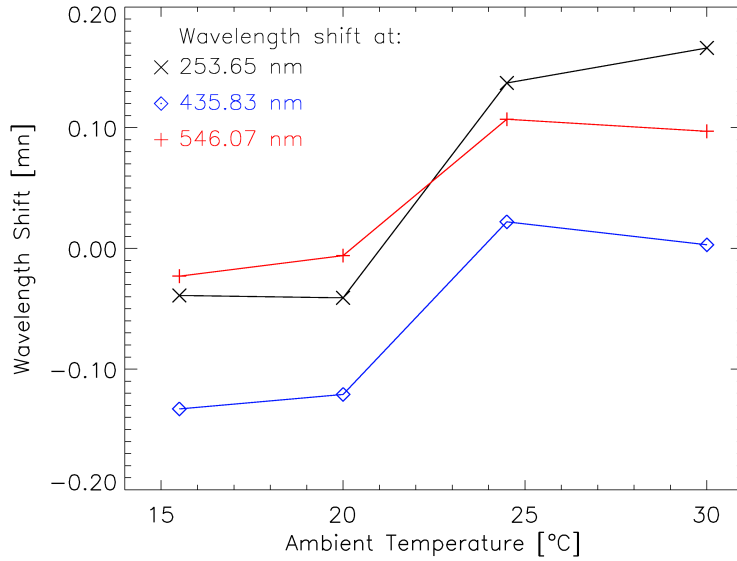


Figure 3.7: Example of wavelength shift at 253.65, 435.83, and 546.07 nm in dependence of ambient temperature. The absolute wavelength shift differs for the three wavelengths. It is negative at 20°C and below, and positive above 24°C.

where $S_M(\lambda)$ is the signal of the spectroradiometer when measuring a source (i.e. the sky).

The overall calibration uncertainty includes all uncertainties associated with the irradiance calibration. Absolute calibration procedures are described in detail by BERNHARD and SECKMEYER (1999). The calibration of the IMUK spectroradiometer is based on a 100 W tungsten halogen lamp. This standard was calibrated by Gigahertz Optik GmbH (<http://www.gigahertz-optik.de>) against lamps calibrated at the German National Standards Laboratory (NSL), the *Physikalisch-Technische Bundesanstalt*, (PTB). Gigahertz Optik maintains a PTB-accredited calibration laboratory. The calibration accuracy of the 100 W standard was additionally verified by comparing the lamp against two independent 1000 W standards of the type Sylvania, which were calibrated in absolute terms by the PTB. The deviation between the 100 W lamp and the two 1000 W standards was less than 3%. This difference is within the typical calibration uncertainty of 3.5% that applies to lamps disseminated by standards laboratories (BERNHARD and SECKMEYER, 1999; KIEDRON et al., 1999).

The calibration certificate of the 100 W lamp is given in wavelength steps of 5 nm. The values were interpolated to intermediate wavelengths with natural cubic splines; the associated uncertainty is 0.2%. The 100 W secondary standard was calibrated at a distance of 50 cm but is deployed at a distance of 40 cm,

3 Development of a NDSC Spectroradiometer

utilising a portable field calibrator, which was already used in earlier campaigns (e.g. SECKMEYER et al., 1995). The inverse square law is applied to scale the irradiance values from a distance of 50 cm to 40 cm. This method is widely employed in the UV community (BERNHARD and SECKMEYER, 1999; GRÖBNER et al., 2004). The scaling factor is accurate to within $\pm 0.3\%$. The uncertainty caused by alignment errors of the lamps and the entrance optics are about 0.1%.

The irradiance collector of the IMUK spectroradiometer contains a shaped diffuser made of Teflon, which is covered by a quartz dome (see Section 3.1). The reference point of the diffuser was determined according to BERNHARD and SECKMEYER (1997) and the associated uncertainty is 0.3%. The influence of the quartz dome leads to an additional uncertainty of 0.2% (BERNHARD and SECKMEYER, 1999).

Although a high quality current source is used to operate the lamps, the precision of the current setting is limited to $\pm 0.01\%$, resulting in an irradiance uncertainty of approximately 0.1% at 300 nm. The combined uncertainty of all factors contributing to the calibration uncertainty is 4.6%.

3.3 Quality Control

Quality Control is defined as maintaining and monitoring the performance of the spectroradiometer over time with own methods. The most important QC procedures are monitoring the radiometric as well as the wavelength stability.

It is recommended to perform radiometric stability checks at least on a weekly basis (SECKMEYER et al., 2001) in order to obtain knowledge about the spectroradiometer's performance over time. At IMUK, such stability checks are performed once a day during campaigns. 100 W halogen lamps are deployed for this purpose inside a portable field calibrator (see Figure 3.8). Such a portable field calibrator has also been provided for the European project QASUME for QC in the field proving that this design of a portable lamp housing is recognised and even employed on an international basis.

To check the wavelength alignment, different emission lines of a Hg-lamp are measured prior to each campaign, when the instrument is already set up on site. In addition, the wavelengths shift is calculated by correlation of the measured solar spectra with the Fraunhofer absorption lines of the sun applying the algorithm SHICrivm (SLAPER et al., 1995), which is freely available on the internet (http://www.rivm.nl/en/milieu/risicos_stoffen/nietioniserende_straling/shic/).

Further routine QC procedures not mentioned yet include

- the comparison of spectral UV measurements with erythemally weighted UV data (MCKINLAY and DIFFEY, 1987) measured by a Solar Light SL501

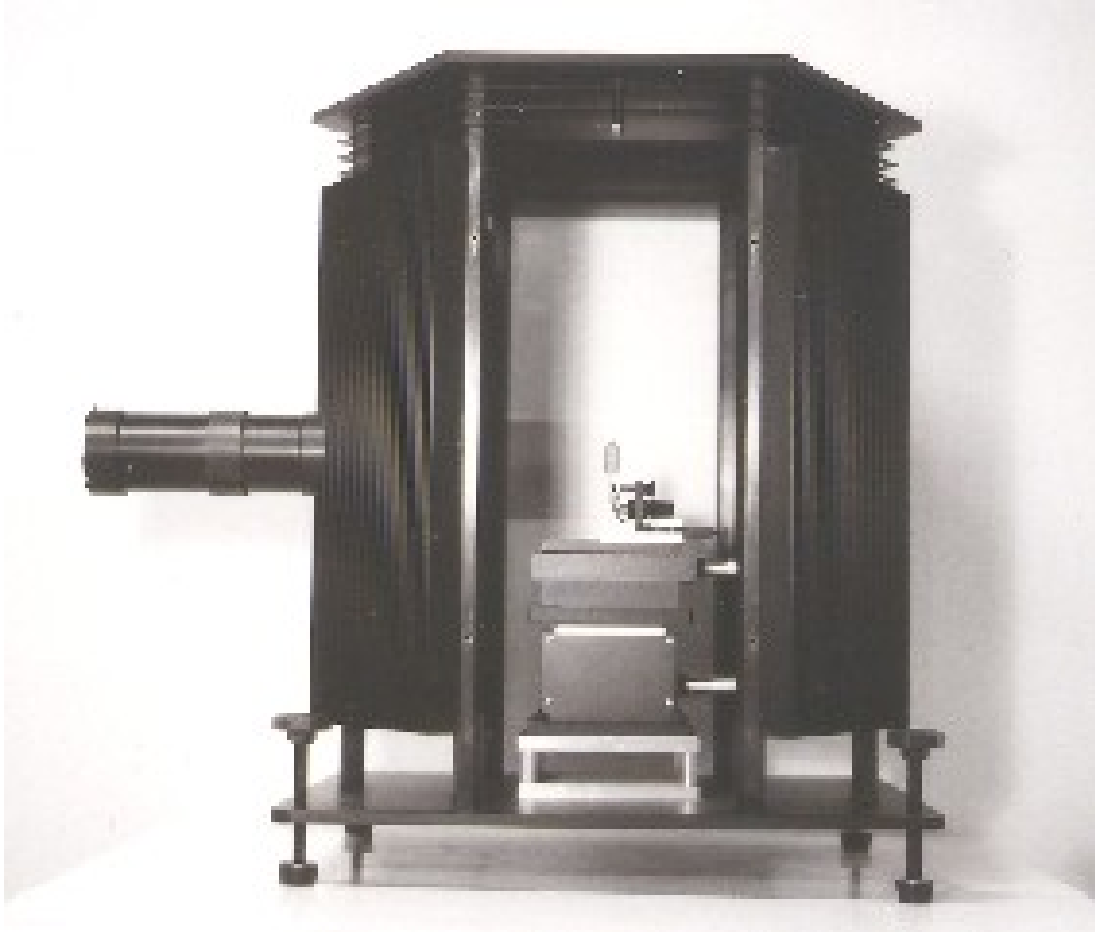


Figure 3.8: Portable field calibrator. The hexagonal shape suppresses stray light to reach the detector which is fitted in the tube on the left when calibrating. The 100 W field calibration lamp is mounted on adjustable units. For calibration purposes and stability checks, the entrance optics is fitted reproducibly in the tube part on the left.

3 Development of a NDSC Spectroradiometer

biometer (SL501),

- model comparisons of measured spectra for cloudless situations,
- ratios of measured spectra to the midday spectrum,
- checks of the diurnal course of irradiance at selected wavelengths,
- comparison of daily doses from days with similar meteorological conditions.

When measuring spectral irradiance, ancillary measurements are performed simultaneously. These include the deployment of a SL501, a pyranometer, and a Microtops Sun Photometer II (Microtops) to perform measurements of total ozone column and aerosol optical depth. Furthermore, cloud and weather observations are performed on a regular basis. The application of QC procedures alone is not sufficient to develop an internationally recognised spectroradiometric system that complies with NDSC or WMO standards. Regular intercomparisons to other instruments are needed in addition.

3.4 Quality Assurance

Intercomparisons of spectroradiometers serve as a successful tool to assure the quality of spectral UV irradiance (SECKMEYER et al., 2001; WEBB, 2000). Further, an intercomparison with a NDSC spectroradiometer is a necessary requirement to rate an instrument as a NDSC spectroradiometer (MCKENZIE et al., 1997).

3.4.1 Ispra Intercomparison

The first serious test for the new IMUK spectroradiometer was an international intercomparison for spectroradiometers hosted by the newly established European Reference Centre for UV Radiation Measurements (ECUV) in Ispra, Italy (45° 48' 43" N, 08° 37' 37" E). This campaign took place from 6 to 17 May 2002. Only instruments that have performed reliably during past intercomparisons have been chosen for this campaign (e.g. GRÖBNER et al., 2000; BAIS et al., 2001), which presented a perfect opportunity to assure the quality of the IMUK spectroradiometer for the first time. The participants were (abbreviations of the groups' spectroradiometers in parentheses):

- Institute for Medical Physics, University of Innsbruck, Austria (ATI)
- Institute for Science and Technology, University of Manchester, Great Britain (GBM)

3 Development of a NDSC Spectroradiometer

- National Institute of Public Health and the Environment, Bilthoven, Netherlands (NLR)
- Finnish Meteorological Institute, Finland (FIJ)
- Laboratory of Atmospheric Physics, Aristotle University of Thessaloniki, Greece (GRT)
- ECUV, Ispra, Italy (two spectroradiometers: JRC and ISQ)
- IMUK, University of Hannover, Germany (IMUK)

This campaign was performed within QASUME funded by the European Commission (EC). All the spectroradiometers were set up next to each other on a flat roof. Solar spectral irradiance from 290 to 500 nm was measured simultaneously on a half hourly basis during the nine days of this intercomparison.

In terms of overall stability for the nine days of measurements, most instruments were constant over time with respect to each other. Example results are shown in Figures 3.9 and 3.10. Extensive information on this intercomparison campaign can be found at <http://lap.physics.auth.gr/qasume>. Figure 3.9 shows the ratio of each instrument to the IMUK spectroradiometer for 8 May 2002. The spread of the ratios is less than 15%, which is worse than expected (HERMAN et al., 1999). For this particular day the IMUK spectroradiometer agrees best with the ATI, JRC, JRX (corrected JRC data due to a new calibration) and ISQ spectroradiometers with deviations ranging from -5% to +5%. The other spectroradiometers measured up to 12% higher irradiances. Most ratios do not show a large wavelength dependence. The ratios GBM/IMUK (light blue) and GRT/IMUK (bluish green) show small spectral dependencies with a deviation of +4% around 300 nm up to +10% at 500 nm, +10% around 300 nm and +7% at 360 nm, respectively.

Figure 3.10 shows the ratio at selected wavelengths between the JRC and IMUK spectroradiometer for all nine days. The JRC instrument was picked for this comparison for various reasons: With the exception of irradiance in the visible part of the spectrum, it was a stable instrument throughout this campaign; its spectra cover the same wavelength range (290 to 500 nm) and are measured in the same wavelength steps (0.25 nm); it took part in a second intercomparison in Hannover in August 2002 (see Section 3.4.2).

First of all the stable behaviour is noted over the course of the intercomparison. The largest changes in ratios can be seen on 12, 14, and 16 May 2002, which were days that started with cloudless skies, implying a zenith and/or azimuth dependency in one or the other instrument. Otherwise the stability is good, general fluctuations with both time and wavelength being within a 10% band. The wavelengths larger than 400 nm show greater deviations (more than 20%) especially during the last days of the campaign. On the last two days (15 and 16 May), the diffuser of the JRC instrument was rotated several times to observe possible

3 Development of a NDSC Spectroradiometer

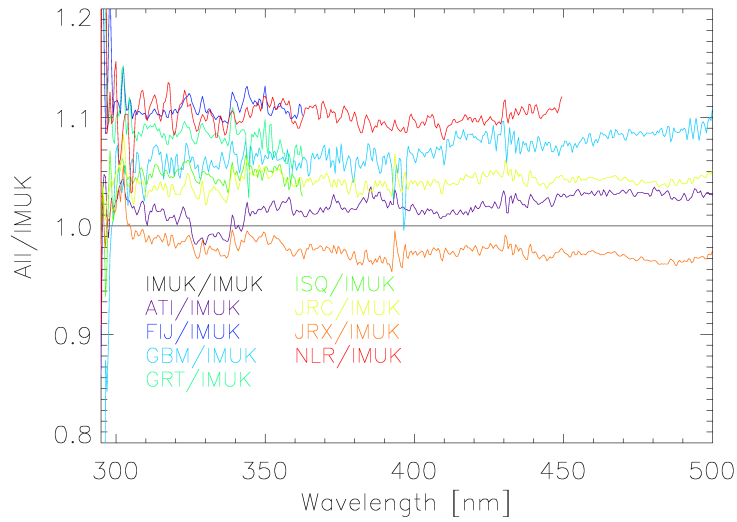


Figure 3.9: Ratios of each spectroradiometer to the instrument of IMUK as a function of wavelength (295 to 500 nm) for 8 May 2002. The spectra are wavelength corrected and convoluted with a triangular slit function with a FWHM of 1 nm. Not every spectroradiometer deployed at the intercomparison was capable of measuring up to 500 nm.

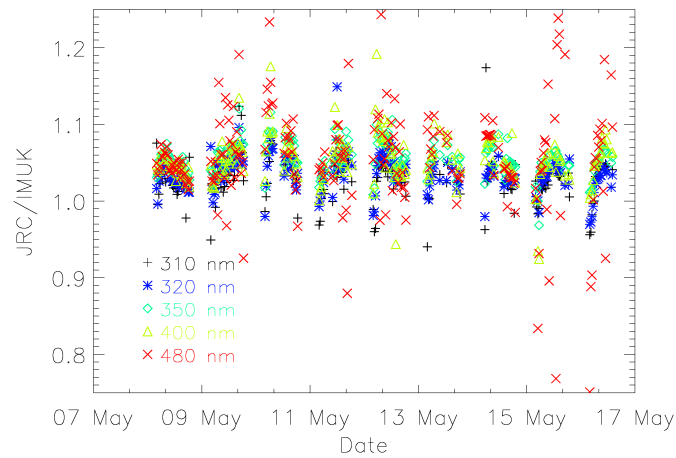


Figure 3.10: Ratio of selected wavelengths for the JRC vs. the IMUK spectroradiometer from 8 to 16 May 2002. The ratios for wavelengths below 400 nm do not show a lot of scatter. In contrast, the ratio at 480 nm deviates more than 20% from unity, especially for the last days of the campaign. This behaviour is most likely due to a problem of the JRC instrument since the ratios of the IMUK instrument to other instruments did not indicate such a behaviour (not shown here).

3 Development of a NDSC Spectroradiometer

azimuth dependencies. After the intercomparison a distinct azimuth dependence of the directional response of the JRC input optics was observed and confirmed both by rotating the input optics during solar measurements, as well as in the laboratory. The directional response varies by up to 6 to 7% with varying azimuth which explains most of the diurnal patterns, and especially the large deviations during the last days of the intercomparison.

In conclusion, this campaign was a first successful test for the IMUK spectroradiometer. The transport to the measuring site, which is always a risk, did not affect the instrument's performance. Compared to the others, the IMUK spectroradiometer was reasonably stable over the complete course of the campaign. The IMUK spectroradiometer measured up to 12% lower absolute irradiance values in comparison with the other stable instruments. This can only partly be explained by the differences of each group's calibration sources.

3.4.2 Ruthe Intercomparison

From 19 August to 1 September 2002 an intercomparison of spectral global solar irradiance measurements between spectroradiometers operated by the JRC and IMUK took place. The visit of the JRC instrument at the IMUK field site followed the previous intercomparison at ECUV in Ispra, Italy, and was also part of QASUME.

During this intercomparison campaign the stability of the IMUK spectroradiometer was found to be not satisfactory. Problems were detected by stability tests and quality control procedures performed during the campaign by the IMUK operator. At least once a day a 100 W halogen lamp was measured inside the portable field calibrator with the same wavelength steps and range as the solar spectra. On some occasions the lamp measurements deviated by more than 30%. On these days data could not be used for any analysis because it was impossible to decide whether the change in stability happened slowly or whether rapid step-like changes in stability occurred. The stability problem was especially pronounced when the instrument was "parked" to its initial position a few times in a row before taking a lamp scan and when the wavelength range and steps were altered. The reason for this behaviour was a defect turret drive of the gratings. The defect components have been replaced by the manufacturer.

Despite the above mentioned problems there were some periods of reliable measurements when the IMUK and JRC spectroradiometers could be compared. On these occasions the lamp measurements showed a reproducible behaviour of the IMUK spectroradiometer. In addition, the stability was cross-checked with SL501 measurements.

The results of the intercomparison of spectral global irradiance measured by the

3 Development of a NDSC Spectroradiometer

two instruments can be summarised as follows:

- Global irradiance measured by IMUK was between 5% lower and 2% higher than those measured by JRC on the three days when simultaneous measurements were performed.
- If measurements on 29 August are excluded, measurements of IMUK are 5% lower than JRC.
- The spectral shape of the global irradiance ratios between IMUK and JRC are spectrally flat to within 2% between 300 and 500 nm.
- The certificate of the primary standard of IMUK is 3% lower than the one used by JRC.

The conclusion drawn from both intercomparisons is that the IMUK and JRC spectroradiometer behaved the same way both times, which is a very good result.

3.4.3 5th North American Intercomparison for UV Spectroradiometers

The IMUK spectroradiometer as well as the NDSC spectroradiometer operated by the National Institute for Water and Atmospheric Research of New Zealand (NIWA) took part in the 5th North American UV Intercomparison for spectroradiometers, which was held from 13 to 21 June 2003 at Table Mountain, located 8 km north of Boulder, Colorado, USA. The campaign was organised by the Central UV Calibration Facility (CUCF) of the National Oceanic and Atmospheric Administration's (NOAA) Air Resources Laboratory. Additionally to IMUK and NIWA, the following agencies participated:

- BSI with their SUV-150 UV spectroradiometer,
- the University of Georgia's National UV Monitoring Center (EPA) with their Brewer MK IV spectroradiometer,
- the Atmospheric Sciences Research Center at the State University of New York (ASRC) with their United States Department of Agriculture (USDA) U111 spectroradiometer and with their Rotating Shadowband spectroradiometer (RSS).

The intercomparison was divided into two parts. During the first six days, all instruments measured spectral irradiance simultaneously in a blind intercomparison. On these blind days the spectral UV data was measured by each participant

3 Development of a NDSC Spectroradiometer

in a wavelength range from 290 to 360 nm in steps of 0.2 nm every half hour. The spectral irradiance was based on each participant's own calibration standard. Exchange of data or general information was permitted during these blind days to achieve an independent intercomparison of measured spectral UV irradiance. The second part comprised the intercomparison between the NDSC spectroradiometer operated by NIWA and the two instruments operated by BSI and IMUK. The BSI instrument was chosen in addition to the NDSC instrument from NIWA, because it is capable of measuring up to 600 nm. Further, this instrument is deployed in the Polar UV Net of the NSF, where stringent QC procedures and thorough maintenance of all instruments is exercised (BERNHARD et al., 2003). BSI and IMUK measured from 280 up to 600 nm, and NIWA from 285 to 450 nm. This was the first time to compare spectroradiometers up to 600 nm.

Six days six instruments

Figure 3.11 shows the diurnal cycle of the erythemal irradiance for 16 June 2003. The absolute value of erythemal irradiance is increasing according to a sinusoidal shape during the morning. In the afternoon, the decrease in incident radiation does not follow this form. Such a diurnal cycle implies a cloudless morning and a cloudy afternoon. Figure 3.12 shows the ratio of erythemal irradiance. The IMUK instrument is always in the denominator to have a direct comparison of each instrument to the IMUK one. The ratio between the EPA and IMUK instruments as well as between the BSI and the IMUK instruments are around unity. Deviations of up to 3% can be seen. The spectroradiometers from ASRC, USDA and NIWA detected the erythemal irradiance to be from 4 to 8% lower than the IMUK instrument. The variation in diurnal deviation is greatest between the EPA and IMUK spectroradiometers. It ranges from -6% in the morning at 11:00 UTC to +2% at midday (19:30 UTC).

The deviations to the other participating instruments, as shown in Figure 3.12, have a maximal value of 8%. This is well within the range of deviations obtained in previous international intercomparisons (BAIS et al., 2001; SECKMEYER et al., 2001; LANTZ et al., 2002). Even the uncertainty of spectral UV measurements with a high quality well maintained spectroradiometer is stated to be between 6.3% at 350 nm and 9.9% at 300 nm (SLAPER et al., 1995). Therefore, better agreements cannot be expected in an intercomparison of spectroradiometers.

3 Development of a NDSC Spectroradiometer

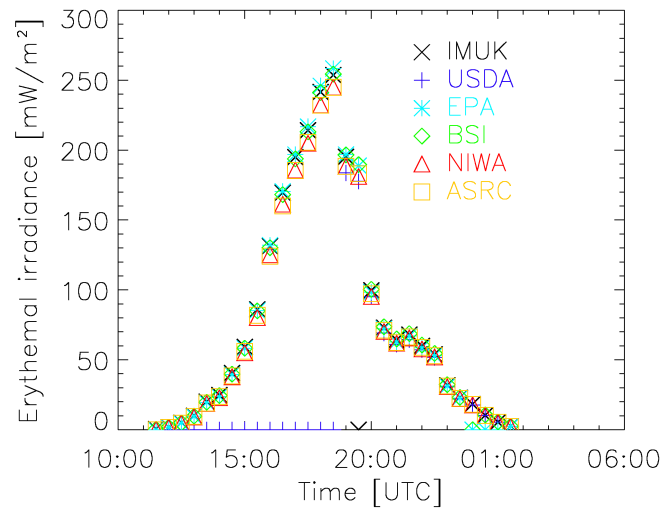


Figure 3.11: Diurnal cycle of erythemal irradiance for 16 June 2003 calculated from the spectral data of all participants. During the morning the sky was cloudless. The afternoon is disturbed by clouds.

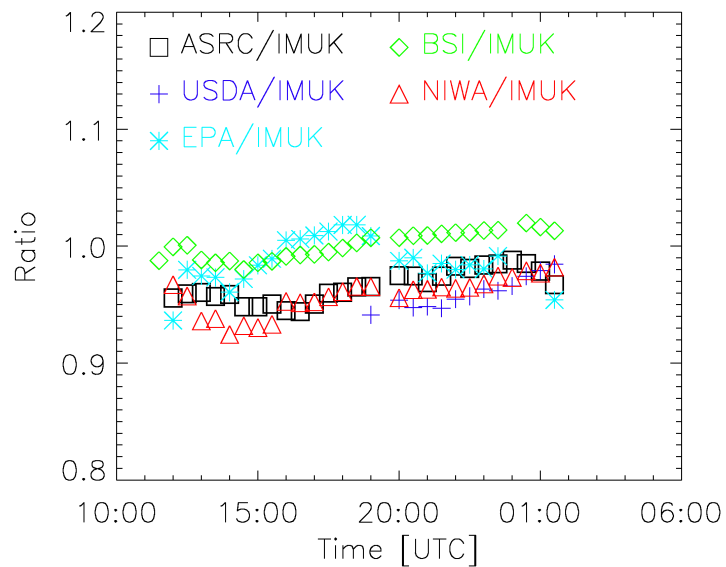


Figure 3.12: Ratios of erythemal irradiance over time for 16 June 2003. Values measured by the IMUK spectroradiometer are always in the denominator to easily compare each instrument to the IMUK one. The best agreement can be observed between the BSI and IMUK spectroradiometers with deviations of $\pm 2\%$ around unity.

3 Development of a NDSC Spectroradiometer

NDSC intercomparison

The intercomparison on 22 June 2003 between IMUK, BSI and NIWA served as a requirement in order for the IMUK and BSI instruments to be considered NDSC spectroradiometers. This day was nearly ideal, only few clouds were present during the afternoon.

For meaningful comparisons of single spectra, the spectral data have been convoluted with a triangular slit function of 1 nm FWHM. All spectra measured by BSI and NIWA were ratioed against spectra measured by IMUK. The ratio spectra at three different times of the day, including midday spectra, are illustrated in Figure 3.13.

For wavelengths between 295 nm and 315 nm all instruments agree to within $\pm 8\%$. In the UVB the deviation between BSI and IMUK is less than 5%. For wavelengths larger than 320 nm, the spectral irradiance measured by IMUK is about 4% lower compared to the BSI instrument. A step change of about 5% occurs at 500 nm, but the deviation between IMUK and BSI stays below 4% for wavelengths longer than 500 nm. At 500 nm the IMUK instrument changes detectors (from PMT to silica diode) and gratings (from 2400 to 1200 grooves per mm). Compared to the NIWA spectroradiometer a slight spectral dependence can be observed. At 298 nm the NIWA instrument measures 8% lower than the IMUK instrument. The ratio increases steadily with increasing wavelength. At 450 nm the irradiance of the NIWA instrument is about 2% higher than the one measured by IMUK.

To evaluate the complete day, ratios of different wavelengths over the course of the day are plotted in Figure 3.14 for BSI/IMUK (panel a) and NIWA/IMUK (panel b). Both ratios show some spectral dependence. All deviations are similar to those found during noontime. The spectral dependence is most pronounced between 16:00 and 21:30 UTC. The ratios at 300 nm are lowest with values of 0.97 for BSI/IMUK and 0.93 for NIWA/IMUK. The ratios increase with increasing wavelength up to 1.03 for BSI/IMUK and up to 1.02 for NIWA/IMUK at 440 nm. A few outliers can also be observed (e.g. at 21:30 UTC, 510 nm). The spectral irradiance measured by the IMUK spectroradiometer agrees generally better with the BSI instrument than with the NIWA instrument.

3 Development of a NDSC Spectroradiometer

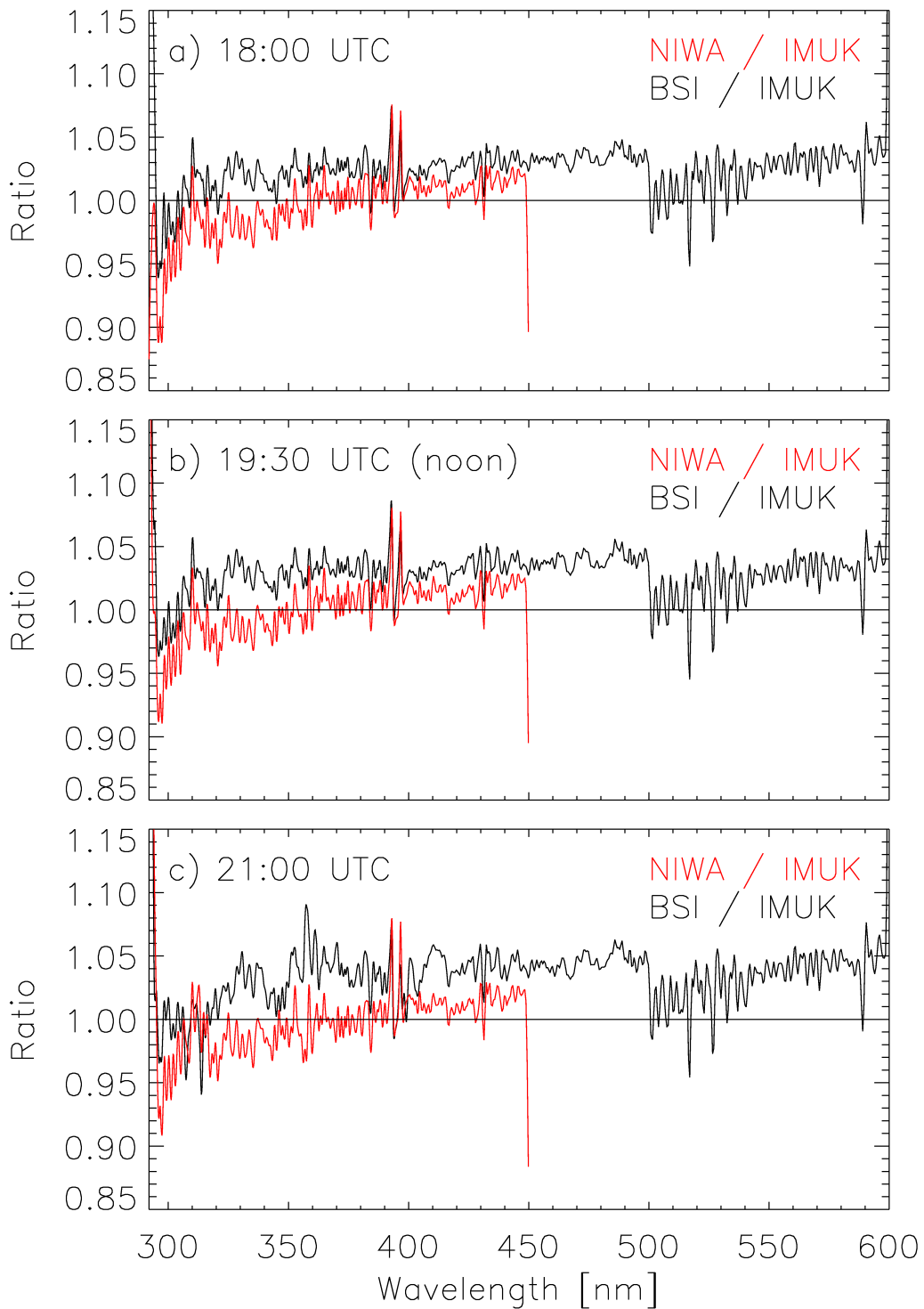


Figure 3.13: Spectral ratios NIWA/IMUK and BSI/IMUK for the noon spectrum (panel b) and 1.5 hours before (panel a) and after midday (panel c) on 22 June 2003. In the NIWA/IMUK ratios a slight spectral dependency is seen. The longer the wavelengths the larger the ratios.

3 Development of a NDSC Spectroradiometer

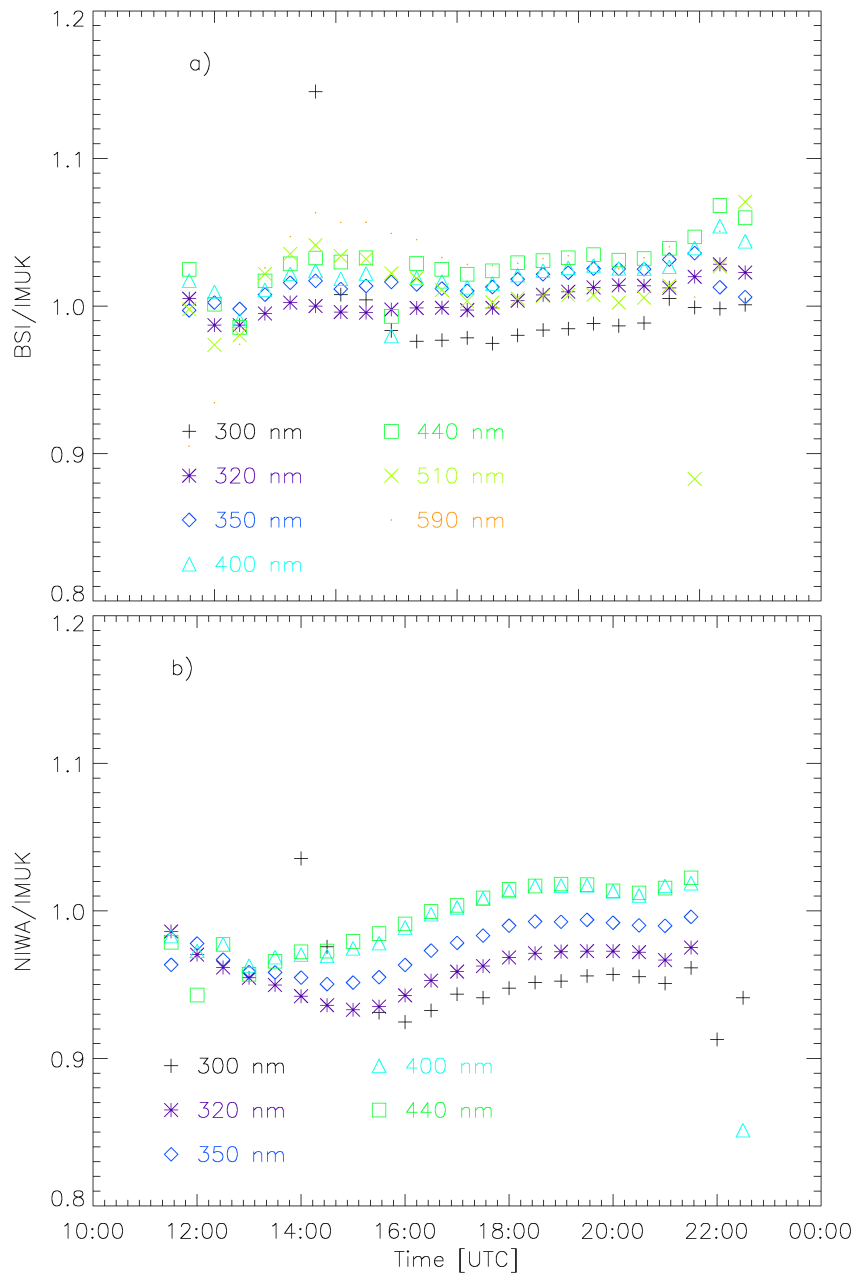


Figure 3.14: Diurnal cycle of ratios at different wavelengths on 22 June 2003. a) BSI/IMUK: The ratios range from 0.97 to 1.05. The smaller the wavelength the lower the ratio, especially between 16:00 and 21:30 UTC. b) NIWA/IMUK: The ratios range from 0.92 to 1.02. The smaller the wavelength the lower the ratio, especially between 16:00 and 21:30 UTC.

3.5 Compliance with NDSC Standards

As mentioned before, two requirements need to be complied with for a spectroradiometer to be recognised as an NDSC instrument:

1. Compliance with the NDSC standards (MCKENZIE et al., 1997), which are summarised in Table 3.1.
2. Successful participation in an intercomparison between a current NDSC instrument and the instrument applying for NDSC status.

The different specifications set up by the NDSC have been tested for the IMUK spectroradiometer (WUTTKE et al., 2004), and are also included in Table 3.1. Remarks to some of the specifications are given below.

Quantity	NDSC specification	IMUK	NIWA
Cosine response error	$< \pm 5\%$ to $< 60^\circ$ isotropic irradiance, and for all angles $< 60^\circ$ from the zenith	$< \pm 3\%$ to isotropic irradiance, and for all angles $< 60^\circ$ from the zenith	$< \pm 1\%$ to isotropic irradiance; $< \pm 3\%$ for all angles $< 70^\circ$ from the zenith
Minimum spectral range	$> 290-400$ nm	290-1050 nm (capable of 250-1050 nm)	285-450 nm
Band width (FWHM)	< 1 nm	0.54 nm at 253.65 nm	0.75 nm at 296 nm
Wavelength alignment	$< \pm 0.03$ nm (precision) $< \pm 0.05$ nm (absolute accuracy)	$< \pm 0.03$ nm (precision) $< \pm 0.05$ nm (absolute accuracy)	$< \pm 0.02$ nm (precision) $< \pm 0.04$ nm (absolute accuracy)
Slit function	$< 10^{-3}$ of max $2.5 \cdot \text{FWHM}$ from line centre $< 10^{-5}$ of max $6.0 \cdot \text{FWHM}$ from line centre	At least $1.76 \cdot 10^{-3}$ of max $2.5 \cdot \text{FWHM}$ from line centre, and likely better	$< 10^{-4}$ of max $2.5 \cdot \text{FWHM}$ from line centre
Sampling step interval	$< 0.5 \cdot \text{FWHM}$	0.25 nm (290-500 nm); 1 nm (500-1000 nm)	0.2 nm
Saturation threshold	$> 1.5 \text{ Wm}^{-2}\text{nm}^{-1}$ (noon max 400 nm)	$> 1.8 \text{ Wm}^{-2}\text{nm}^{-1}$ (noon max 400 nm)	$> 2.0 \text{ Wm}^{-2}\text{nm}^{-1}$ (noon max at 450 nm)

3 Development of a NDSC Spectroradiometer

Quantity	NDSC specification	IMUK	NIWA
Detection threshold	$< 10^{-6} \text{ Wm}^{-2}\text{nm}^{-1}$ (for S/N = 1 at 1 nm FWHM)	$9 \cdot 10^{-7} \text{ Wm}^{-2}\text{nm}^{-1}$ (for S/N = 1 at 1 nm FWHM)	$< 10^{-6} \text{ Wm}^{-2}\text{nm}^{-1}$ (for S/N = 1)
Scan time	< 10 min	Typical 9 min 30 sec (290-400 nm); 33 min (290-1050 nm)	4.5 min (285 to 450 nm). A full measurement usually consists of a reverse scan + forward scan
Overall calibration accuracy	< 5% (unless limited by threshold)	$\pm 4.6\%$	$\pm 5\%$
Stray light	As defined by the detection threshold	Only noise below the detection threshold	Only noise below the detection threshold
Temperature	Monitored, & with stability sufficient to maintain overall stability (typical T-stability $< \pm 2 \text{ K}$)	Stabilised and monitored (T-stability $< \pm 1 \text{ K}$)	$29.0 \pm 0.5 \text{ C}$, Stabilised and monitored
Scan date and time	Recorded with each spectrum (so that timing is known to within $\pm 10 \text{ s}$ at each wavelength)	Date: recorded with each scan; Time: Recorded at each wavelength; time-base: GPS	In-built GPS for accurate timing, recorded with each spectrum
Diffuse/direct measurements	Capability of distinguishing each component	Diffuse measurements possible with shading disk positioned manually	Diffuse measurements possible with shading disk positioned manually

Table 3.1: NDSC specifications for UV spectroradiometry. The specifications are given in terms of final data quality desired (MCKENZIE et al., 1997).

Cosine Error: The cosine error of the IMUK spectroradiometer is shown in Figure 3.2. The cosine error of the NIWA spectroradiometer was determined at azimuth angles of 0° , 90° , 180° , and 270° at 400 nm. The values stated in Table 3.1 are an average of these measurements.

Bandwidth (FWHM) and Slit Function: The slit function of the IMUK instrument is shown in Figure 3.6. The slit function of the NIWA instrument is

3 Development of a NDSC Spectroradiometer

also based on scans of a mercury line, but at 296.73 nm. Both are mirrored at the centre wavelength. Figure 3.15 shows the slit functions of both spectroradiometers, but on a logarithmic scale to easily estimate the orders of magnitude. The slit function of BSI is also shown to demonstrate the difference when a laser is used as a line source. The values of the FWHM are adjustable for both instruments if necessary.

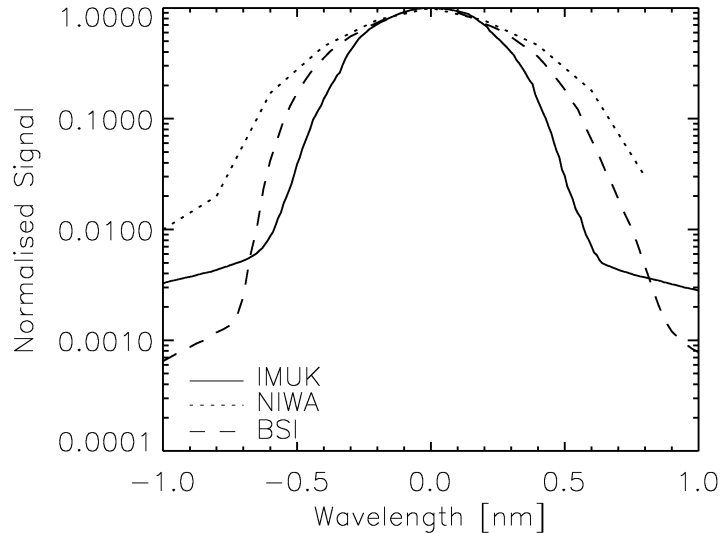


Figure 3.15: Normalised mean slit function of the IMUK, NIWA, and BSI spectroradiometers. They are shown on a logarithmic scale to easily estimate the orders of magnitude. The slit function of BSI is the only one determined by measuring a laser.

Saturation Threshold: $1.8 \text{ Wm}^{-2}\text{nm}^{-1}$ is the maximum spectral irradiance observed during the Boulder campaign. Comparisons with model results and between the instruments of NIWA and IMUK indicate that none of the systems is saturated at this radiation level.

Stray Light: Only noise is detected by the IMUK and NIWA spectroradiometers when sky irradiance is measured at wavelengths below 285 nm, indicating that stray light levels are below the detection limit.

3.5.1 Assessment of Complying with NDSC Specifications

The IMUK spectroradiometer complies with all specifications set up by the NDSC with the exception of the slit function criterion, which could not be validated with sufficient accuracy. This criterion requires that the slit function is smaller

3 Development of a NDSC Spectroradiometer

than 10^{-3} of its maximum at $2.5 \cdot \text{FWHM}$ (i.e. 1.35 nm) away from the centre. Measurements based on the 253.65 nm mercury line indicate that the slit function is at least $1.76 \cdot 10^{-3}$ at the specified distance. The actual value is likely smaller, but this could not be proven since the emission continuum of the mercury lamp limits the measurement to about 2.5 orders of magnitude. A more accurate measurement would have required a laser, which was not available.

3.5.2 Assessment of NDSC Intercomparison

Spectral measurements performed by the IMUK spectroradiometer on 22 June 2003 agree well with results from the NDSC spectroradiometer operated by NIWA. Deviations in the UVA and visible are smaller than $\pm 5\%$. Differences in the UVB are smaller than $\pm 8\%$. Considering the low absolute irradiance levels and the strong increase of the solar spectrum in the UVB, deviations of 8% are still acceptable. Small differences in absolute irradiance levels and small wavelength shifts between the instruments are likely responsible for the somewhat larger deviation at shorter wavelengths. The ratio NIWA/IMUK exhibits a small (i.e. 5% between 320 and 450 nm) wavelength dependence for unknown reasons. The outliers observed in Figure 3.14 (e.g. at 21:30 UTC, 510 nm) may be due to synchronisation problems during cloudy periods in the afternoon. However these deviations are within the stated uncertainties (BERNHARD and SECKMEYER, 1999; BAIS et al., 2001) of UV spectroradiometry. It should be noted that none of the instruments distinguish between direct and diffuse measurements yet. However, all instruments are able to measure diffuse irradiance with manually located shading disks. In conclusion, the IMUK instrument complies with the standards for NDSC spectroradiometers to measure UV radiation (WUTTKE et al., 2004).

4 Antarctic Campaign - Methods

Antarctic measurements have been performed in the context of the project "Characterisation of the specific solar radiation conditions in polar regions with respect to climate change and ozone depletion" (CASE) funded by the *Deutsche Forschungsgemeinschaft* (DFG). One of the aims of CASE was to conduct measurements of various radiation quantities in an Antarctic environment. Such a goal may seem technical for a scientific project, but conducting measurements in Antarctica is not comparable to campaigns elsewhere. Despite the technical achievements of the last decades and centuries, Antarctica remains one of the least accessible regions on Earth. Compared to campaigns in the "civilised" world, an Antarctic campaign has to be planned and prepared with much more attention. Logistic demands are almost excessive. For example, transporting the equipment takes at least two months one way. Instrument specific spare parts are not available. Testing the instruments' performance in advance in such adverse weather conditions as encountered in Antarctica is nearly impossible.

In this chapter, the instruments deployed as well as the strategy to measure the different radiation parameters are presented.

4.1 Measurements at Neumayer

Measurements of various spectral radiation parameters have been performed at the German Antarctic Neumayer Station, which is situated on the Ekström Ice Shelf on the Weddell Sea at 70° 39 'S, 8° 15' W during the austral summer 2003/04. The location is shown on the map in Figure 4.1.

Neumayer is a favourable site to conduct radiation measurements. The main part of the station is underneath the snow surface. Only during the summer campaign, a few containers are set up on the station area to accommodate additional scientific and technical staff. Thus, obstructions of the measurements due to large buildings is minimised (see Figure 4.2). Since Neumayer is located on an ice shelf, the surrounding surface is very homogeneous representing a flat snow covered surface. Atka Bay is covered by sea ice most of the year.

4 Antarctic Campaign - Methods

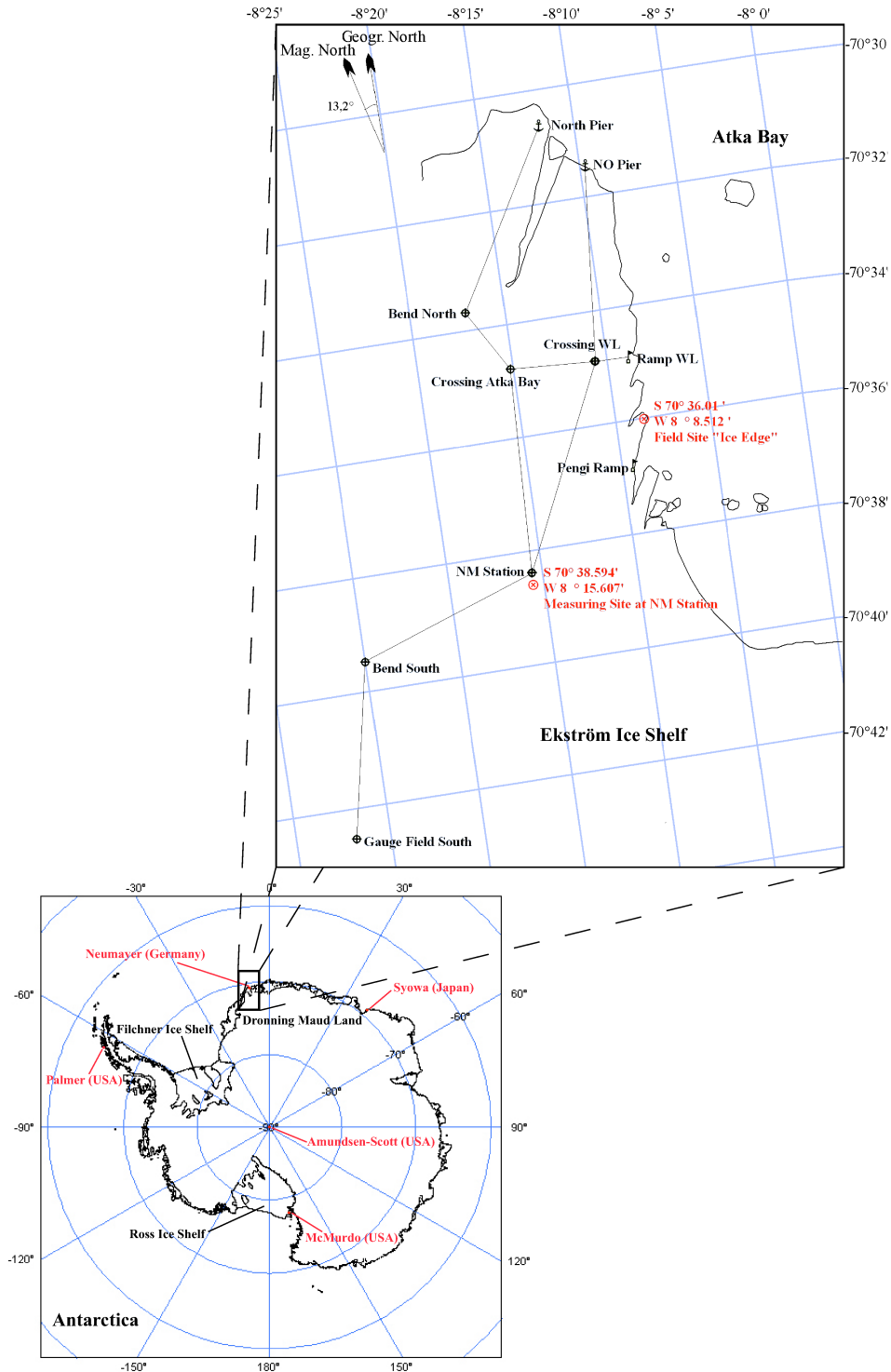


Figure 4.1: Map of Antarctica showing the spectral UV monitoring stations. An enlargement of the surroundings of Neumayer is also provided. The measurements have mainly been conducted at the measuring site at Neumayer (NM) Station. Only albedo measurements with the SL501 have been performed at the field site "Ice Edge" [courtesy Ulf Müller].

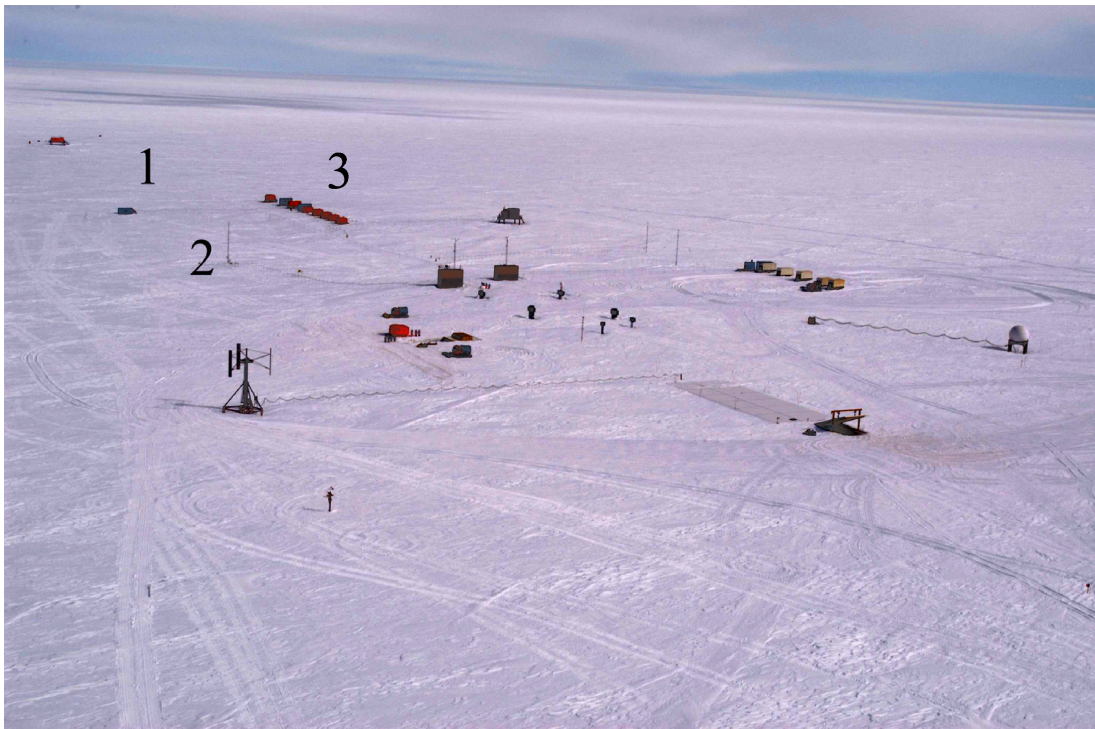


Figure 4.2: Neumayer Station photographed from an airplane during the summer season 2003/04. (1) Container with IMUK instruments. (2) AWI meteorological field site. (3) Summer camp [courtesy Johannes Käßbohrer].

4 Antarctic Campaign - Methods

For protection against the harsh weather conditions in Antarctica, the instruments to measure solar radiation were located inside a 20'-container, which was kindly provided by the Alfred Wegener Institute for Polar and Marine Research (AWI; see Figure 4.3). It was set up about 100 m east of the summer camp and 200 m south of the AWI meteorological field site. The container was heated to guarantee a temperature above +5°C at all times for the instruments and PCs inside this container to operate reliably.

Spectral irradiance and sky luminance, as well as the broadband erythemal and global irradiance, have been measured throughout the summer campaign in any type of weather conditions. These measurements are run automatically. Spectral radiance and albedo measurements have been conducted for cloudless cases or overcast situations. The rationale for deciding upon the periods of measurements for the four main radiation parameters is given in the following list.

Spectral irradiance: The IMUK spectroradiometer has been successfully compared to international recognised spectroradiometers for a variety of weather conditions (see Section 3.4). Thus, a reliable performance not only for cloudless situations is proven. Further, it is meaningful to conduct spectral irradiance measurements as often as possible to connect spectral irradiance sampled at Neumayer with spectral irradiance measured at other Antarctic stations, in particular the NSF sites.

Albedo: Since spectral surface albedo is measured with only one radiation sensor (see Section 4.3), it could only be determined for stable cloud conditions. Thus, surface albedo measurements have been performed during cloudless cases or situations with a stratiform cloud cover.

Luminance: It was planned to use the luminance measurements as an indication of the cloud situation to interpret the spectral irradiance measurements. Therefore, luminance had to be measured as often as possible.

Spectral radiance: The decision about the periods of spectral radiance measurements have been based on model calculations performed prior to the campaign. The viewing direction opposite the sun (solar azimuth angle + 180°) has been found to be most interesting because the variation of radiance for different viewing zenith angles (VZA) was maximal during cloud free cases. Cloudless situations have been also favoured due to the planned model evaluation. To account for the influence of cloud cover, zenith radiance has been measured for both, overcast and cloudless sky.

A summary of the radiation parameters measured during the campaign at Neumayer is given in Table 4.1. The instruments deployed are also given. In the following sections, the performance of the spectroradiometer over the duration



Figure 4.3: Container for radiation measurements during the summer campaign 2003/04. On the left, the Skyscanner (1) is mounted. The metal tube (2) on the right part of the roof holds the input optics for spectral irradiance measurements.

of the campaign is presented in the context of spectral irradiance measurements. Furthermore, the methods to acquire surface albedo, luminance, spectral radiance, and the most important ancillary parameters are addressed.

4.2 Spectral Irradiance

Spectral irradiance measurements have been performed in a wavelength range from 280 to 500 nm in steps of 0.25 nm and 501 to 1050 nm in steps of 1 nm. Spectra have been recorded 24 hours per day. It takes about 35 minutes to record a spectrum of irradiance in these wavelength steps, this amounts to about 42 spectra per day. To guarantee a reliable quality of the spectral data the QC procedures described in Section 3.3 have been followed on a regular schedule. The most important tasks include checks of the radiometric and wavelength stability.

4.2.1 Radiometric Stability during Irradiance Measurements

100 W quartz halogen lamps are deployed inside a portable field calibrator (see Figure 3.8) in order to obtain knowledge about the radiometric stability over time. During the CASE campaign, stability checks have been conducted daily. The stability time series are shown in Figure 4.4.

Two different time series are illustrated; one shows the stability for the PMT, the

4 Antarctic Campaign - Methods

Parameter	Instrument	Amount of data
Spectral irradiance	Spectroradiometer with cosine diffuser	2725 spectra on 86 days
Spectral albedo	Spectroradiometer with cosine diffuser	1026 spectra of up- and downwelling irradiance on 12 days
Broadband UV albedo	SL501	5-minute means on 15 days
Luminance	Skyscanner	Collected every minute on 88 days
Spectral radiance	Spectroradiometer with Skyscanner	336 spectra on 20 days
Erythematol irradiance	SL501	1-minute means on 90 days
Global irradiance	Pyranometer	1-minute means on 100 days
Total ozone column	Microtops Sun Photometer	119 total ozone columns on 37 days

Table 4.1: Summary of the radiation data collected during the Antarctic campaign at Neumayer in the austral summer 2003/04.

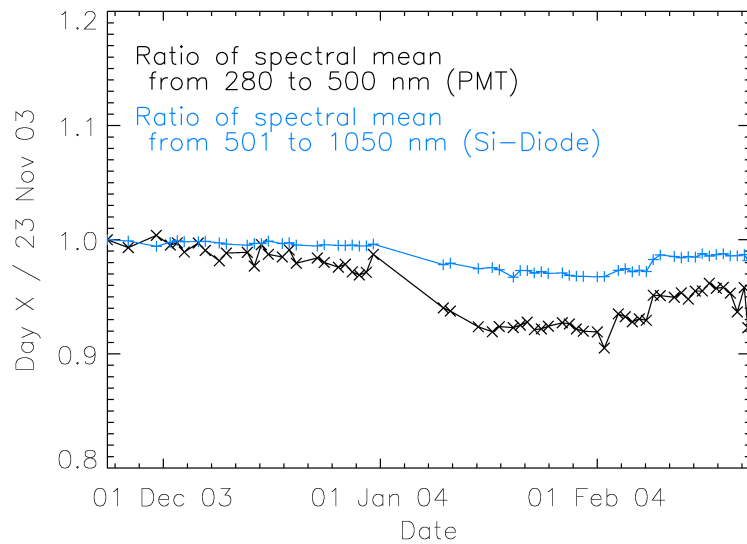


Figure 4.4: Stability of the spectroradiometer over the duration of the campaign with the irradiance entrance optics as sensor. The 100 W lamp measurements of each day have been divided by the ones on 23 Nov 03.

4 Antarctic Campaign - Methods

second depicts the stability for the silica diode. They are shown separately for each detector, because each one can behave differently over time. Lamp measurements have been related to the first day of lamp measurements within the campaign. It can be seen in Figure 4.4 that the silica diode shows a more stable performance than the PMT. The spectroradiometric system is stable to within 2% considering the silica diode. The change in responsivity considering the PMT is larger with 9%. For both detectors, the responsivity decreases over time. To account for this loss, the each day's lamp measurements are considered for the absolute calibration of spectral irradiance (see Section 3.2.6). No stability checks have been performed during the first ten days of January 2004 because albedo measurements have been performed with the entrance optics mounted to the metal rods (see Section 4.3). This prevented the use of the portable field calibrator.

4.2.2 Wavelength Stability during Irradiance Measurements

During the campaign, the wavelength shift is monitored daily by applying the algorithm SHICrvm (SLAPER et al., 1995) to the spectral irradiance data. The wavelength shift of the spectroradiometer on three days as well as the mean shift on these days is shown in Figures 4.5 and 4.6.

The wavelength shift varies over the course of the day with 0.03 nm. The absolute shift for all wavelengths is 0.05 nm from the nominal wavelength. The shape of the wavelength shift shows a periodic structure. This structure does not change over the complete course of the campaign. In the lower panel of Figure 4.6 the mean wavelength shift for 8 Dec 2003, 13 Jan and 20 Feb 2004 is shown, indicating no significant change in the spectroradiometer's wavelength alignment over time.

4 Antarctic Campaign - Methods

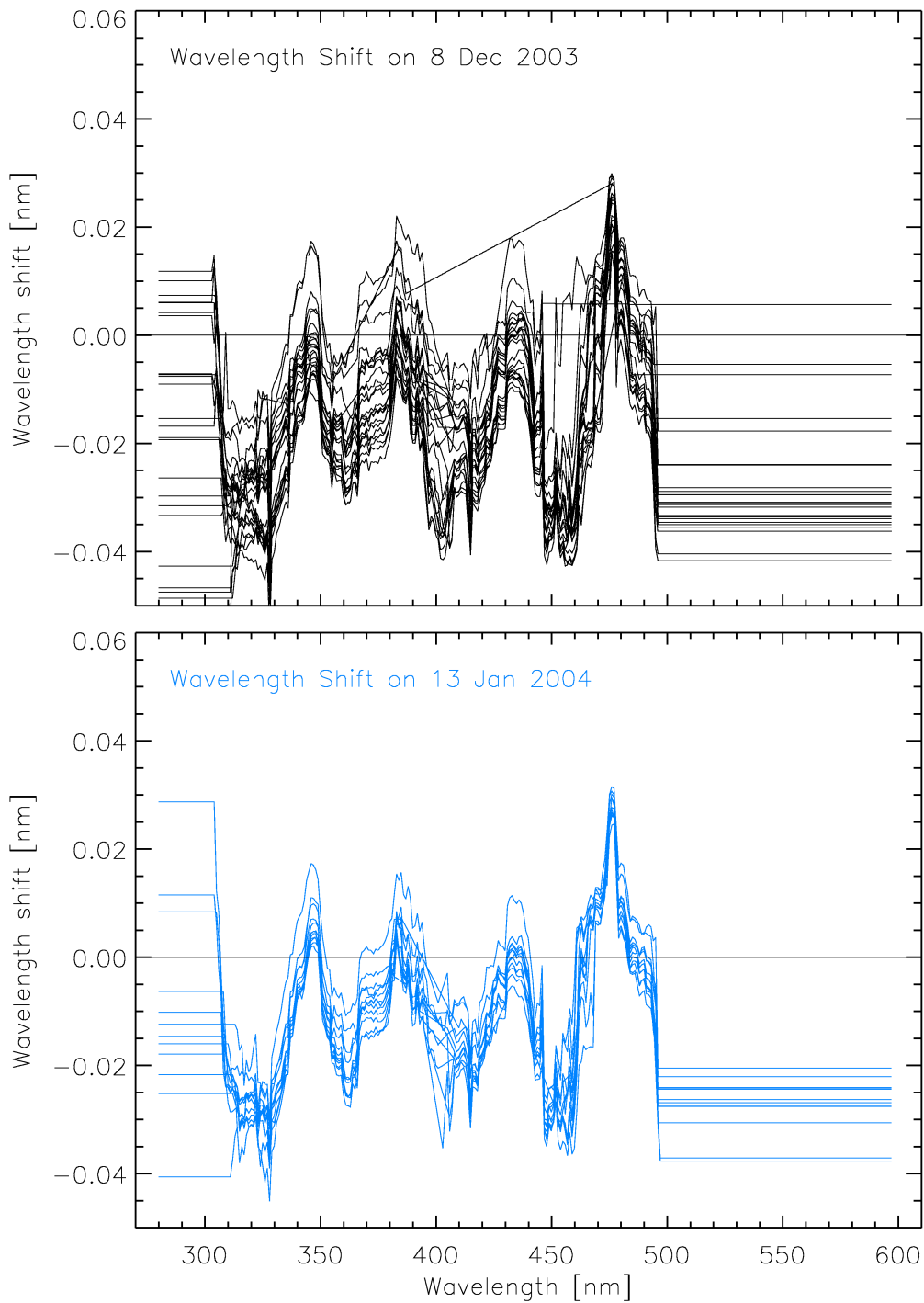


Figure 4.5: Wavelength shift of the IMUK spectroradiometer on 8 Dec 2003 (upper panel) and 13 Jan 2004 (lower panel). Each line represents the spectral wavelength shift for one measured spectrum of solar irradiance. The shift varies over the day due to a slight change in temperature inside the temperature stabilised box.

4 Antarctic Campaign - Methods

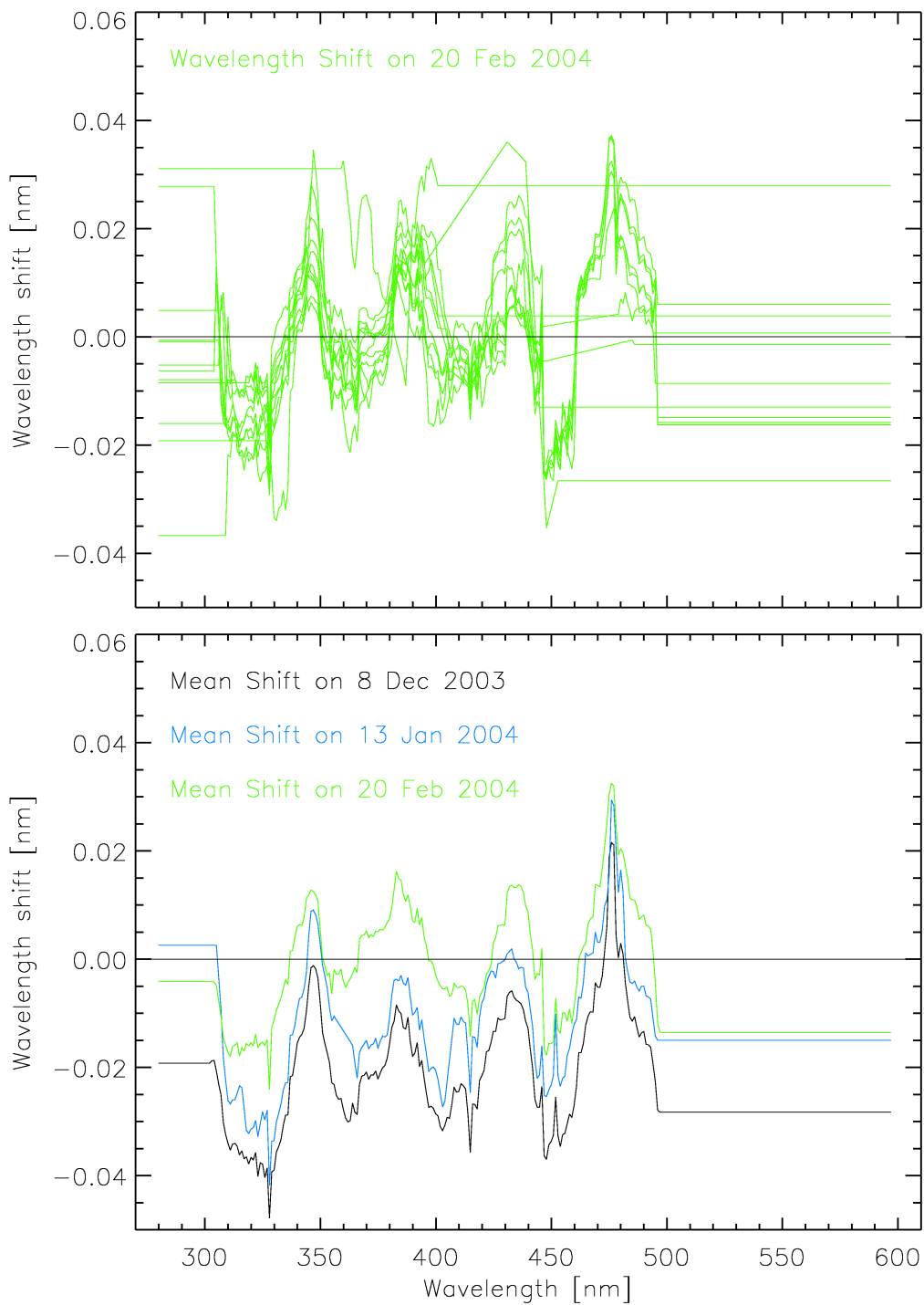


Figure 4.6: Upper panel: Wavelength shift of the IMUK spectroradiometer on 20 Feb 2004. Each line represents the spectral wavelength shift for one measured spectrum of solar irradiance. The shift varies over the day due to a slight change in temperature inside the temperature stabilised box. Lower panel: Mean wavelength shift for three days. The wavelength shift does not change its spectral behaviour and remains between -0.05 and 0.04 nm over the duration of the campaign.

4.3 Albedo

Surface albedo measurements have been performed at two sites (Figure 4.1). Directly at the station, albedo has been measured with the spectroradiometer in a wavelength range from 280 to 1050 nm as well as with the SL501. At the ice edge about 6.2 km away from the station, albedo measurements have been conducted only with the SL501. At both sites, albedo measurements have been performed over a field of natural undisturbed snow. The set-up of the albedo measurements at the ice edge is depicted in Figure 4.7.

According to SECKMEYER et al. (2001) albedo should be measured with two radiometers with cosine-weighted field of view in about 2 to 4 m height above the ground. The entrance optics employed to measure albedo during the Antarctic campaign is optimised for its cosine response, thus accounting for most part of the cosine error (see Figure 3.2). To be able to detect up- as well as downwelling radiation the sensors have been fixed to a rotatable rod, which was attached to a supporting frame roughly 2 m above the ground. The method of turning a radiation sensor has been applied previously, for example, by FEISTER and GREWE (1995) or BLUMTHALER and AMBACH (1988). The collected light is led into the monochromator through an optical fibre. Due to the limited length of the optical fibre, the temperature stabilised box containing the spectroradiometer was set up only 2 m away from the footprint of the entrance optics. Thus, a shadowing effect of the box needs to be accounted for. The supporting frame is white to minimise the difference in reflectivity between the white snow surface and the supporting frame.

During the spectral albedo measurements, the SL501 was additionally mounted on the rod. While the cosine diffuser faced upwards, the SL501 measured reflected radiation. This way, the albedo could be determined independently with two different types of sensors.

4.3.1 Measuring Spectral Albedo

Albedo spectra have been collected either during cloudless or overcast sky conditions. This way it is assured that the atmospheric conditions are sufficiently stable in order to measure subsequent spectra of reflected and incident irradiance. The two most important influencing factors are the change in *SZA* and the presence of clouds. Also the length of the spectra recorded for the calculation of albedo has to be considered. The cosine diffuser was turned roughly every ten minutes. The time needed to scan each spectrum depends on the spectral range and step width. Four different data collection protocols concerning wavelength range and step have been developed and applied.



Figure 4.7: Photograph of albedo measurements performed at the ice edge. The SL501 is currently measuring incident radiation. The supporting frames of the equipment is painted white to minimise the shadowing effect.

1. From 290 to 400 nm in steps of 0.25 nm; 1 January 2004: This range and step width has been chosen to be able to calculate erythemal irradiance from the spectral data. Thus, the albedo measured with the SL501 can be compared to the one derived from the spectral measurements. Reflected and incident irradiance have been recorded alternately because the scan time of one spectrum amounted to 9 minutes.
2. From 304 to 306 nm, 319 to 321 nm, 349 to 351 nm, 399 to 401 nm, 498 to 500 nm in steps of 0.25 nm; 694 to 699 nm, 796 to 804 nm, 996 to 1004 nm in steps of 1 nm; 2 to 4 January 2004: Choosing these wavelength steps, different wavelength regions could be covered with the routine wavelength step of 0.25 or 1 nm. It took only 4 minutes to measure a spectrum with these wavelength steps. Therefore, two spectra of incident irradiance were measured in a row before two spectra of reflected irradiance were recorded.
3. From 300 to 310 nm, 315 to 325 nm, 345 to 355 nm, 395 to 405 nm, 490 to 500 nm in steps of 0.25 nm; 540 to 590 nm, 670 to 720 nm, 775 to 825 nm, 975 to 1025 nm in steps of 1 nm; 5 January 2004: One spectrum takes ten minutes to record so that reflected and incoming irradiance are measured in an alternating order. These short wavelength intervals are chosen to cover different spectral regions with the same spectral resolution as irradiance

4 Antarctic Campaign - Methods

and radiance measurements.

4. From 290 to 1050 nm in steps of 2 nm; 6 and 8 January 2004: The complete spectrum is covered in equidistant wavelength steps. Spectra of incident and reflected radiation have been measured alternately.

To account for the difference in SZA when measuring the reflected and downwelling spectrum a correction factor was calculated with the help of the freely available radiative transfer model UVSPEC contained in the libRadtran package (<http://www.libradtran.org>; MAYER et al., 1997). For each measured spectrum (downwelling or reflected) a spectrum of downwelling irradiance was modelled with a radiative transfer solver applying the discrete ordinate method developed by STAMNES et al. (1988) for wavelengths lower than 500 nm. For wavelengths larger than 500 nm the radiative transfer equation is solved according to pseudo-spectral calculations with a molecular absorption parameterisation adopted from RICCHIAZZI et al. (1998). The atmosphere was considered aerosol free. Ozone column was taken from the Total Ozone Mapping Spectrometer (TOMS) data which is available on the internet (http://toms.gsfc.nasa.gov/ep_toms/ep_ovplist_1.html). A homogeneous cloud layer has been included when applicable. A surface albedo of 0.99 is used as input. To verify that the correction factor does not depend on the input albedo, spectral irradiance was modelled with an input albedo of 0.92 in addition. All other input parameters remained constant. The ratio between the model spectrum with an input albedo of 0.99 and 0.92 is shown in Figure 4.8 for one example day. For all SZA occurring on a summer day at the location of Neumayer the ratio between spectra with an albedo of 0.99 and 0.92 is unity. The deviation of up to 1% is seen between spectra including clouds and cloud free sky spectra. Thus, it is important to include stratiform clouds in the model spectra to calculate the correction factor when applicable. The effect of the variable input albedo with unchanging cloud cover is zero. Thus, an albedo of 0.99 can be used as input parameter.

To calculate the correction factor K , two consecutively modelled spectra of irradiance are divided by each other:

$$K = \frac{E_{MODE}}{E_{MODR}} . \quad (4.1)$$

E_{MODE} is the spectrum modelled with the SZA according to the measured downwelling spectrum of irradiance. E_{MODR} is the spectrum with the SZA according to the following measured reflected spectrum. In all modelled spectra, a wavelength dependent SZA has been used to account for the change in SZA during the period of recording a spectrum.

The measured spectrum of downwelling irradiance is then divided by the correction factor K :

$$E_{MESK} = \frac{E_{MES}}{K} \quad . \quad (4.2)$$

E_{MES} is the measured spectrum of downwelling irradiance. E_{MESK} is the spectrum corrected for SZA at the time of recording the following reflected spectrum.

The temperature stabilised box of the spectroradiometer as well as the metal rods, which hold the radiation sensors, are in the field of view of the sensors when measuring reflected radiation. Thus, they cause a shadowing effect which has to be accounted for when calculating the albedo. The equipment covers 3% of the cosine diffuser's field of view when directed downwards. Thus, the reflected radiation R_{MES} would be underestimated by 3% if the box had a reflectance of zero. The box is made of aluminium. The reflectance of sand-blasted aluminium is about 0.45 (KÖNIG and ADEN, 1999). It has a slight spectral dependence. It is 0.43 at 300 nm, and slightly increasing for longer wavelengths. Taking the mean reflectance value of 0.45 the reflected irradiance is only underestimated by 1.65%, leading to an underestimation in albedo by the same amount. The reflected irradiance corrected for the shadowing effect R_{MESK} is calculated according to

$$R_{MESK} = R_{MES} + R_{MES} \cdot 0.0165 \quad . \quad (4.3)$$

Now the albedo a_K , taking into account the change in SZA and the shadowing effect, can be calculated with the downwelling irradiance corrected for SZA E_{MESK} and the measured reflected irradiance corrected for the shadowing effect R_{MESK} :

$$a_K = \frac{R_{MESK}}{E_{MESK}} \quad . \quad (4.4)$$

The spectral dependence of the albedo is not included in Equations 4.1 to 4.4. The spectral albedo a_λ is defined in this study by referring both, R_{MESK} and E_{MESK} , to wavelength (see Equation 2.7):

$$a_\lambda = \frac{R_{MESK,\lambda}}{E_{MESK,\lambda}} \quad . \quad (4.5)$$

The spectral albedo presented in Chapter 5 is determined according to Equation 4.5. The method of correcting for the shadowing effect is further discussed in Chapter 6.

4.3.2 Measuring Broadband UV Albedo

The albedo measured with the SL501 is also corrected for the effect of changing SZA and the shadowing effect and determined according to Equation 4.4. A value

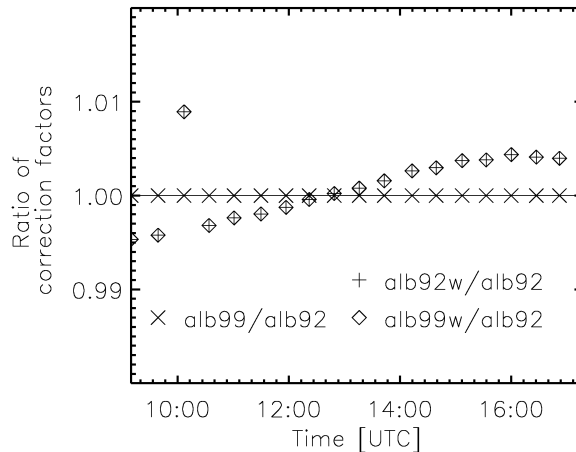


Figure 4.8: Ratios of correction factors modelled with different input albedos for an example day. The ratios do not deviate for the same cloud conditions. A deviation of 1% can be observed between cloudy and cloud free conditions. The reason for the outlier at 10:00 UTC has not been found so far. The abbreviations used in the legend represent the type of albedo and cloud input parameter for UVSPEC: alb92: albedo 0.92, no clouds; alb99: albedo 0.99, no clouds; alb92w: albedo 0.92, stratiform cloud cover; alb99w: albedo 0.99, stratiform cloud cover.

of erythemal irradiances is stored every minute by the data logger that belongs to the SL501. The sensor is rotated every 10 minutes. An 8-minute mean value of erythemal irradiance has been calculated in order to determine the albedo. The first and last recorded value has been neglected to be sure that the act of turning the rod is not affecting the calculated albedo. The broadband UV albedo has been calculated according to Equation 4.4, with R_{MESK} and E_{MESK} describing the 8-minute means of reflected and incident erythemal irradiance, respectively.

4.4 Luminance

Sky luminance (see Equation 2.12) is detected with the Skyscanner during all types of weather conditions. Only during spectral radiance measurements luminance could not be detected because the Skyscanner was employed to point the radiance entrance optics to the desired direction.

The response of the luminance sensor $s(\lambda)$ is close to the response of the human eye ($V(\lambda)$). Both responses, $s(\lambda)$ and $V(\lambda)$, are shown in Figure 4.9. Figure 4.10 depicts the ratio between $s(\lambda)$ and $V(\lambda)$. The limited wavelength range from 420 to 750 nm is plotted as well, because the deviation below 420 nm exceeds 40%.

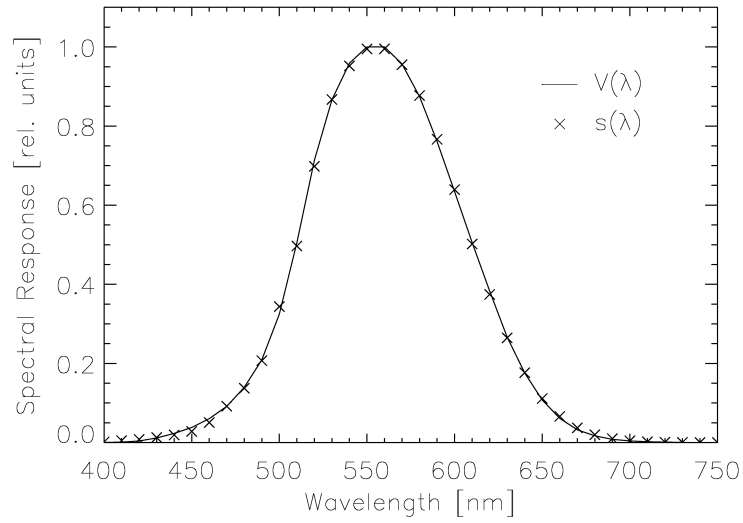


Figure 4.9: The response of the luminance sensor $s(\lambda)$ and the response function of the human eye $V(\lambda)$ are shown. Deviations can only be seen around 450 nm where the response is low anyway.

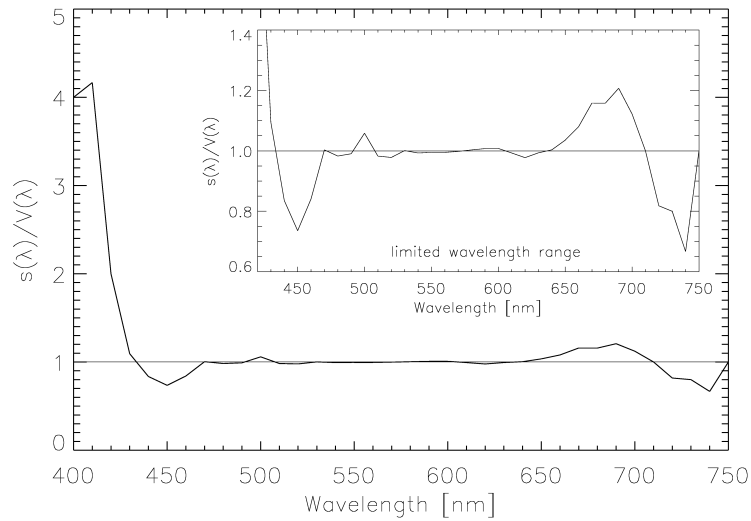


Figure 4.10: Ratio of the response of the luminance sensor $s(\lambda)$ to the response of the human eye $V(\lambda)$. As the deviation exceeds 40% below 420 nm a limited wavelength range is also shown.

The Skyscanner was specifically developed to be deployed in harsh climates. 150 points evenly distributed in the sky are scanned to measure the sky luminance distribution. Such a scan of the complete sky takes about 40 seconds and is performed every minute. During one scan, the zenith luminance is measured six times for quality control as it is expected to stay constant during one scan. For each zenith measurement the azimuth position of the detector is different. Fast moving clouds, for example, can cause a deviation in zenith luminance even within the short period of one scan. Improper levelling of the Skyscanner is another reason for varying zenith luminance. In this case, the zenith is missed in each of the six zenith measurements and each time a different spot of the sky is measured. Therefore, it is recommended to check the spirit level of the Skyscanner daily.

4.5 Spectral Radiance

Spectral radiance has been collected in the wavelength range from 280 to 1050 nm under a cloudless sky or stratiform cloud cover. Two different data collection protocols have been developed and applied:

1. Zenithal scans of radiance have been performed in limited wavelength regions. A zenithal scan is always performed with a constant viewing azimuth angle (VAA) and varying viewing zenith angles (VZA). In most cases, radiance was detected from the zenith to the horizon in steps of 10° . The preferred VAA was opposite the sun ($SAA + 180^\circ$), thus in the backward scattering part of the principal plane. The principal plane denotes the plane of the azimuth of the sun, passing through the zenith and back down to the horizon at $SAA + 180^\circ$. Only limited wavelength regions have been chosen in order to minimise the scan time for one spectrum. To account for various spectral ranges the following wavelength intervals have been sampled: 304 to 306 nm (UVB), 319 to 321 nm (boundary between UVB and UVA), 349 to 350 nm (UVA), 399 to 401 nm (boundary between UVA and visible), and 498 to 499 nm (visible with PMT) in steps of 0.25 nm; 691 to 699 nm (visible with silica diode), 796 to 804 nm (boundary between visible and IR), and 996 to 1004 nm (IR) in steps of 1 nm.
2. Zenith radiance has been measured in the same wavelength range and step width as spectral irradiance, hence from 280 to 500 nm in steps of 0.25 nm and from 501 to 1050 nm in steps of 1 nm.

Due to the design of the IMUK spectroradiometer, it is only possible to measure one spectral parameter at once. Therefore, spectral irradiance measurements cannot be performed simultaneously. It is also impossible to perform luminance

measurements at the same time because of the fast movements performed during one scan of luminance distribution. For the detection of radiance the Skyscanner is employed to point the entrance optics at particular positions in the sky as can be seen in Figure 4.11. The FOV of the radiance input optics is described in Section 3.2.2.

4.5.1 Radiometric Stability during Radiance Measurements

During the campaign, the stability of the instrument with the tubus as entrance optics was monitored. 100 W lamp measurements have been performed on each day of radiance measurements and on some extra days in addition. The time series shown in Figure 4.12 illustrates the ratio of each 100 W lamp measurement divided by the 100 W lamp measurement performed on the first day of radiance measurements. As in Figure 4.4, a single time series for each detector is plotted. With the tubus entrance optics, the response of the spectroradiometric system increases over time for both detectors. The increase in stability is 4 and 5% for the silica diode and the PMT, respectively.

4.5.2 Absolute Radiance Calibration

The absolute radiance calibration was performed at the IMUK radiation laboratory after the Antarctic campaign. For the absolute calibration a 100 W quartz halogen lamp has been measured in different distances. This was necessary because it had to be assured that the lamp is completely within the FOV of the entrance optics. Further, the radiometric inverse square law (DIN 5031, 1982) had to be verified. It is not trivial that the input tubus responds according to this law as the illumination of the entrance slit of the monochromator is not diffuse. The radiometric square law is fulfilled for distances between 95 and 175 cm. The 100 W lamp has additionally been measured at a distance of 141.5 cm. Then the irradiance of the lamp was transferred to this distance. Now, the spectral responsivity of the instrument can be calculated according to Equation 3.2. Then the spectral irradiance according to Equation 3.3 can be determined. To obtain the absolute spectral radiance a division by the value of the FOV in sr (see Section 3.2.2) is necessary. On the day when the 100 W lamp was measured at large distances in the IMUK radiation laboratory, it has also been measured in the portable field calibrator. This way, the stability tests performed at Neumayer have been linked to the calibration day. The daily response of the spectroradiometer could be accounted for when computing absolute spectral radiance.



Figure 4.11: Skyscanner with the optical fibre attached for radiance measurements. Currently the entrance optics points near the horizon opposite the position of the sun. The optical fibre is protected by a flexible heated insulated tube.

4 Antarctic Campaign - Methods

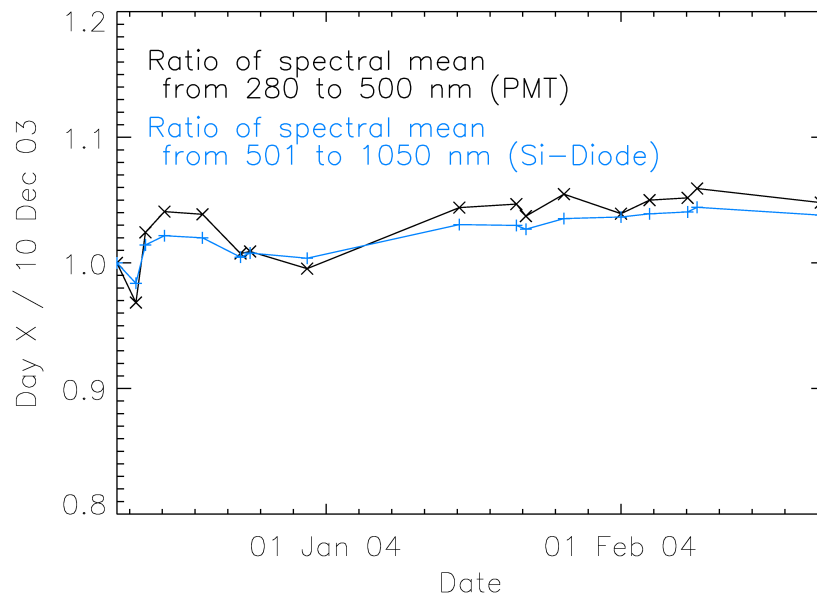


Figure 4.12: Time series of the stability of the spectroradiometer over the complete duration of the campaign with the tubus input optics for radiance measurements. 100 W lamp measurements from each day are divided by the lamp measurements conducted on 10 Dec 2003.

4.6 Ancillary Measurements

Ancillary measurements are crucial for quality control. They also provide valuable information concerning the model evaluation. In this section only the measurements of total ozone, sunshine duration and cloud base height are mentioned as they proved to be most important for the data analysis.

4.6.1 Total Ozone Column

Total ozone column has been measured by a hand-held Microtops when the sun was not obscured by clouds. It has five channels, which are limited by appropriate optical filters. Direct solar ultraviolet irradiance at three discrete wavelengths within the UV (305, 312 and 320 nm) is measured and stored. Three values of total ozone column are derived from these three UV channels taking into account the different absorption efficiencies of each channel. One value is based on the difference of the 305 and 312 nm channels. The second total ozone column is derived from the 312 and 320 nm channels. The third value represents a mean value. The Microtops can also measure total water vapour (936 nm) and aerosol optical thickness (AOT) at 1020 nm.

4.6.2 Cloud Base Height and Sunshine Duration

To decide upon the cloud conditions, data from two AWI instruments are exploited. One is the Laser Ceilograph LD-WH X manufactured by Impulsphysik GmbH. It is a light detection and ranging (LIDAR) instrument. It transmits light out to a target, in this case the clouds. The transmitted light interacts with and is changed by clouds if they are present. Some of this light is reflected and/or scattered back to the instrument where it is analysed. The time for the light to travel out to the cloud base and back to the LIDAR is used to determine the cloud base height. The other sensor used is the Sunshine Duration Sensor Solar 111 from Haenni, Switzerland. This sensor has two outputs, 1 and 0 for unobscured and obscured sun, respectively. Each minute, the signal is updated. Thus, a signal showing 1 means one minute of unobscured sun.

5 Antarctic Results

The results obtained in the Antarctic campaign at Neumayer in the summer 2003/04 are presented in this Chapter. The first section deals with the albedo measurements, as this is a parameter influencing spectral irradiance and radiance as well as luminance. Following the albedo results, Section 5.2 presents the results of measured luminance distribution. In sequence, the spectral radiance results are given. This way, both directional parameters are presented consecutively. Section 5.4 comprises results of spectral irradiance. In the last section, examples of the most important ancillary measurements are illustrated.

5.1 Albedo

Table 5.1 summarises the conditions, when albedo measurements have been performed. In addition, the daily mean albedo as measured with the SL501 is included in the last column. Results derived from the spectral albedo measurements are not included in Table 5.1 due to the different data collection protocols. All albedo values, spectral and broadband, are corrected for a change in SZA as well as for the shadowing effect of the temperature stabilised box (see Section 4.3.1).

Date	SZA range	Location	Type	Sky conditions	T_{max} [°C]	Albedo (SL501)
11.12.03	49.14° to 57.48°	NM	B	Cloudless sky	-4.8	0.96
19.12.03	50.22° to 58.46°	NM	B	Overcast	-0.7	0.96
20.12.03	47.52° to 50.42°	NM	B	Cirrus, fields of altocumulus, sun sometimes obscured	-1.4	0.95
21.12.03	47.23° to 62.22°	IE	B	Fields of altocumulus, sun sometimes behind thin cirrus	-1.3	0.91

5 Antarctic Results

Date	SZA range	Location	Type	Sky conditions	T_{max} [°C]	Albedo (SL501)
22.12.03	47.22° to 61.51°	IE	B	Sun most of day behind thin cirrus	0.5	0.94
02.01.04	47.66° to 62.00°	NM	B, S	Overcast, stratus	-1.7	0.92
03.01.04	47.75° to 57.53°	NM	S	Overcast, stratus, light snow drift	0.4	N/A
04.01.04	47.85° to 60.57°	NM	B, S	Morning: overcast (stratus, stratocumulus), afternoon: cloudless sky	-0.1	0.94
05.01.04	47.95° to 50.24°	NM	B, S	Few cirrus and altocumulus	0.2	0.94
06.01.04	48.49° to 49.27°	NM	B, S	Stratocumulus, sometimes transparent	0.3	0.97
08.01.04	48.30° to 50.86°	NM	B, S	Overcast Stratoscumulus	-1.3	0.93

Table 5.1: Summary of the conditions when albedo measurements have been performed. The date, range of SZA, location (NM: Neumayer Station, IE: Ice Edge; see also Figure 4.1), type of instrument used (B: SL501 (broadband), S: spectroradiometer) sky conditions, maximum temperature, and the measured broadband UV albedo are shown.

5.1.1 Spectral Behaviour of Albedo

An overview of daily mean spectral albedo in the wavelength range from 295 to 1050 nm is shown in Figure 5.1. Additionally, a spectrum of modelled diffuse as well as direct albedo is included. In Figure 5.2 the mean spectral daily albedo is shown for a limited wavelength range (295 to 500 nm). The spectra are modelled with the tool SNOWALBEDO contained in the libRadtran package (<http://www.libradtran.org>), which is based on an albedo model suggested by WISCOMBE and WARREN (1980).

The albedo in the UV is between 0.95 and 0.99. It increases slightly with increasing wavelength to reach its maximum around 0.99 at 430 nm on most days (see Figure 5.2). 5 January 2004 presents an exception with the mean albedo reach-

5 Antarctic Results

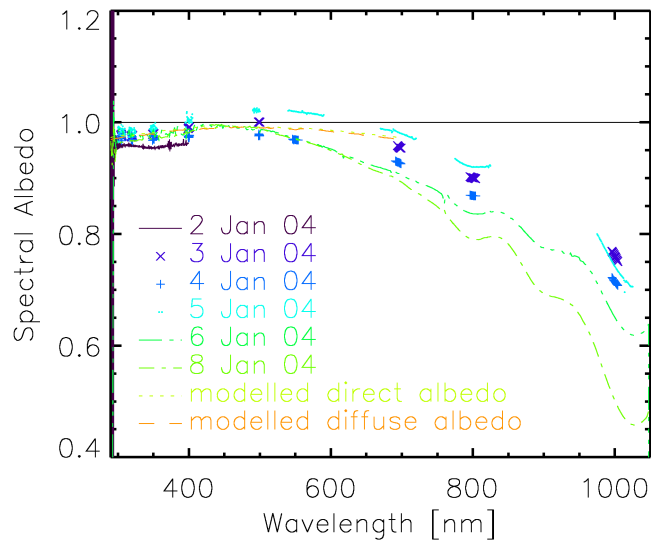


Figure 5.1: Daily mean spectral albedo measured at Neumayer on different days. The maximum value is reached at about 500 nm. The albedo decreases slightly towards shorter wavelengths. The decrease in albedo for longer wavelengths becomes more pronounced in the infrared part of the spectrum for wavelengths greater than 800 nm.

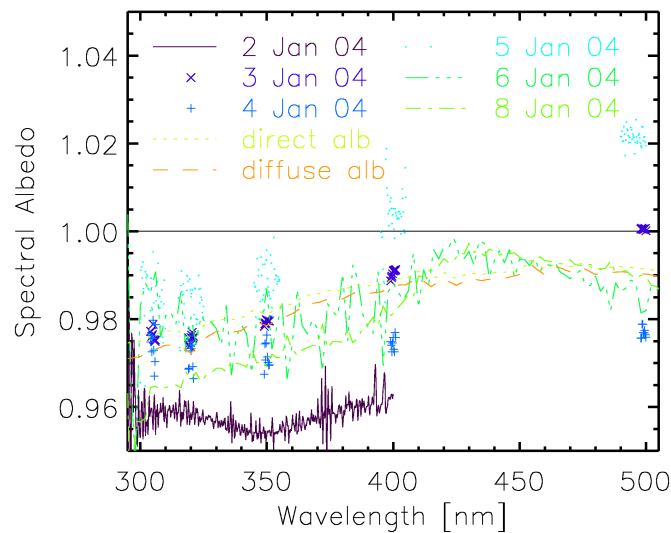


Figure 5.2: Same as Figure 5.1, but the wavelength range is limited (295 to 505 nm). It can be seen, that the maximum is reached around 430 nm for a few days. On 5 Jan 04, the albedo is larger than unity with 1.02 at 500 nm.

ing a maximum of 1.02 at 500 nm. The albedo remains high at up to 800 nm in the visible. The decline of the slope for increasing wavelengths is steeper for wavelengths longer than 800 nm. At 1000 nm, the observed albedo values range between 0.45 and 0.75. It cannot be decided which albedo spectrum is highest. This depends on wavelength as the spectra cross each other. The spectral behaviour of the albedo, in particular the albedo being larger than unity, is discussed in the next chapter. The uncertainties occurring in the albedo measurements are also addressed (see Section 6.1.1).

5.1.2 Effect of SZA and Snow Grain Size on Albedo

The afternoon of 4 January 2004 was the longest period where albedo measurements under cloudless sky conditions have been performed. Both, the mean spectral and broadband albedo, show a tendency of being smaller the later in the day it was measured. Thus, it decreases with increasing SZA. This can clearly be observed in Figure 5.3 where the diurnal course of the albedo derived from different radiation sensors is shown. The absolute level of the albedo derived from the measurements with the SL501 is highest. It is lowest for the albedo calculated from the AWI BSRN data based on pyranometer measurements. A discussion on this behaviour is presented in Section 6.1.2.

On 2 January 2004, the sky was covered with stratiform clouds. For this day, the diurnal cycle of different integrals of UV albedo is shown in Figure 5.4. Additionally to UV integrals derived from the spectral albedo, the diurnal cycle of albedo measured with the SL501 is shown. No significant diurnal variation in dependence of SZA can be observed. The albedo measured by the SL501 is slightly lower than the albedo values derived from spectral measurements. The daily mean value for each wavelength range derived from the spectral measurements (UVA, UVB, UV, CIE) is 0.93. The daily mean albedo measured with the SL501 is 0.92.

All albedo values derived from measurements conducted with the SL501 are shown in Figure 5.5. The albedo was measured in a range of solar zenith angles from 47° to 63° . Except for two occasions, the albedo values are between 0.88 and 0.99. One value is at 0.83 and one is at 1.02. A dependence of albedo on SZA cannot be observed. For a discussion of these results, see Section 6.1.2.

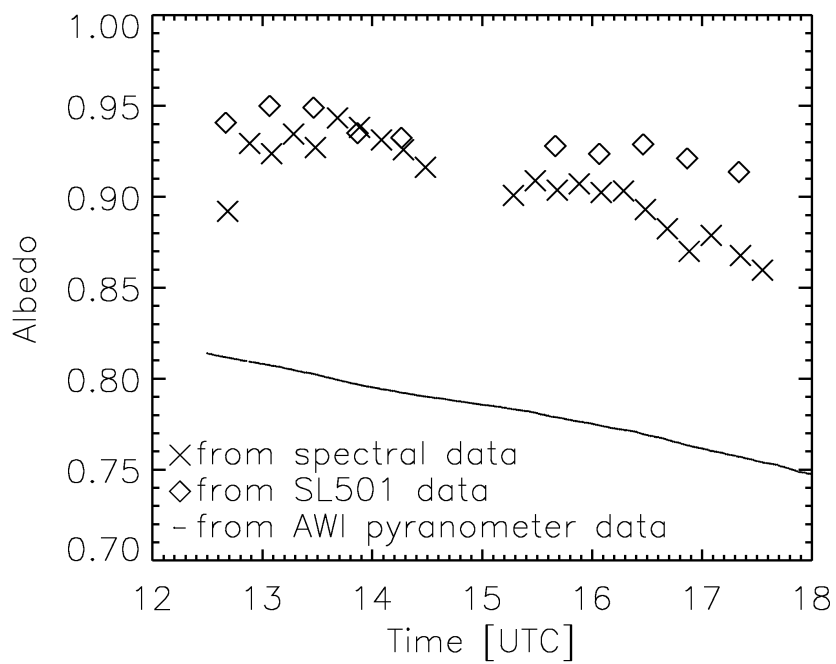


Figure 5.3: Diurnal cycle of mean albedo on 4 January 2004 derived from different radiation sensors. For the period shown, the sky was cloud free. All sensors show a decrease in albedo the later in the day it is.

5 Antarctic Results

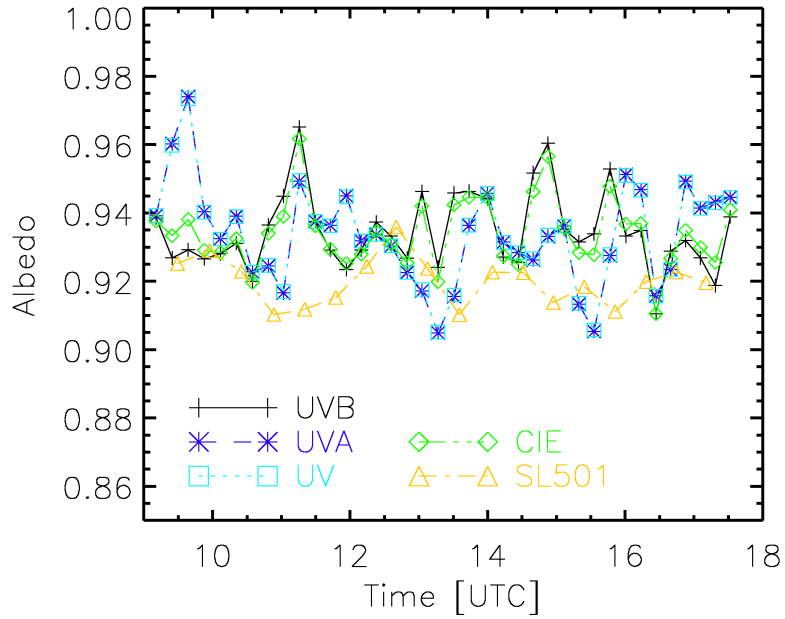


Figure 5.4: Diurnal cycle of different integral albedo values measured on 2 January 2004. The sky was covered by stratiform clouds. A dependence of albedo on time cannot be observed for this day.

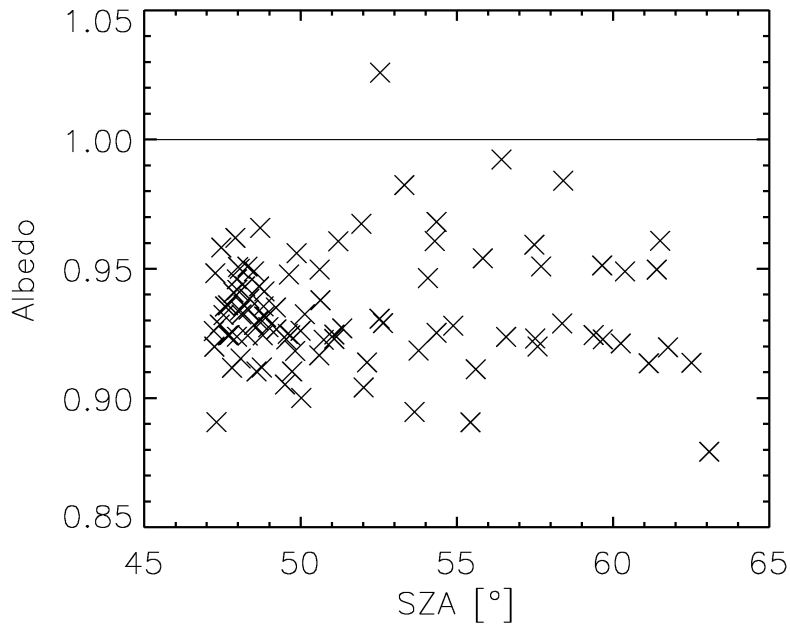


Figure 5.5: All albedo values derived from measurements with the SL501 as a function of SZA. A dependence of albedo on SZA cannot be observed.

5.2 Luminance

Two different sky luminance distributions are shown in Figures 5.6 and 5.7, for a cloudless and an overcast sky situation, respectively. The sky dome is projected onto a plane. The absolute luminance is meant to resemble a three dimensional picture. The geographical directions are indicated by N (north), S (south), W (west), and O (east). The orange spot represents the position of the sun.

The cloudless luminance distribution is measured on 12 December 2003 at 13:02 UTC (see Figure 5.6), a rim at the horizon with higher values compared to the centre of the luminance distribution (lower zenith viewing angles) is observed. This feature is called horizon brightening.

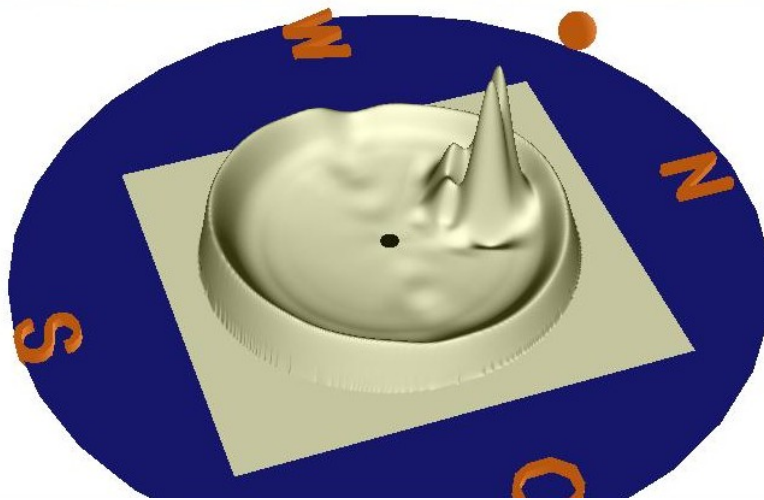


Figure 5.6: Sky luminance distribution for a cloudless situation measured on 12 December 2003 at 13:02 UTC. Geographical directions are indicated by N (north), S (south), O (east), and W (west). The orange spot represents the sun. Horizon brightening can be observed. The maximum luminance occurs in a circumsolar ring around the sun (aureole). For more details, see text.

It is also observed in the measurements of spectral sky radiance (see Section 5.3). The maximum values are in the aureole, which describes the circumsolar region. As the direct luminance of the sun is four to five orders of magnitude higher than the sky luminance it is not measured. The luminance detector is not designed to cover such a large dynamic range. When the sky luminance entrance optics is directed towards the sun, a shutter prevents the strong direct radiation to enter the system. Directly east of the aureole, a small local minimum is seen.

The overcast sky shows a different distribution of luminance (see Figure 5.7). This situation has been measured on 2 January 2004 at 12:20 UTC. The distribution

5 Antarctic Results

of sky luminance is quite uniform. Horizon brightening is observed, but it is not as distinct as for the cloudless case. A local minimum stretches from the east to the west for all VZA.

Possible causes for the features observed in the measured sky luminance distributions are discussed in Section 6.2.

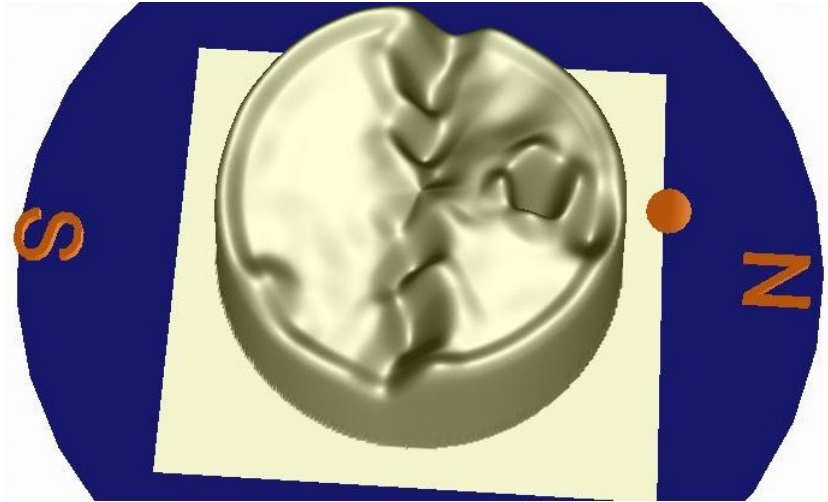


Figure 5.7: Sky luminance distribution when the sky was covered by clouds with eight octas, measured on 2 January 2004 at 12:20 UTC. The directions N (north) and S (south) are indicated. The orange spot represents the sun. Except for the local minimum stretching in east-west direction and the rim at the horizon, the sky luminance distribution is quite uniform. For further details, see text.

5.2.1 Zenithal Scans of Luminance

Three zenithal scans in the principal plane (explanation see Section 4.5) are depicted in Figure 5.8. The luminance is normalised to the zenith luminance. Two cloudless cases measured at Neumayer on 11 and 12 December 2003 with an SZA of 86° and 48° , respectively, and one cloudy situation (5 January 2004, SZA = 76°) are shown. The situation for 12 December 2003 is already shown in Figure 5.6. Horizon brightening can only be observed for the cloudless zenithal scans. For the overcast situation the luminance only varies to $\pm 50\%$.

To assess the influence of the surface albedo, Figure 5.9 shows two zenithal scans measured at Neumayer and two measured at Boulder, Colorado. All four scans are measured under cloudless conditions. The two zenithal scans for Neumayer are also shown in Figure 5.8. The two zenithal scans shown for Boulder are measured on 22 June 2003, the day of the NDSC intercomparison (see Section 3.4.3). At

5 Antarctic Results

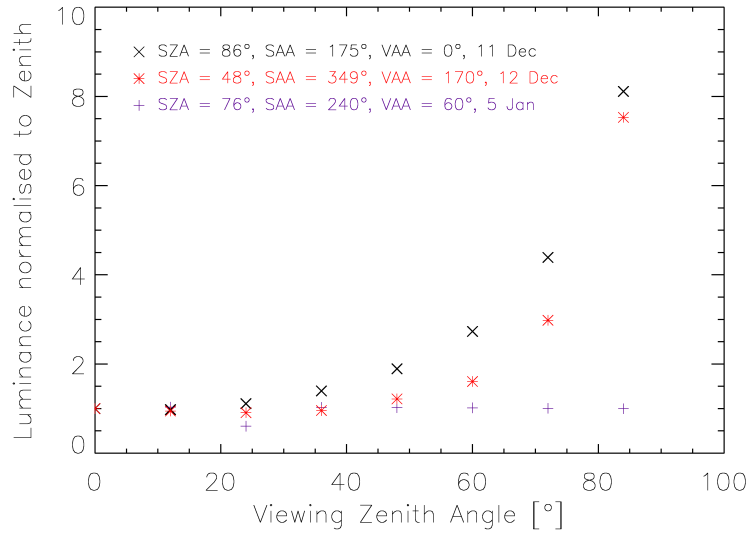


Figure 5.8: The zenithal scans on 11 and 12 December were measured under a cloudless sky, the zenithal scan for 5 January under an overcast sky. The solar zenith angle (SZA), solar azimuth angle (SAA) as well as the viewing azimuth angle (VAA) are given in the legend. Horizon brightening is clearly observed for a cloudless situation. For a SZA of 86° , the luminance at a VZA of 84° exceeds the zenith luminance by a factor of 8.2. For the overcast situation the luminance only varies to $\pm 50\%$.

Neumayer, for a SZA of 86° , the luminance at a viewing zenith angle of 84° exceeds the zenith luminance by a factor of 8.2. Horizon brightening is slightly lower for a SZA of 48° with 7.6. For the luminance scans at Boulder, horizon brightening is clearly observed for an SZA of 86° reaching a factor of 5. At a SZA of 48° , the luminance at a viewing zenith angle of 84° only exceeds the zenith luminance by a factor of 1.7. A further discussion about the physical principles of zenithal scans of luminance is presented in Section 6.2.1.

5.2.2 Diurnal Cycle of Luminance

The diurnal cycle of zenith luminance for 4 and 5 January 2004 is plotted in Figure 5.10. Both, cloud free and cloudy sky situations occurred. A stratiform cloud cover of eight octas was present until noon of 4 January. The sky remained cloudless until noon of the next day, then another stratiform cloud cover moved in. The zenith luminance during both cloudy situations reaches $1.7 \cdot 10^4 \text{ cdm}^{-2}$, whereas it stays low with $1.5 \cdot 10^3 \text{ cdm}^{-2}$ for the cloudless situation. Thus, the cloudy zenith luminance is about one order of magnitude higher than the zenith

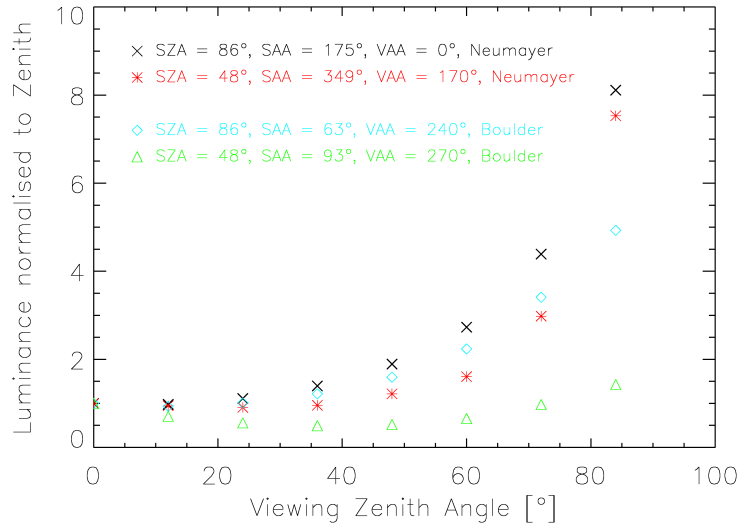


Figure 5.9: Four zenithal scans of luminance for cloudless sky. Horizon brightening is clearly observed at Neumayer for both SZAs and at Boulder for a SZAs of 86°. The SZAs, solar azimuth angle (SAA) as well as the viewing azimuth angle (VAA) are given in the legend. For more details, see text.

luminance observed under cloud free conditions.

5.3 Spectral Radiance

In this section different cases of sky radiance are presented. Radiance spectra are shown as well as the variation of radiance for different viewing zenith angles opposite the position of the sun. Measured to modelled radiance is compared. A discussion on the physical reasons for the different cases of observed radiance is presented in Section 6.3, where connections to luminance are shown as well.

5.3.1 Cloudless Zenith Radiance

The first important question to answer is how a spectrum of radiance looks like. Figure 5.11 shows spectra of zenith radiance for cloudless situations recorded on 11 and 12 December 2003 at different times. The top and middle panel show the spectra on a linear and logarithmic scale, respectively. On the bottom panel, the same spectra are shown, but each one is normalised to its maximum value.

The spectrum measured at 11:56 UTC is maximal. The spectra scanned at 18:19

5 Antarctic Results

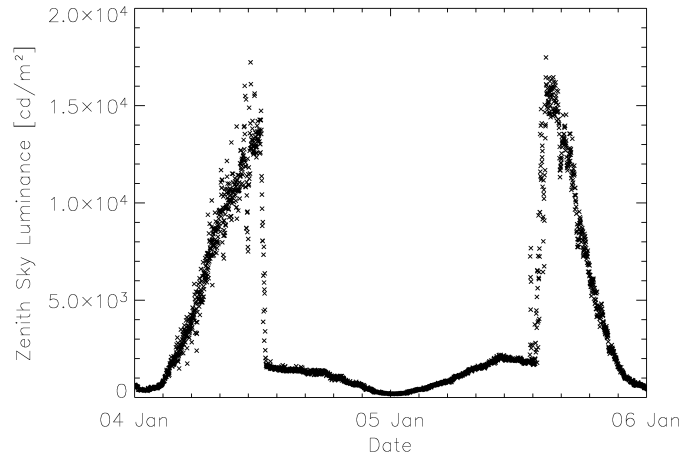


Figure 5.10: Diurnal cycle of zenith luminance on 4 and 5 January 2004. The sky was cloud free from midday 4 to midday 5 January. The zenith luminance is lower by one order of magnitude during cloudless sky conditions.

and 05:40 UTC show a different spectral structure. They decrease much less for wavelengths larger than 500 nm compared to the other three spectra. On the lowest panel of Figure 5.11, it can be seen that the maximum value of the noon spectrum is at 330 nm. The same value is also almost reached at 400 nm. For the three radiance spectra with the largest SZA at 18:19, 00:24, and 05:40 UTC, the maximum radiance is shifted to 450 nm.

The diurnal cycle of zenith radiance for the period from 10 to 13 December 2003 is depicted in Figure 5.12. The sky was cloudless up to 19:30 UTC on 12 December. Local maxima can be observed around 6:00 as well as 18:30 UTC for wavelengths larger than 499 nm. These local maxima coincide with the spectra at 18:19 and 5:40 UTC showing a different spectral behaviour (see Figure 5.11). As soon as clouds moved in the zenith radiance increased.

5.3.2 Cloudless vs. Overcast Zenith Radiance

In Figure 5.13 a cloudless and a cloudy spectrum of zenith radiance is shown (upper panel: linear scale, middle panel: logarithmic scale, bottom panel: linear scale and normalised). Both spectra are measured around noon, thus both SZA are roughly the same (47.7° on 19 Dec 2003, cloudy; 51.2° on 22 Jan 04, cloudless). At 500 nm, for example, the cloudy spectrum reaches $620 \text{ Wm}^{-2}\text{nm}^{-1}\text{sr}^{-1}$. At the same wavelength, the cloudless spectrum only shows a value of $80 \text{ Wm}^{-2}\text{nm}^{-1}\text{sr}^{-1}$. Looking at the middle panel of Figure 5.13, it can be seen that the cloud free spectrum decreases towards longer wavelengths by

5 Antarctic Results

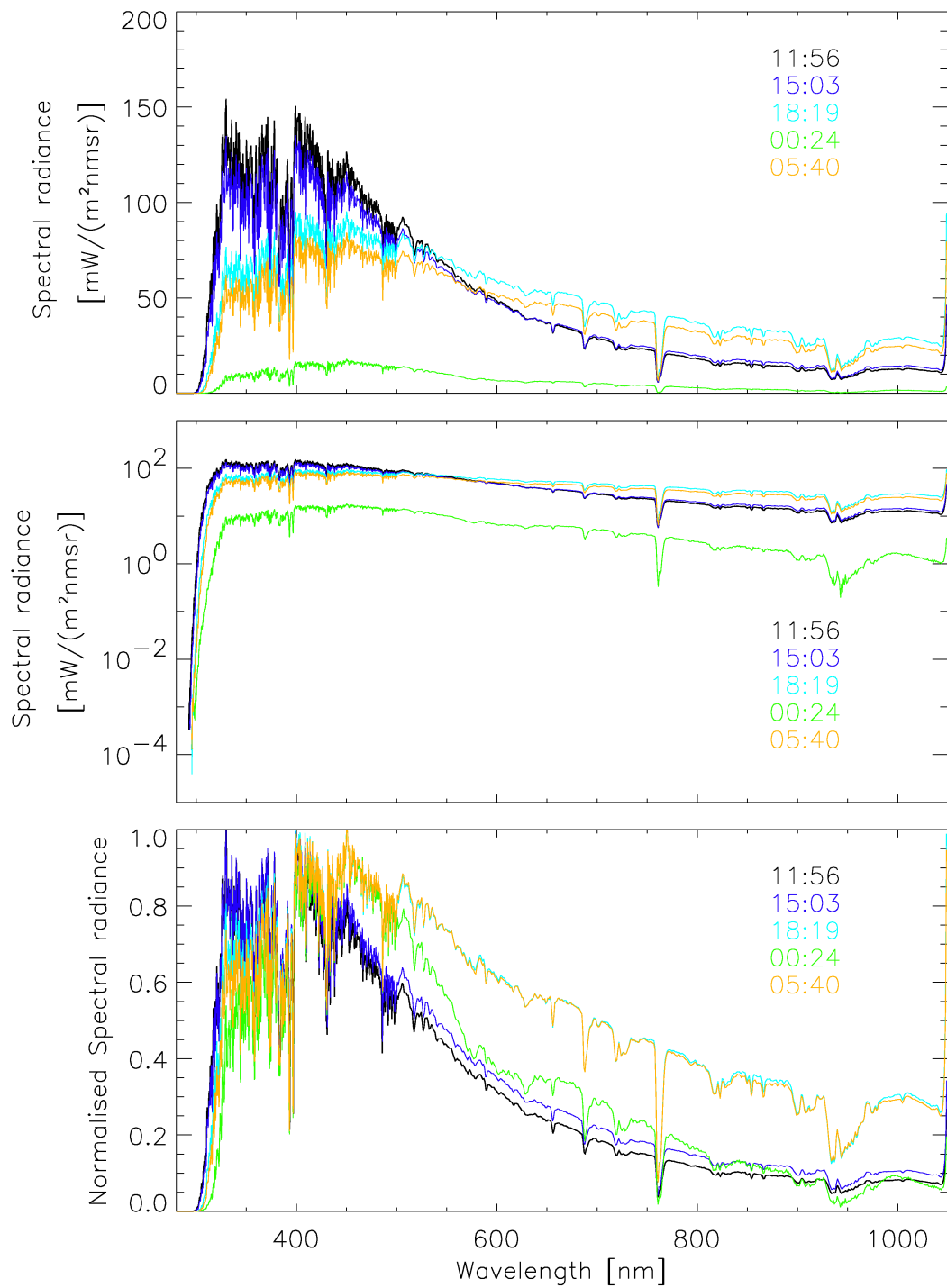


Figure 5.11: Spectra of zenith radiance on 11 and 12 December 2003 for cloudless situations. The upper panel shows the spectra on a linear scale, the middle panel on a logarithmic scale. The lowest panel shows the spectra normalised to the maximum value. For additional descriptions, see text.

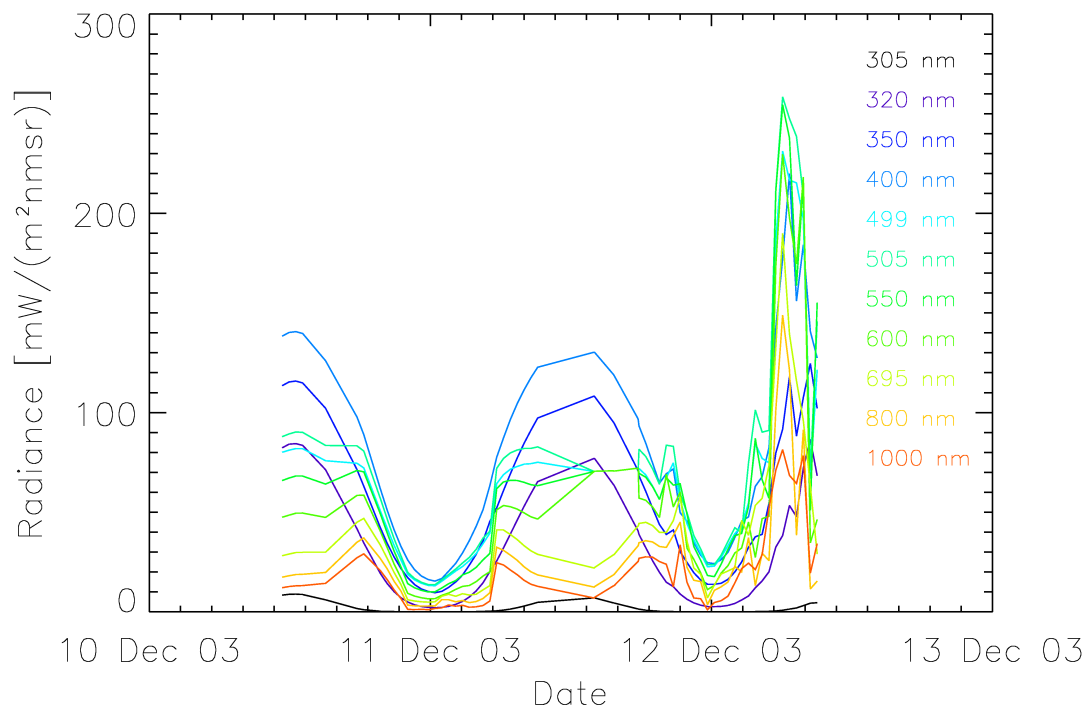


Figure 5.12: Diurnal cycle of zenith radiance from 10 to 13 December 2003 for various wavelengths as indicated in the legend. Clouds were present from 12 Dec 19:30 UTC. Up to then cloud free conditions prevailed. Zenith radiance for the cloudy situation is much higher compared to the cloudless case.

about two orders of magnitude. The cloudy spectrum, in contrast, only shows a very slight decrease. The maximum value of the cloudless spectrum is at 400 nm. The maximum of the measured cloudy spectrum is at about 510 nm (see lowest panel in Figure 5.13).

5.3.3 Zenithal Scans of Radiance

A set of radiance spectra for a complete zenithal scan from the zenith to the horizon in steps of 10° is shown in Figure 5.14. The spectra have been measured at a few small wavelength intervals in the principal plane opposite the sun (SAA + 180°) under a sky without cloud cover on 9 February 2004. The upper panel shows absolutely calibrated radiance spectra, the lower panel shows the spectra normalised to the maximal value. The maximum of the spectrum is shifted to longer wavelengths the larger the VZA. Up to 500 nm the absolute radiance is lower the larger the viewing zenith angle is. For wavelengths larger than 500 nm the radiance is larger the larger the VZA. Thus, horizon brightening can only be observed for wavelengths in the visible and near infrared part of the solar spectrum.

Figure 5.15 shows the zenithal scan for different wavelengths in dependence on viewing zenith angle, normalised to the VZA of 10° . It was aimed at normalising the zenithal scan to the zenith radiance, however, the difference between measurement and model for the zenith direction amounts to a factor of 5. This is not the case for the VZA of 10° . Further, modelled radiance distributions for VZA $< 20^\circ$ are constant to within $\pm 5\%$ (see Figures 5.15 and 6.5). Therefore, it is justified to normalise the radiance to radiance with a VZA of 10° instead of the zenith.

Modelled and measured zenithal radiance scans are shown in Figure 5.15. It takes 40 min to record such a zenithal scan. Horizon brightening is clearly observed for wavelengths larger than 400 nm. The model results show a horizon brightening, which is larger than the measured horizon brightening. The maximal horizon brightening is seen at the longest wavelength (1000 nm) with a factor of 18 for a VZA of 85° for modelled radiance. The measured radiance only shows a horizon brightening with a factor of 11 for the same viewing geometry. At 320, 350, and 400 nm the maximum of the zenithal scan is at a VZA between 70° and 80° , for both, measured and modelled radiance. At 305 nm the radiance even decreases for larger viewing zenith angles.

5.3.4 Model vs. Measurement

All cloud free radiance spectra have been modelled with UVSPEC, a radiative transfer model contained in the libRadtran package (MAYER et al., 1997). Cloud-

5 Antarctic Results

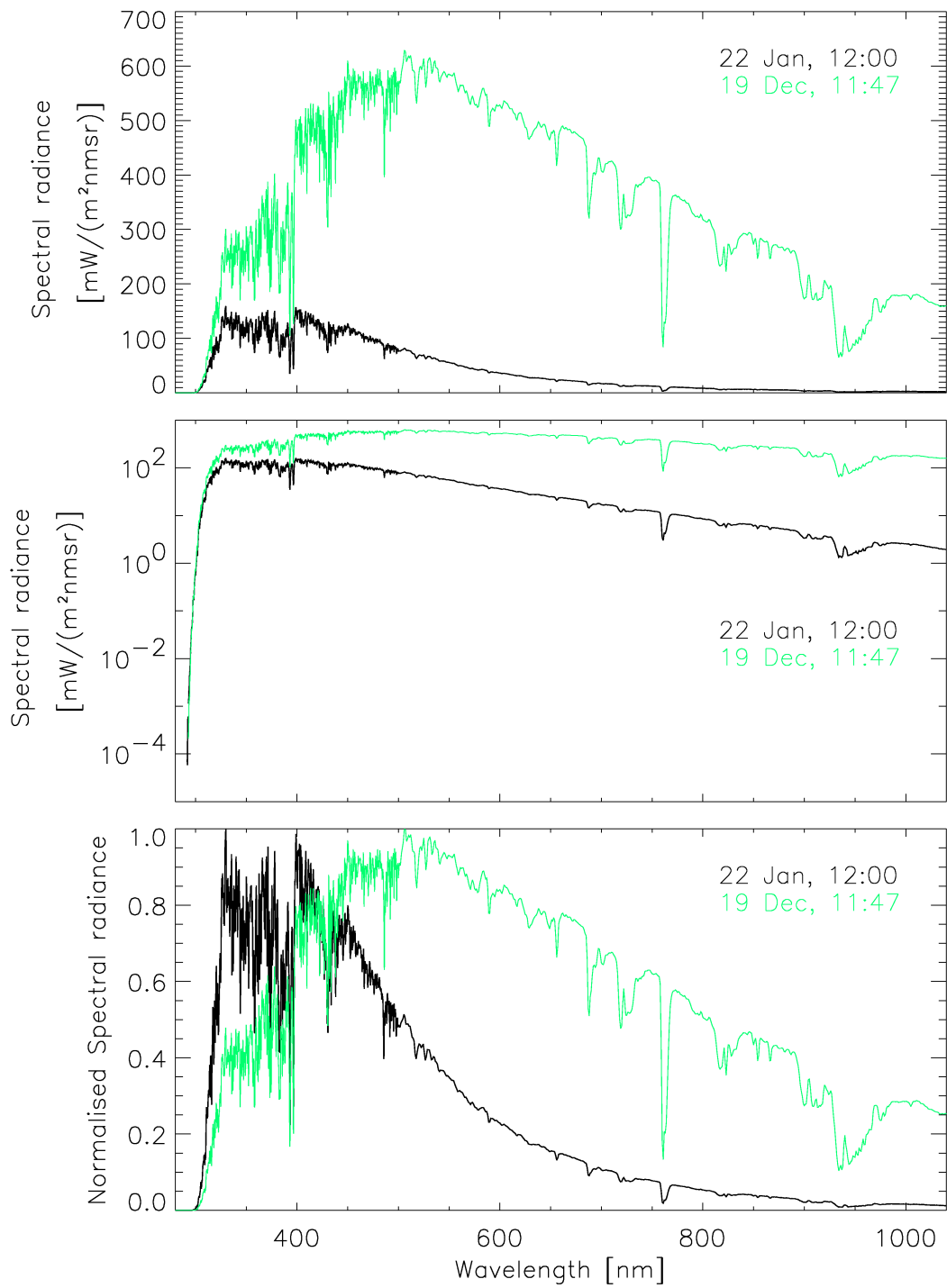


Figure 5.13: Cloudless (22 Jan) and cloudy (19 Dec) spectrum of zenith radiance. The upper panel shows the spectra on a linear scale, the middle panel on a logarithmic scale. Normalised zenith radiance spectra are shown in the bottom panel on a linear scale. For more descriptions, see text.

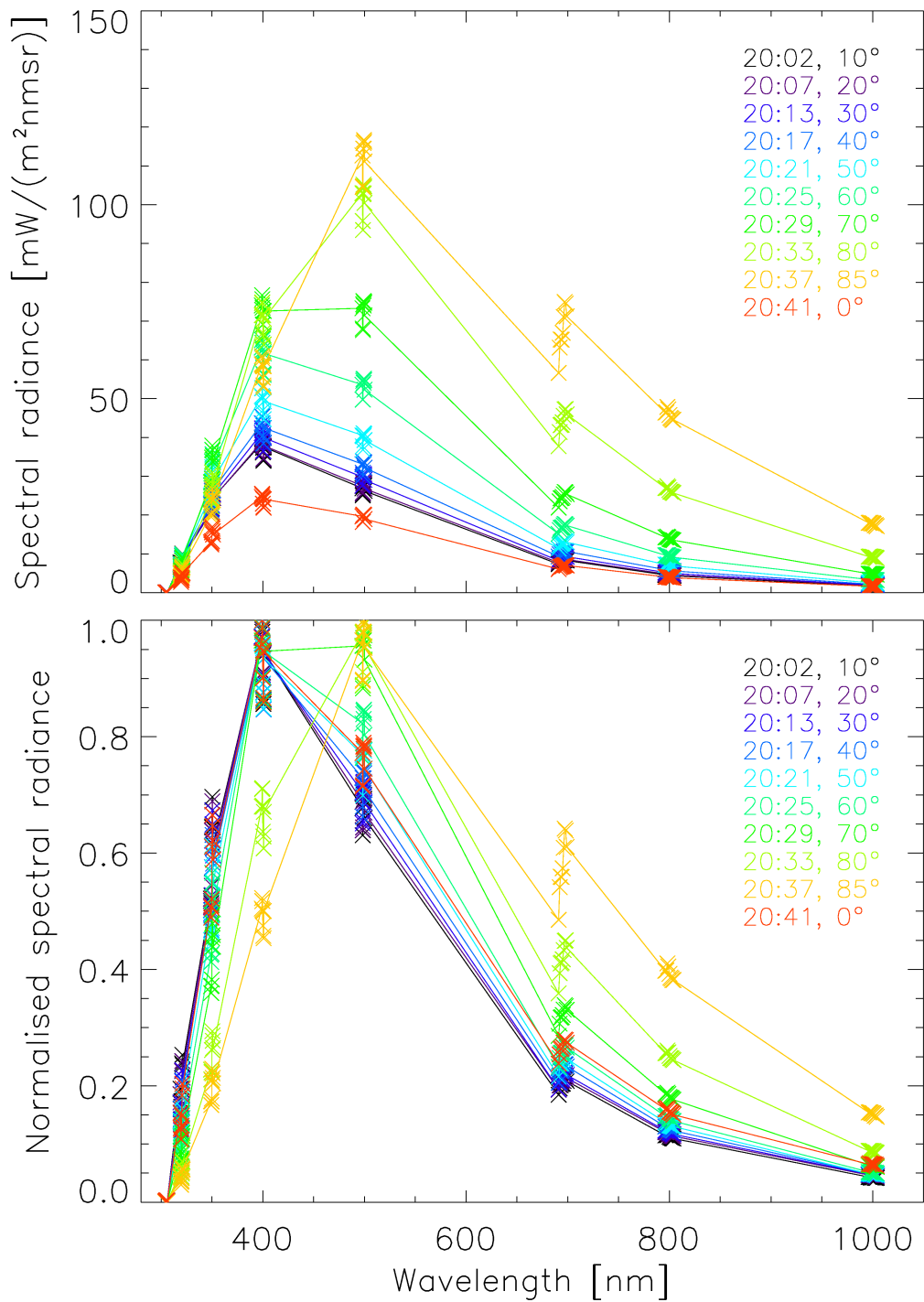


Figure 5.14: Set of radiance spectra measured in one zenithal scan on 9 February 2004. The spectra have been measured from the zenith (0°) to the horizon in the backscattering principal plane in steps of 10° . The upper panel shows absolute radiance, whereas the lower panel shows spectral radiance normalised to the zenith radiance.

5 Antarctic Results

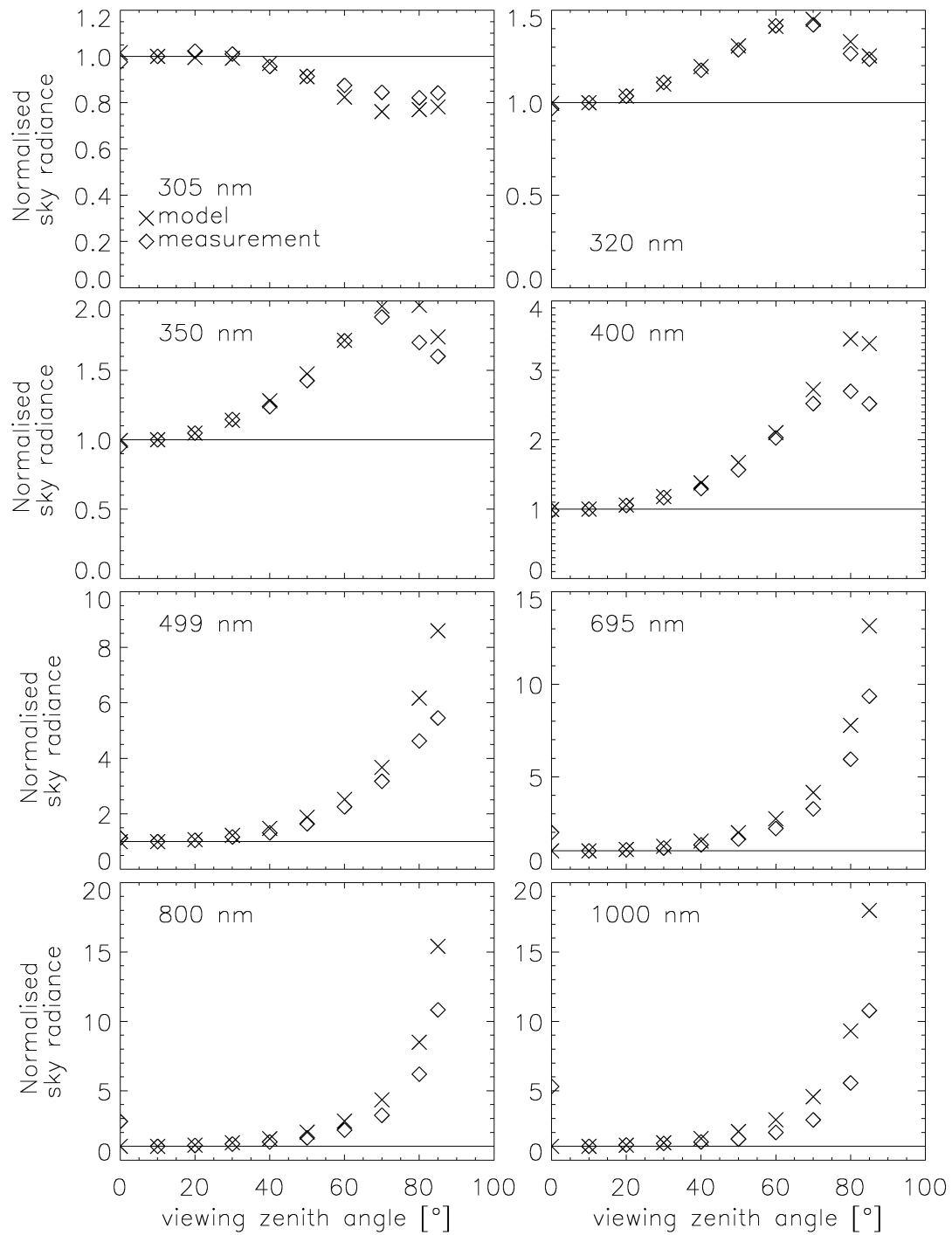


Figure 5.15: Measured and modelled zenithal scans in the backscattering principal plane on 9 February 2004 for various wavelengths. The sky was cloud free. Horizon brightening can be clearly observed for wavelengths larger than 400 nm. In the UVA the maximum radiance is at a VZA of 70°. At 305 nm the radiance decreases the larger the VZA. Horizon brightening for the modelled radiance is larger compared to the measured spectral radiance.

5 Antarctic Results

less situations and input parameters are determined in the same way as described in Section 5.4. The ratio between modelled and measured radiance as a function of SZA is shown in Figure 5.16 for selected wavelengths. The measured radiance mostly exceeds the radiance resulting from model calculations. The deviation between measurement and model is lowest at 320 and 350 nm with an average ratio of 1.2. For wavelengths longer than 400 nm a dependence of the ratio on SZA can be seen. The ratio increases for increasing SZA up to 75° , then the ratio decreases again steeply until values of 1.2 are reached. For a few cases the ratios stay around 1.3 for all SZA. A few outliers can also be observed. One is, for example, at a SZA of 50° at 320 and 350 nm. The results obtained here are discussed in Section 6.3.

5 Antarctic Results

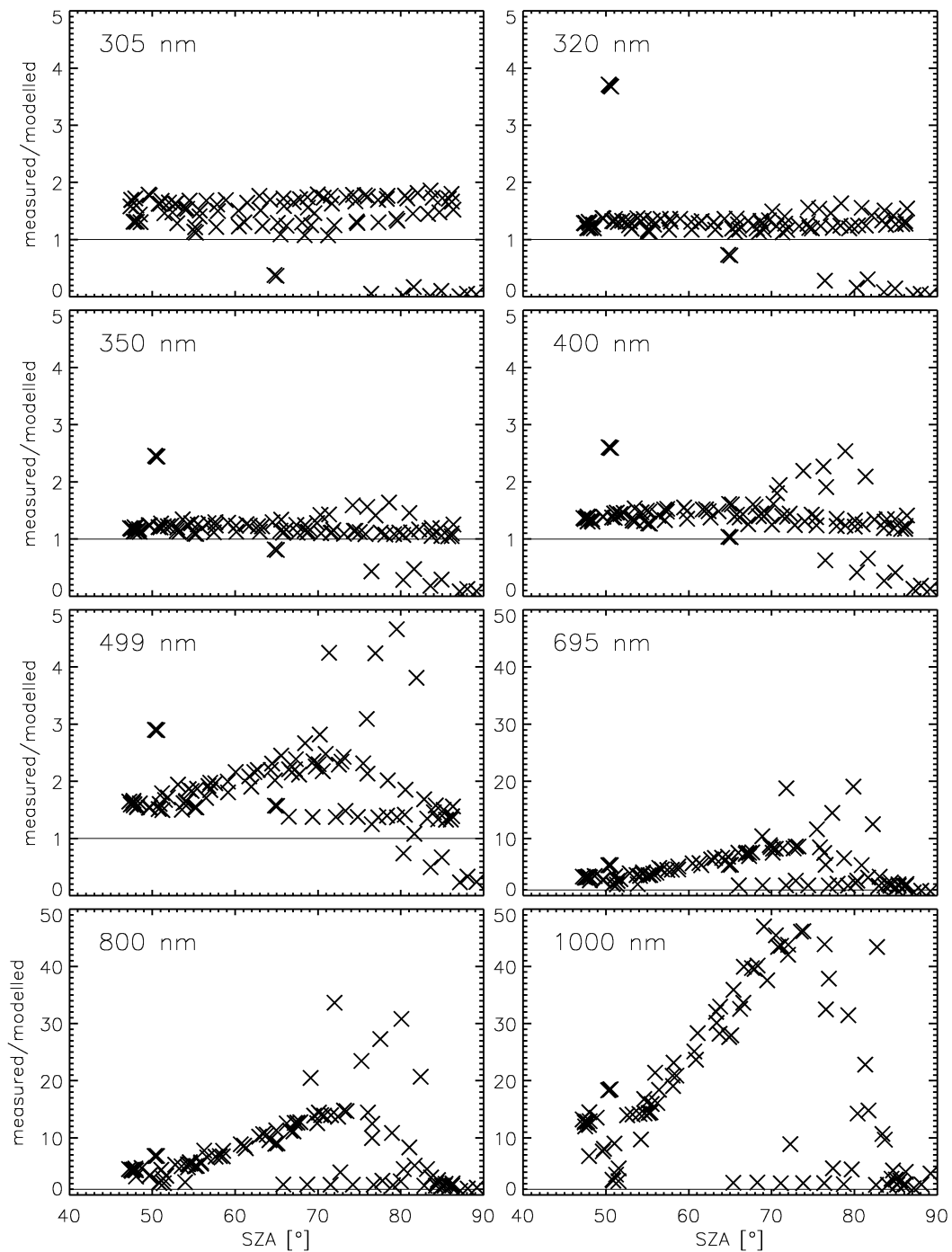


Figure 5.16: Ratio of measured to modelled radiance as a function of SZA for all cloudless situations. The ratio is shown for different wavelengths. For wavelengths longer than 400 nm the ratio is very large with values up to 47 for SZA of 75°. At 320 and 350 nm it is minimal with values around 1.2.

5.4 Spectral Irradiance

Figure 5.17 shows the ratio of modelled to measured irradiance in dependence on SZA for eight different wavelengths. Spectral irradiance has been modelled with UVSPEC. The results of this comparison between modelled and measured irradiance will serve

- as a tool for controlling the quality of the measured data and
- to assess whether the spectral irradiance measured within this campaign is useful for a model evaluation.

For this comparison only cloudless situations have been considered. A situation is considered cloud free when the AWI sunshine duration indicator showed the signal for unobscured sun and when no clouds have been detected by the AWI LIDAR. For an example diurnal cycle of both AWI sensors see Section 5.5. Model input parameters comprise

- the SZA dependent on wavelength according to the scan time,
- the measured spectral snow albedo from the cloudless afternoon of 4 January 2004,
- the total ozone column derived from TOMS data (ftp://jwocky.gsfc.nasa.gov/pub/eptoms/data/overpass/OVP323_ept.txt),
- no aerosols, and
- subarctic atmospheric profiles.

Instead of TOMS ozone data, Microtops ozone data could have been used. Reasons for this decision are discussed in Section 6.4. The assumption of zero aerosols is justified as the Antarctic atmosphere is known to be very clean (PIEL, 2004). Antarctic atmospheric profiles would have been favourable, but they are not contained in the standard distribution of libRadtran.

The deviation from unity is lowest for 350 nm with deviations of $\pm 10\%$ for all SZA. The deviation at 320 and 400 nm is also low within $\pm 15\%$, but mostly lower. At 305 nm large deviations are seen. They range from -30 to +100%. For the three largest wavelengths (695, 800, and 1000 nm) a clear dependence on SZA can be observed. The ratio between measurement and model increases the larger the SZA, and reaches up to +80% for an SZA of 88° .

The time series of the UV irradiance integrated over the wavelength range from 280 to 400 nm is shown in Figure 5.18.

5 Antarctic Results

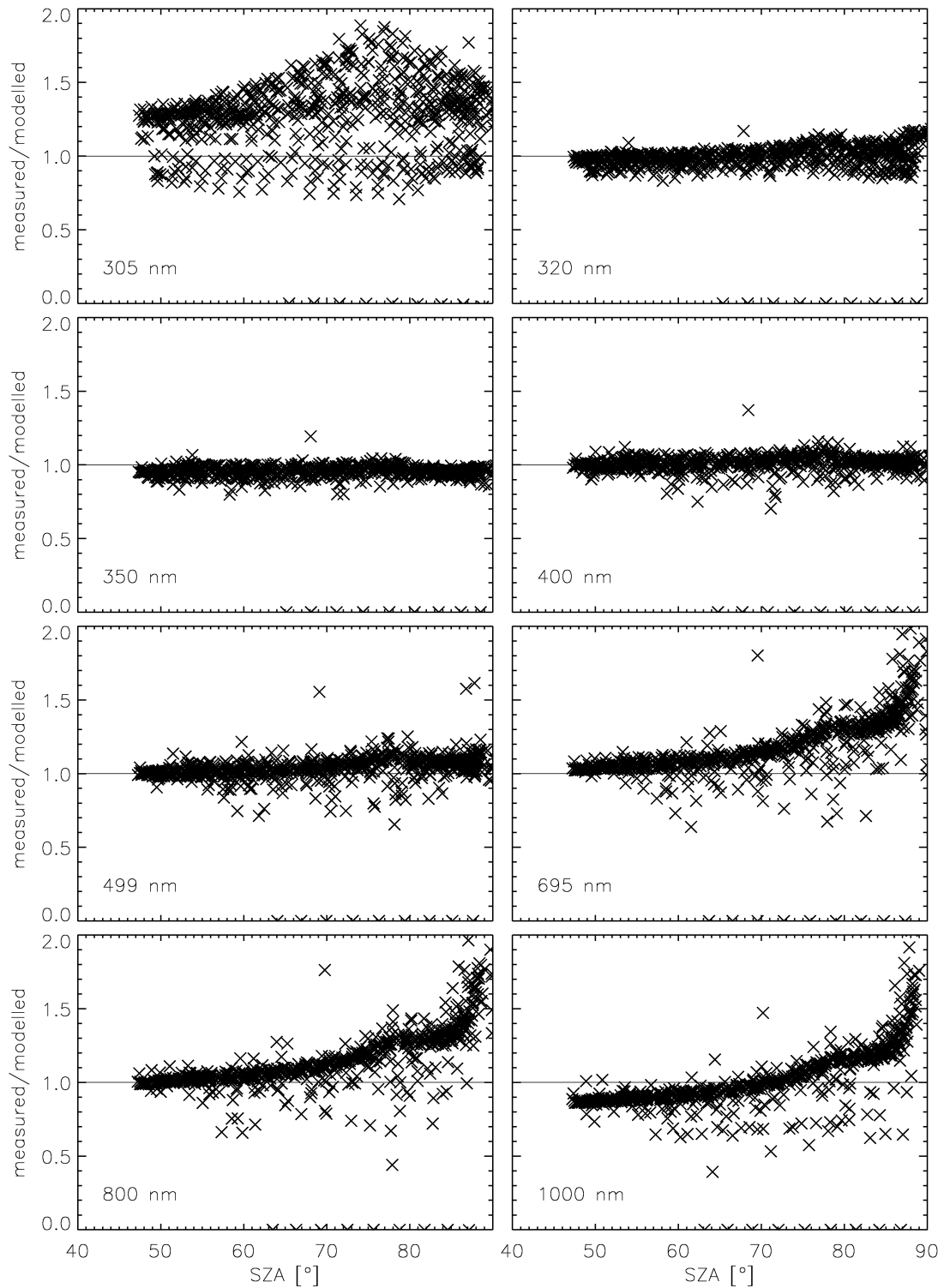


Figure 5.17: Ratio of modelled to measured irradiance in dependence of SZA for different wavelengths. The deviation from unity is lowest at wavelengths in the UVA, with no dependency on SZA. For 695, 800, and 1000 nm the ratio increases with increasing SZA.

5 Antarctic Results

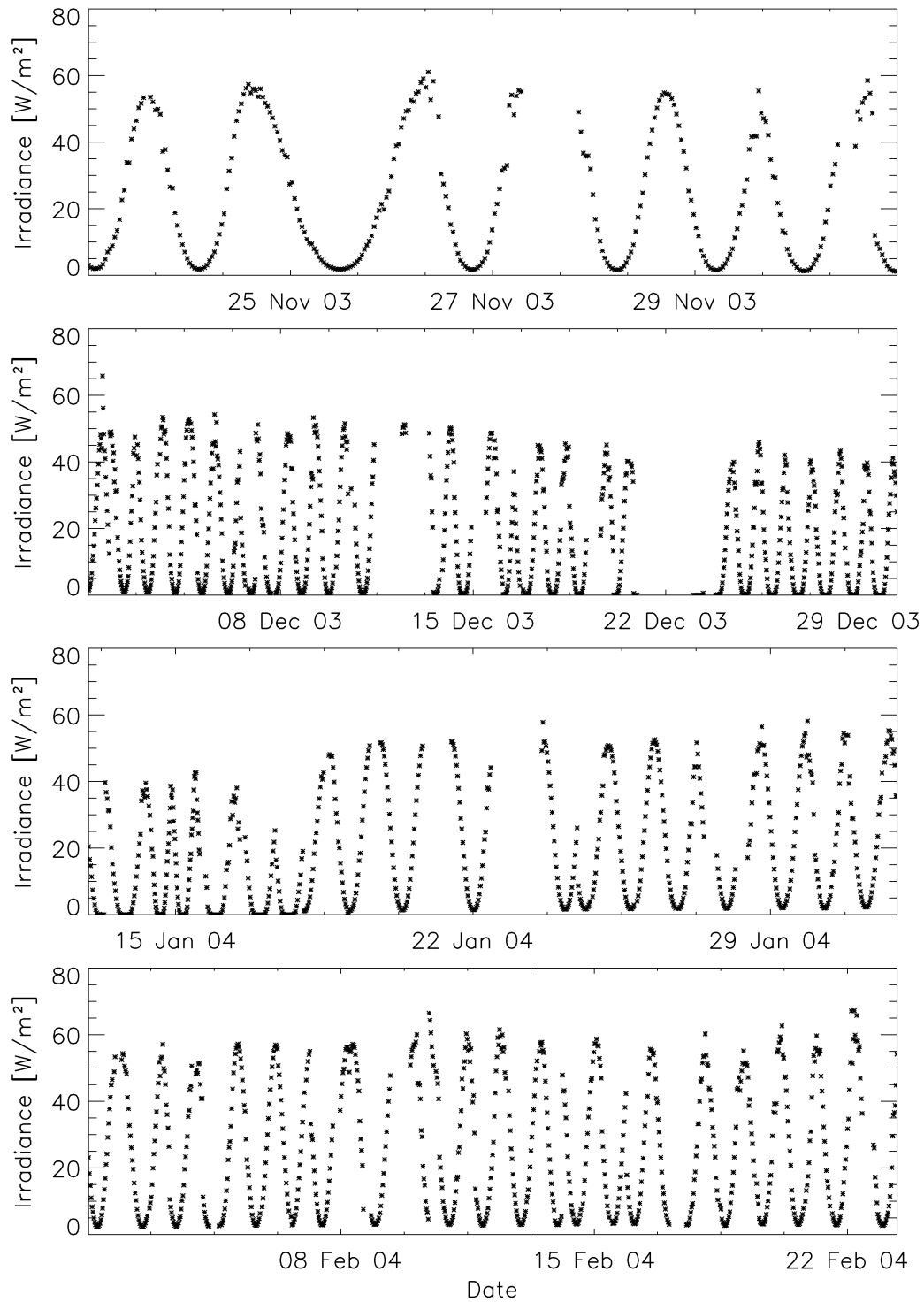


Figure 5.18: Time series of wavelength integrated UV irradiance for each month of the campaign. The measurements started on 23 November 2003 and lasted until 23 February 2004. The first ten days of January 2004 are omitted because the spectroradiometer was employed for albedo measurements.

Each panel represents the time series for one month of the campaign. The measurements started on 23 November 2003 and lasted until 23 February 2004. The first ten days of January 2004 are omitted because the spectroradiometer was employed for albedo measurements. The UV was further chosen to be depicted because other Antarctic stations monitor UV irradiance (see Figure 4.1). This way, the spectral irradiance collected at Neumayer can be compared to other stations' data. The maximum value occurs on 22 February 2004 with 67 Wm^{-2} , which was a day with broken clouds.

5.5 Ancillary Measurements

Only results from the most important ancillary parameters (total ozone column, cloud base height and sunshine duration) are shown in the following sections.

5.5.1 Ozone

Total ozone column measured by the Microtops is compared to the total ozone column derived from TOMS data (see Figure 5.19) for each of the three values delivered by the Microtops.

Microtops measurements have been performed when the sun was not obscured by clouds. The deviation between both instruments is within $\pm 20\%$ for most situations. The lowest mean ratio is obtained for the ratio between the mean Microtops channel and TOMS (red triangles). The ozone value derived from the 312 and 320 nm channels (blue crosses) are always lower than the TOMS data.

5.5.2 Cloud Base Height and Sunshine Duration

5 January 2004 is chosen to illustrate the importance of ancillary data. The diurnal cycles of the height of the cloud base and the sunshine duration is depicted in Figure 5.20. This day started with a cloudless sky. A low layer of stratiform clouds formed quickly around noon. This can be easily observed in both parameters. The occurrence of the clouds in the AWI LIDAR measurements coincide with the signal for obscured sun in the AWI sunshine duration sensor.

5 January 2004 was a day of spectral albedo measurements. In addition, a zenithal luminance scan for the cloudy period during the afternoon is shown in Figure 5.8. These few examples already underline the importance of high quality ancillary data for the interpretation of the measured radiation quantities.

5 Antarctic Results

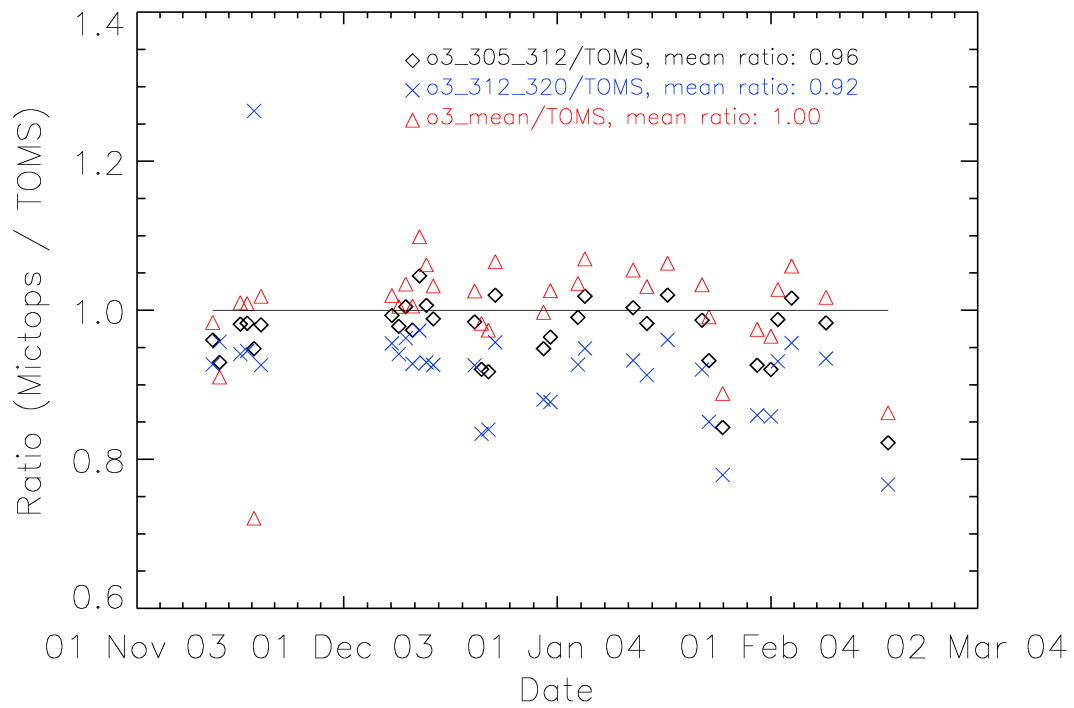


Figure 5.19: Ratio between total ozone column measured by the Microtops and TOMS for each channel of the Microtops for situations when the sun was unobscured by clouds. For more details see text.

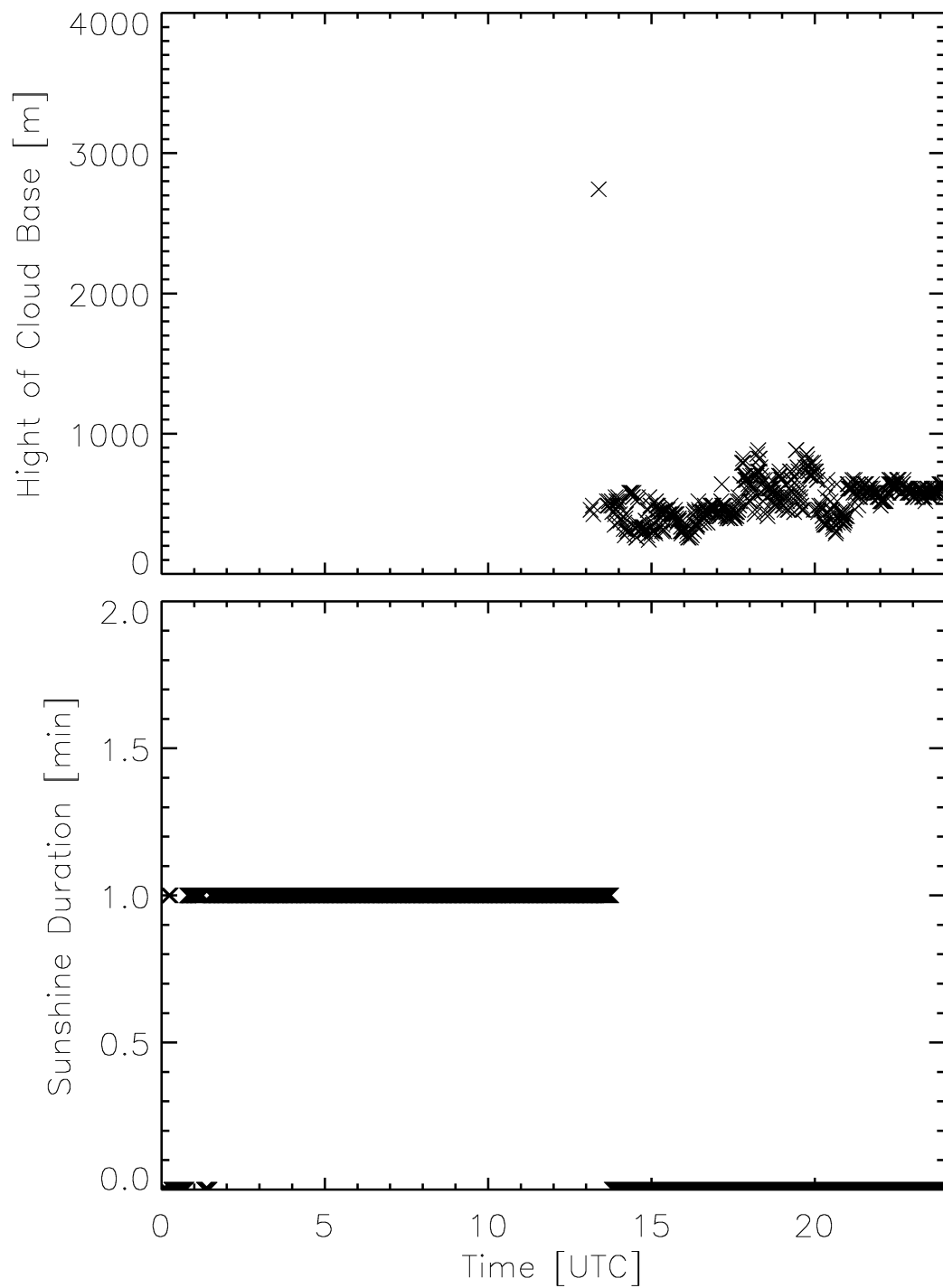


Figure 5.20: Diurnal cycle of cloud base height (upper panel) and sunshine duration (lower panel) based on the AWI BSRN data for 5 January 2004. The morning was cloudless, in the afternoon a stratiform cloud cover prevailed.

6 Discussion

The result presented in the last Chapter are discussed here in the same order. In the first section the albedo measurements are assessed. Then, the discussion on directional parameters luminance and spectral radiance is given. The last section comprises the assessment of spectral irradiance.

6.1 Albedo

This section is divided into the discussion on methodical uncertainties and the effect of snow grain size and solar zenith angle on albedo.

6.1.1 Methodical Uncertainties

The albedo measured at Neumayer agrees to within $\pm 6\%$ with the albedo of a snow surface experimentally determined in previous studies (GRENFELL et al., 1994; SMOLSKAIA et al., 1999). Uncertainties due to the way of measuring the albedo with only one sensor have to be discussed. Two main sources of errors based on the method to measure albedo lead to uncertainties:

- shadowing effect of the equipment,
- levelling of the sensor after rotating the rod.

Shadowing effect

To determine the shadowing effect of the equipment, the reflectivity of the temperature stabilised box has to be known (see Section 4.3.1). The temperature stabilised box is made of aluminium, which is dull and scratched due to outdoor use and multiple transports. Further, some patches needed for transportation purposes stick on the outside of the box. Therefore, the reflectivity of the box varies across its surface. To determine the albedo of the box multiple measurements at different positions are necessary to be able to attain the mean reflectivity. It was not possible to determine the reflectivity of the temperature stabilised box at IMUK. To determine the reflectivity of a surface according to DIN 5036 (1979),

a spectralon plaque of known reflectivity is needed, which had not been available. This was the reason for relying on a reflectivity value of sand-blasted aluminium determined by KÖNIG and ADEN (1999).

A counter argument for using particularly the reflectivity of this type of aluminium is based on the fact that the spectral reflectivity varies drastically for different types of aluminium. Especially in the UVB, some types of aluminium have a much lower reflectivity compared to the visible (Seckmeyer, 2004, personal communication). If the box of the IMUK spectroradiometer had such a low reflectivity in the UVB, the correction factor applied for the shadowing effect in Section 4.3.1 would be spectrally dependent. The correction factor would be larger, the shorter the wavelength. The upper limit of the correction factor would be 3% of the measured reflected irradiance because this is the fraction of the FOV covered by the equipment. With the reflectivity of 0.45 determined by KÖNIG and ADEN (1999) the reflected irradiance was only underestimated by 1.65% as the equipment does reflect 45% of the incident irradiance. With a lower reflectivity of the aluminium box, the reflected irradiance would still be underestimated by up to 1.35%. Thus, the remaining systematic uncertainty of the measured reflected irradiance is 1.35%. If the albedo in the UV was higher by 1.35% due to the underestimated reflected irradiance the observed decline in albedo towards shorter wavelengths in the UV may be an artefact of the spectrally independent correction factor applied. Providing the correction factor increases with decreasing wavelength, the albedo would remain high in the UV range with values between 0.97 and 1 (see Figure 5.2).

Uncertainty due to levelling the detector

Another source of uncertainty arises from turning the rod to level the detector between measurements of incident and reflected irradiance measurements. Exact levelling of the detector parallel to the horizontal is not possible because it could not properly be controlled. Therefore the same effect as for an albedo of a tilted surface can be expected. GRENFELL et al. (1994) observed albedo for a surface with a slope of 2% and a solar zenith angle of 70°. The variation in albedo is about 20% giving apparent albedo values between 0.89 and 1.08, depending on the direction of the slope and the position of the sun relative to the slope. For high sun the slope effect is modest, but at large SZA typical for polar latitudes, it increases rapidly. A perfectly flat surface is almost impossible to encounter on an Antarctic ice shelf as most areas are covered by sastrugi (snow dunes). Such sastrugi vary in dimension. Their height can range from a few centimetres to 50 cm and more. In the horizontal one sastrugi can extend over several metres. Sastrugi tend to reduce the albedo, which is explained in detail by WARREN et al. (1998).

The mislevelling of the sensor is most probably the reason for the outlier albedo value of 1.02 in Figure 5.5. Also the mean spectral albedo being larger than unity on 5 January 2004 can also be explained by the mislevelling (see Figure 5.1). An albedo larger than unity is most likely to be seen during cloud free periods such as on 5 January 2004 (see Figure 5.20). On cloudless occasions the reflectance of the snow surface has a larger directional component compared to overcast situations (DIRMHIRN and EATON, 1975). However, since the error based on the inaccurate levelling of the detector occurs randomly over the day, the error is reduced the more albedo values are measured.

Assessment of uncertainties

A quantification of the overall uncertainty is difficult as it is hardly possible to quantify each single uncertainty. It could be argued that the spectral behaviour of the snow albedo measured at Neumayer resembles the modelled spectral snow albedo (see Figure 5.2) thus providing an excellent result. The modelled snow albedo also decreases with decreasing wavelength. It accounts for the extreme anisotropy of scattering by snow particles using the δ -Eddington approximation for multiple scattering (LENOBLE, 1993), together with Mie theory for single scattering (LIOU, 1980). This model has neither been validated with spectral measurements of high resolution nor for the UV. To be sure of a reliable performance of the snow albedo model a profound validation needs to be performed. Until then, it cannot be proven whether the slight decrease in albedo in the UV is an artefact due to the shadowing effect of the equipment.

6.1.2 Effect of SZA and Snow Grain Size on Albedo

Effect of SZA

In previous studies, for example by GRENFELL et al. (1994) or WISCOMBE and WARREN (1980), an increase in albedo for increasing SZA is observed. In contrast, if a dependence of the albedo on SZA can be observed in our measurements, albedo decreases with increasing SZA by 0.08 for a SZA ranging from 48° at 12:30 UTC to 63° at 17:40 UTC (see Figure 5.3). On most days no dependence on SZA has been observed at all (see Figure 5.5). For a closer investigation, the albedo of snow is modelled according to WISCOMBE and WARREN (1980). Input parameters are the equivalent depth of liquid water in the snow pack ($0.1\text{g}/\text{cm}^2$), the mean grain radius ($100\mu\text{m}$), the albedo of the underlying surface (1.0) and a variable SZA. The ratio of spectral albedo modelled with different SZA has been calculated (see Figure 6.1). In both albedo ratios the albedo modelled with the larger SZA is in the denominator. Both ratios are below unity by 1 to 3% depending on the chosen SZA and the wavelength considered. Thus, the albedo

6 Discussion

is larger for a larger SZA. Under a cloudless sky, the snow albedo increases with increasing SZA because of the strong forward scattering from the snow grains in the snow cover (DIRMHIRN and EATON, 1975; LI and ZHOU, 2003).

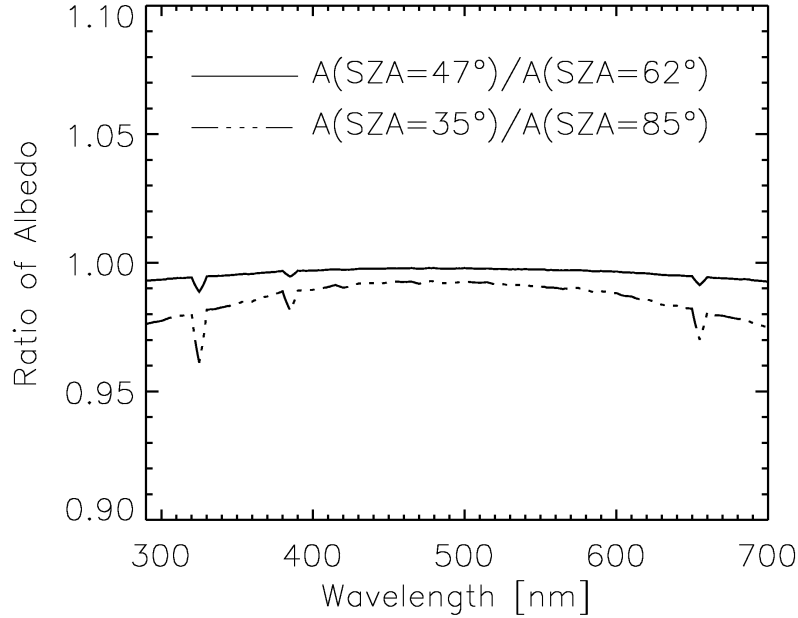


Figure 6.1: Ratios of modelled snow albedo (A) for varying SZA. In both cases, the ratio is between 0.96 and 1.0 for all wavelengths. Thus the albedo is larger at larger SZA compared to smaller SZA. The local minima at 320, 385, and 650 nm are due to Mie scattering processes. This phenomenon will be explained in more detail in the context of Figure 6.3.

The deviation from unity is lowest around 460 nm, increasing towards longer as well as shorter wavelengths. The ratio of albedo spectra modelled with a SZA of 47° and 63° represents the total range of SZA under which albedo measurements at Neumayer have been performed. The deviation from unity for this ratio is always below 1%. A more sophisticated model developed by LI and ZHOU (2003) also shows a low dependency of albedo on SZA for the UV and visible wavelength range.

The albedo spectra measured at Neumayer with the same SZA, but at different times (morning and/or afternoon; different days) even show a deviation of clearly more than 1% (see Figure 6.2). The difference in albedo spectra is lowest at 400 nm with 0.08 and it becomes larger the larger the wavelength. These observed differences in albedo spectra with the same SZA are based on other parameters, such as snow grain size or cloud conditions. Thus, it is impossible to

6 Discussion

extract a dependency of the spectral albedo on SZA for our measurements.

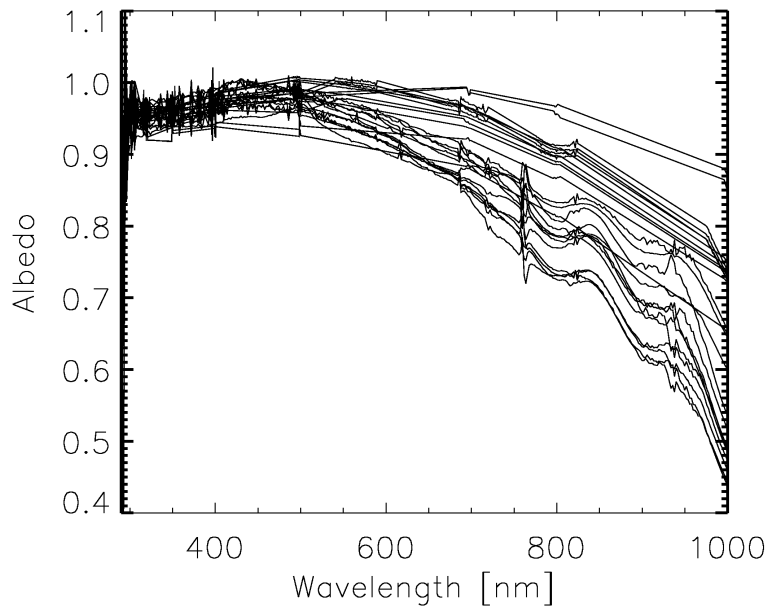


Figure 6.2: All of these albedo spectra are measured at Neumayer with solar zenith angles between 48° and 49° on different days and times (morning and/or afternoon). The difference in albedo spectra is lowest at 400 nm with 0.08 and it becomes larger the larger the wavelength.

During the afternoon of 4 January 2004 a decline of albedo for increasing SZA is observed with three different instruments (see Figure 5.3). This dependency is opposite from the one predicted by theory (GRENFELL et al., 1994; LI and ZHOU, 2003). A possible levelling error cannot be the source for this observed diurnal cycle, because particularly the AWI instruments are checked regularly and do not need to be rotated. They are mounted to a permanent frame (see <http://www.awi-bremerhaven.de/MET/Neumayer/radiation.html>). The reason for this opposite dependence of albedo on SZA is more to likely be based on changing snow conditions due to the steady solar insolation. Albedo under a cloudless sky is much more difficult to measure than albedo under a diffuse sky (GRENFELL et al., 1994). This is based on the lacking direct component of incident irradiance for the diffuse (overcast) case. Under diffuse sky conditions, a diurnal dependence of albedo on SZA has not been observed at all (see Figure 5.4). This may be due to the wavelength region measured on this day, which was limited to the UV.

The deviation in absolute albedo in Figure 5.3 is due to the different wavelength sensitivities of the radiation sensors. The AWI pyranometers integrate the incoming radiation from 300 to 3000 nm, the SL501 has a response similar to the erythemal action spectrum (MCKINLAY and DIFFEY, 1987). The spectral measure-

ments have been averaged over short wavelength intervals from 304 to 1004 nm to display the diurnal cycle. As the SL501 is mainly sensitive to wavelengths in the UVB, it shows the highest albedo on an absolute level. The spectrally averaged albedo comprises not only UV, but also visible wavelengths and reaching up to 1004 nm, thus being slightly smaller than the SL501 albedo. The albedo derived from pyranometer data is lowest because the largest portion of infrared radiation is included. The location of the AWI instruments is about 200 m north of our measuring site (see Figure 4.2). Thus, they detect albedo over a different field of snow providing independent results.

Effect of snow grain size

It can be seen in Figure 6.3 that the influence of different snow grain sizes on albedo is larger than the effect of SZA. The grain size of the snow flakes increases as the snow ages (WISCOMBE and WARREN, 1980). The albedo is modelled again with the tool SNOWALBEDO. The parameters are the same as in Fig. 6.1, but the SZA is constant with 50° . The influence of the grain size is lowest at 460 nm. Between the largest particle (800 μm) and the smallest particle (54 μm) possible to use as input parameters into SNOWALBEDO the deviation in modelled albedo is 9% for 300 nm as well as for 700 nm. It is roughly 4% for 460 nm. The local minima seen at 315, 380 and 650 nm are due to the fact that the model results are based on Mie-calculations applying single grain sizes and not grain size distributions which occur in nature. Interferences cause these local minima. They appear when the grain size is, for example, a whole-numbered multiple of the wavelength. They would disappear if the model used a real grain size distribution. Thus, these features seen especially in the black ratio have a physical explanation and are therefore not observable in the measurements.

Snow grain size has not been determined for Neumayer station during the albedo measurements. However, investigations on snow grain size by GAY et al. (2002) suggest surface grain sizes of 100 to 200 μm for a variety of Antarctic locations. According to Table 5.1 snow fell on 2 January 2004, so the albedo should be larger on this day compared to the following days. Another factor responsible for the aging of snow is the temperature. As snow melts the grain size increases drastically LEFEBRE et al. (2003).

The dependence on grain size is indicated in our measurements (see Table 5.1). Snow fell on 2 and 3 January 2004. The albedo is expected to increase after such an event. The daily mean albedo measured with the SL501 shows an increase in albedo from 0.92 on 2 January 2004 to 0.94 on 4 and 5 January 2004. The SL501 albedo on 6 January 2004 may not be representative for the complete day, as it is based on a short time period of roughly one hour. The maximum temperature on 5 and 6 January reached positive values, thus the mean grain radius increased

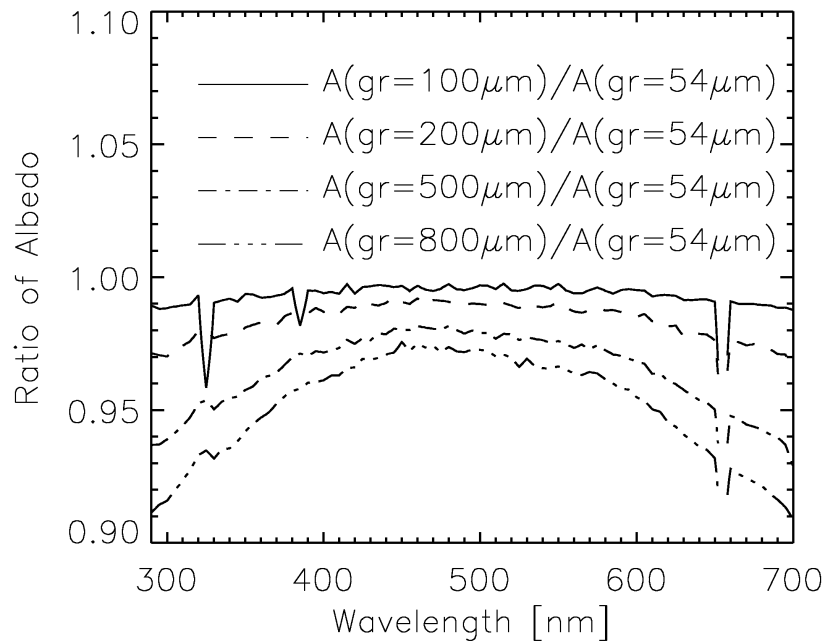


Figure 6.3: Ratios of snow albedo (A) modelled with different grain size radii. The larger the grain size the lower the albedo. The local minima are due to Mie scattering processes. For more details, see text.

comparably fast. On 8 January 2004 a slightly lower albedo was observed as expected for a larger grain size. The low albedo on 2 January 2004 can also be explained by comparably large particle sizes due to high maximum temperatures during the previous days (i.e. 1.5°C on 29 December 2003).

Such dependencies are much more difficult to observe in the daily mean albedo spectra (see Figures 5.1 and 5.2). One reason is that they cross each other at different wavelengths. Another reason may be the method of measuring spectral albedo and the uncertainties originating in this method (see Section 6.1.1).

When snow albedo is determined experimentally, it is difficult to distinguish between its influencing factors. They have to be considered in a combined way when analysing measured snow albedo.

6.2 Luminance

Since it takes less than a minute to record one scan of sky luminance distribution, an almost instantaneous picture of the sky is obtained. The two different sky luminance distributions, shown in Figures 5.6 and 5.7, illustrate the differ-

ence based on the cloud situation. For the cloudless situation, the maximum sky radiance is observed in the aureole. This maximum occurs because of single scattering in the forward peak of the aerosol scattering phase function (LENOBLE, 1993). Aerosols in the Antarctic are advected by long range transport of their source region in the surrounding Southern Ocean (PIEL, 2004). The small local luminance minimum close to the aureole (see Figure 5.6) is not described in the scientific literature and a possible reason has not been found.

6.2.1 Horizon Brightening

The second feature observed under a cloudless sky is the horizon brightening (see Figures 5.6 and 5.8). Radiation originating from the horizon has the longest path through the atmosphere compared to all other viewing directions. Thus, multiple scattering occurs more frequently. This is the cause for the enhanced luminance observed close to the horizon in comparison with smaller viewing zenith angles.

Horizon brightening is stronger for larger SZA. The path of the direct beam through the atmosphere is very long for large SZA. Attenuation of the direct beam due to scattering is more likely with increasing SZA. Thus, scattered, i.e. diffuse, radiation is dominant for large in comparison with small SZA. Together with the increased possibility of multiple scattering for increasing viewing zenith angles the enhanced horizon brightening for large SZA is explained.

The high albedo of the snow surface further increases the horizon brightening compared to a low albedo surface, such as grass. This is already shown in Figure 5.9, where zenithal scans of normalised luminance measured at Boulder and Neumayer are shown. To compare the zenithal scans of normalised luminance measured over grass (Boulder) and snow (Neumayer), the ratio Boulder/Neumayer is shown in Figure 6.4 for a SZA of 86° and 48° .

Both ratios are below unity and decrease for increasing VZA. The ratio with a SZA of 86° deviates less from unity than the ratio at a SZA of 48° . Two questions arise:

1. Why does the high albedo of the snow covered surface enhance horizon brightening compared to a low albedo surface?

Due to the high snow albedo of about 0.98 at 550 nm (see Section 5.1.1) almost all incident radiation is reflected. Backscattering from atmospheric molecules is possible. The longer the path of the radiation through the atmosphere, the more reflection and backscattering events occur. In contrast, for a low albedo surface such as grass with an albedo of 0.09 at 550 nm (FEISTER and GREWE, 1995), the incoming radiation is almost completely absorbed by the surface. This prevents a reflection and in turn backscattering.

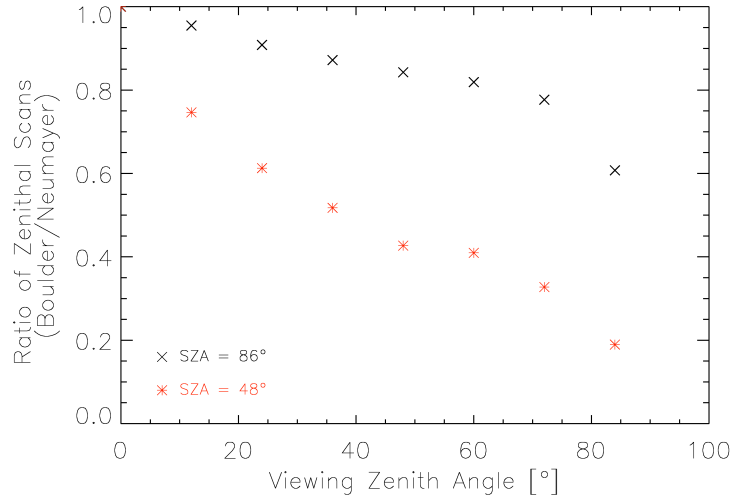


Figure 6.4: Ratios of zenithal luminance scans (Boulder/Neumayer) for two SZA. The zenithal scans on which these ratios are based, are shown in Figure 5.9. Both ratios are lower than unity and decrease for increasing VZA. This implies a stronger horizon brightening for a high albedo surface compared to a low albedo surface. For a detailed explanation, see text.

2. Why is the enhancement in horizon brightening due to a high albedo surface larger for smaller SZA?

Due to the shorter path through the atmosphere, the direct beam for low SZA is not attenuated as strongly as for high SZA. Therefore, the fraction of diffuse radiation on global irradiance is less for lower SZA compared to high SZA. For UV wavelengths at different SZA the ratio direct/global irradiance is shown by MAYER et al. (1997). In case of an albedo of 0.09 (grass) reflection of incident radiation at the surface hardly occurs. Therefore, the diffuse component of the global irradiance remains low at low SZA. In contrast, the highly reflective snow covered surface with an albedo of nearly unity allows a reflection of the incident direct irradiance also at low SZA. This facilitates backscattering by the atmosphere and leads to an enhancement in diffuse radiation compared to a surface with low albedo.

At high SZA the path of the direct beam is long and scattering events are more likely to occur before the photons reach the surface. Therefore, horizon brightening can also be observed for low albedo surfaces. However, the effect of horizon brightening is larger with increasing albedo.

Since these luminance measurements have been performed at different locations, parameters influencing the radiative transfer (e. g. aerosols, ozone column, alti-

tude) are not alike. Additionally, the Rocky Mountains arise west of the inter-comparison site at Boulder. It is most probable that an unobscured view of the horizon at a VZA of 84° is not guaranteed when measuring luminance westwards. In spite of these constraints, it has been shown that for these specific cases, horizon brightening is enhanced over a highly reflective surface. This enhancement is 80% and 40% for a SZA of 48° and 86° , respectively, thus being more pronounced for decreasing SZA.

6.2.2 Luminance under Overcast Sky

The diurnal cycle of zenith luminance shown in Figure 5.10 demonstrates that zenith luminance during cloudy situations exceeds the zenith luminance for a cloudless sky by one order of magnitude. This is to be explained by the dominant Mie scattering (LENOBLE, 1993) based on the presence of cloud droplets. Incident radiation is attenuated by the cloud droplets, which scatter the radiation in any direction. Some photons are scattered out of the clouds, some undergo multiple scattering events before they leave the cloud. This way, a quite uniform distribution of sky luminance for all VZA is observed under overcast conditions.

The local minimum stretching from east to west for all VZA (see Figure 5.7) needs to be addressed in more detail. Up to now, no explanation for this characteristic has been found. A first idea was that the container with all the instruments (see Figure 4.3) leads to a lower luminance due to its blue colour. Less radiation is reflected from the container compared to the snow surface surrounding it. The influence of the container was tested by turning the Skyscanner about 90° . After turning, the local minimum was observed in a north-south direction. Thus, the container cannot be its source. Discussions with the manufacturer did not lead to a solution to this problem so far. Currently, it is assumed that the Skyscanner itself interferes with the measurements. The order in which the different directions are measured is calculated for each scan by a method developed by TREGENZA (1987). It mainly depends on SZA. A systematic behaviour combining the order of scan points and the occurrence of the local minimum cannot be observed. Detailed experiments have to be performed in order to investigate this effect.

6.2.3 Link to Previous Studies

In the context of Antarctic radiation research, luminance measurements have been performed for the first time. Another novelty is the use of luminance data as ancillary data for the interpretation of spectral irradiance and radiance.

However, a range of luminance measurements and models exist (IGAWA et al., 1999; VIDA et al., 1999; INEICHEN, 1996), which are developed in the context of engineering topics. One application is to use the natural light effectively for a

low energy consuming daylight design of buildings (WALKENHORST et al., 2002; IGAWA et al., 1999). The luminance distributions discussed in these technical studies agree qualitatively with the Antarctic measurements. Horizon brightening as well as the aureole is observed for cloudless situations (VIDA et al., 1999). They do not focus on a varying surface albedo. Detailed comparisons are necessary to evaluate the connection between both approaches of luminance investigations and to quantify possible deviations.

6.3 Spectral Radiance

The spectral behaviour of radiance for different atmospheric conditions is explained. A discussion about horizon brightening focussing on the wavelength dependence follows. The last issue is the discussion on modelled vs. measured radiance.

6.3.1 Cloudless vs. Overcast Spectral Radiance

The shape of different spectra of radiance can be explained by scattering processes. One example is the difference between cloudless and overcast radiance spectra (see Figure 5.13). In a cloudless situation Rayleigh scattering is dominant. The strong dependence of Rayleigh scattering on wavelength (LENOBLE, 1993) leads to the steep decrease in spectral radiance with increasing wavelength. For cloudy situations Mie scattering at cloud droplets becomes the major process. Mie scattering is hardly dependent on wavelength (LENOBLE, 1993). Therefore, the spectral radiance hardly decreases with increasing wavelength.

The higher absolute radiance of the overcast compared to the cloud free radiance spectra is due to multiple reflections between the surface and the clouds. Enhancements in absolute irradiance levels due to a high surface albedo in combination with cloud cover have been observed before (KYLLING et al., 2000; NICHOL et al., 2003), however, not explicitly for radiance. The effect of snow cover on radiance has been investigated by HUBER et al. (2004), the effect of clouds by WEIHS et al. (2000). Both are case studies covering a limited range of atmospheric and surface conditions. The combined effect of clouds and albedo on spectral radiance has not been reported in the scientific literature so far.

The shift of the maximum radiance from 330 to 510 nm for cloudless and overcast situations, respectively, is also due to enhanced Mie scattering during cloudy situations in combination with the high surface albedo.

6.3.2 Horizon Brightening

An effect based on multiple scattering due to longer path lengths of radiation through the atmosphere for larger viewing zenith angles is the horizon brightening, which is shown in Figure 5.15. Even in Figure 4.7, a photograph of albedo measurement at the ice edge, the horizon brightening can virtually be seen. The dependence of horizon brightening on albedo and SZA has already been discussed for luminance in Section 6.2. Therefore, it is focused on the dependence of horizon brightening on wavelength in this section.

In general, horizon brightening increases the longer the wavelength. At short wavelengths in the UVB multiple scattering of diffuse irradiance occurs uniformly across the sky due to the strong wavelength dependence of Rayleigh scattering (LENOBLE, 1993). For radiation with long wavelengths, multiple scattering can only be produced by longer paths through the atmosphere, which is the case for directions close to the horizon. Therefore, inhomogeneous radiance distributions are better seen the longer the wavelength. A complete distribution of sky radiance could not be measured because of the long time needed to record a spectrum (see Section 4.5). Another restriction was the positioning of the tubus entrance optics, which is not yet automated. Therefore modelled distributions of sky radiance for different wavelengths are shown in Figure 6.5.

These sky radiance distributions have been modelled for a possible situation at Neumayer with a low SZA, no cloud cover and aerosols (clear sky). The albedo was set to 0.9 for all wavelengths. North is at the bottom of these distributions because downwelling radiance is shown resembling an upwards directed radiation detector. The position of the sun is marked by a black spot. The radiance is normalised to the zenith radiance. Horizon brightening is seen more clearly the larger the wavelength. At 305 nm, the radiance at the horizon is even lower compared to the zenith. At 695 nm the radiance at the horizon opposite the position of the sun exceeds the zenith radiance by a factor of 15.

In order to assess the influence of a snow surface compared to a grass surface, zenithal scans of radiance at different wavelengths have been modelled for a varying surface albedo (see Figure 6.6). The zenithal scan over a snow covered surface with a SZA of 82° represents the situation on 9 February 2004 around 20:15 UTC, which is shown in Figure 5.15. The albedo for grass according to FEISTER and GREWE (1995) has been used. Since FEISTER and GREWE (1995) present the albedo values only up to 800 nm, the zenithal scan at 1000 nm is omitted. In addition, both albedo situations have been modelled for a SZA of 48° . The input albedo for snow and grass in dependence of wavelength are shown in Table 6.1.

UV: For all UV wavelengths, horizon brightening is observed for the case with snow albedo and SZA of 48° . At 400 nm, radiance with a VZA of 86° exceeds the zenith radiance by a factor of 3.5.

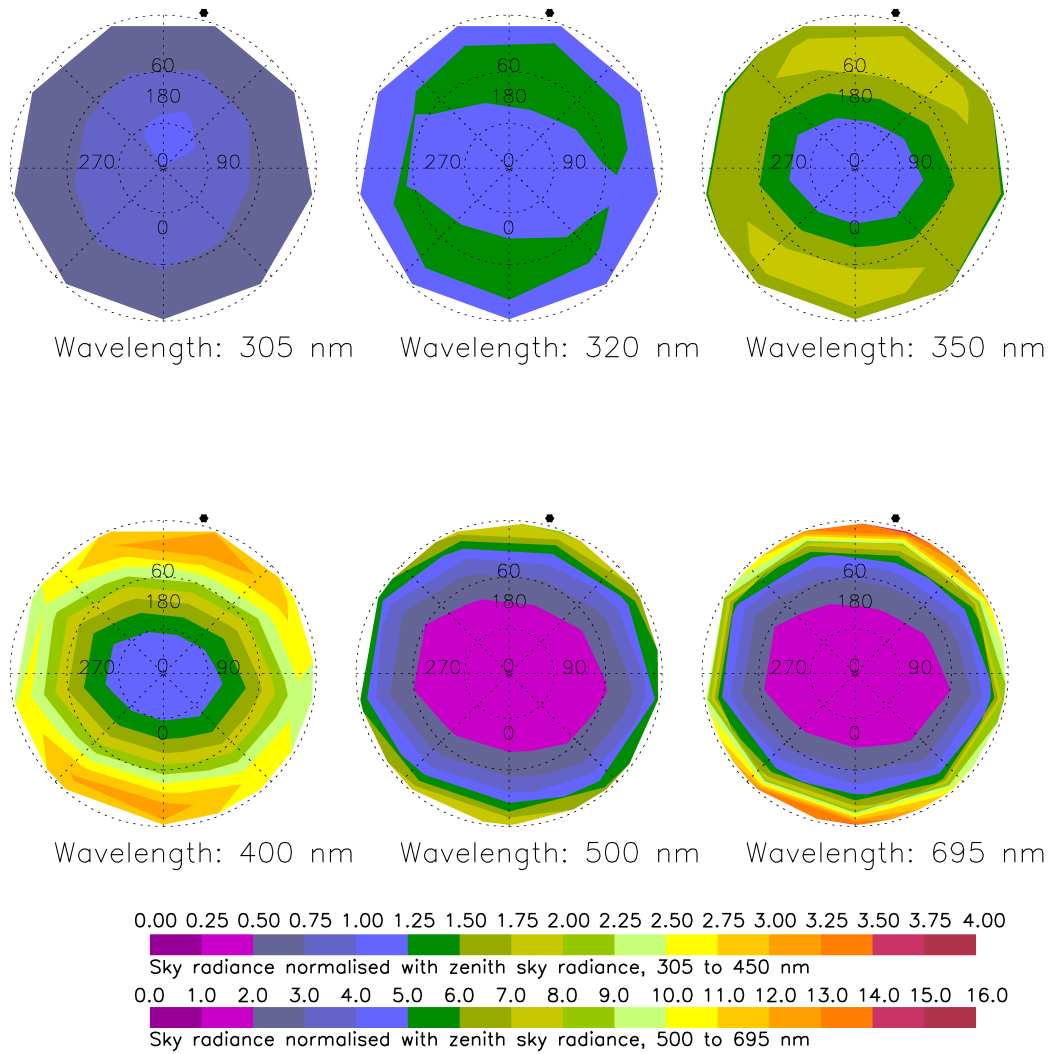


Figure 6.5: Modelled sky radiance distributions for different wavelengths. The input parameters have been chosen to resemble possible atmospheric conditions at Neumayer with high SZA. The black dot in the panels represents the position of the sun. Note the different legend scaling for 500 and 695 nm. Horizon brightening is more clearly seen the larger the wavelength. For more details, see text.

6 Discussion

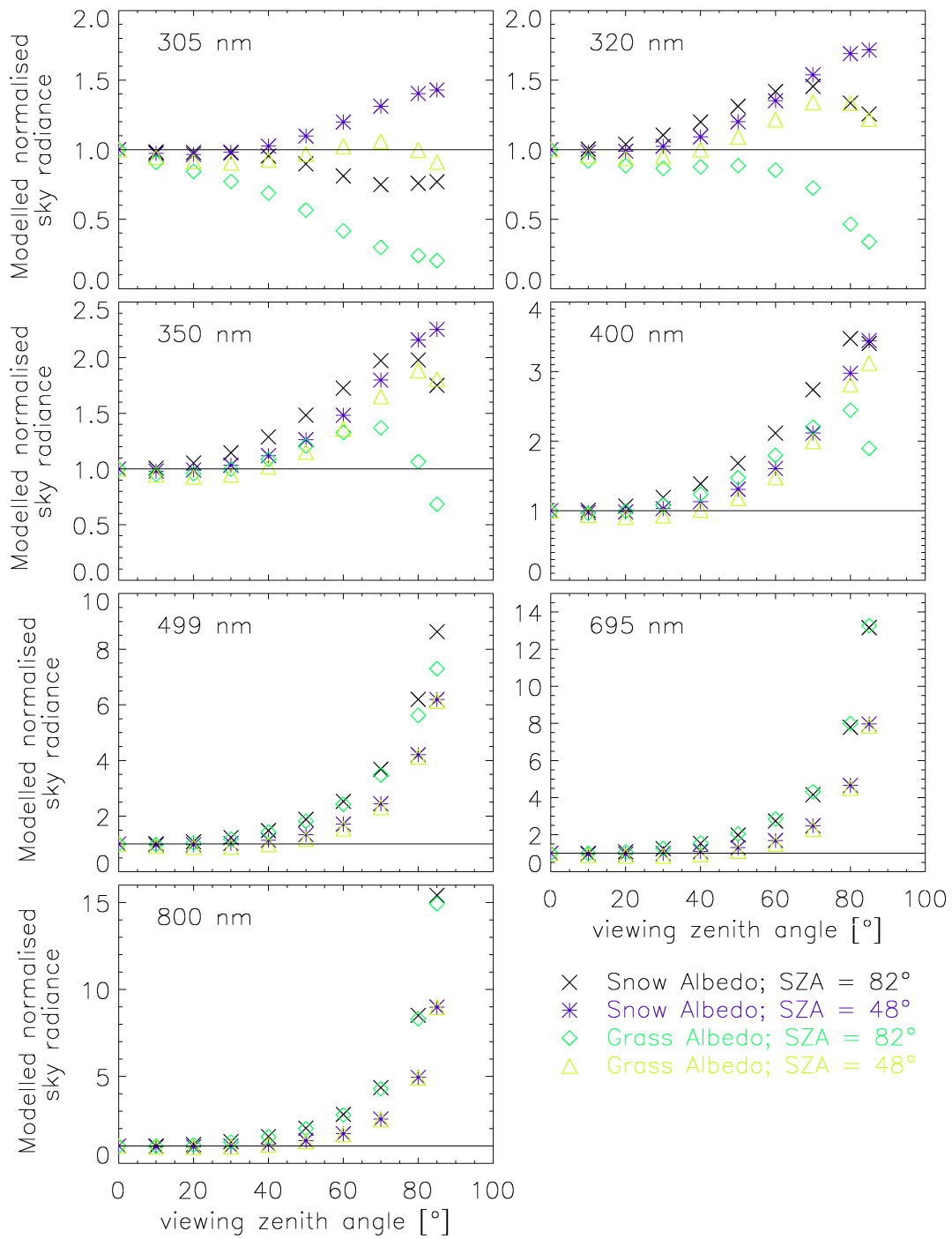


Figure 6.6: Modelled zenithal scans of radiance for a SZA of 82° and 48° over grass and a snow covered surface. For all cases, horizon brightening is seen for all wavelengths in the visible. In the UV, horizon brightening is only observed for the case with snow albedo and SZA of 82°. For more details, see text.

6 Discussion

Wavelength [nm]	Albedo of grass	Albedo of snow
305 nm	0.017	0.971
320 nm	0.017	0.961
350 nm	0.018	0.966
400 nm	0.022	0.967
499 nm	0.035	0.965
550 nm	0.089	0.962
695 nm	0.040	0.900
800 nm	0.587	0.830

Table 6.1: Albedo of snow and grass for different wavelengths. The albedo of grass is taken from FEISTER and GREWE (1995) and the albedo of snow was measured within this study at Neumayer on 4 January 2004.

For grass albedo and SZA of 82° , for example, the radiance decreases for increasing VZA for 305 and 320 nm. At 350 and 400 nm, the radiance increases up to a VZA of 70° , and then decreases again.

This maximal radiance at a VZA between 70° and 80° is also observed for the grass albedo at 48° SZA at 305, 320 and 350 nm as well as for the snow albedo at 82° at 320, 350 and 400 nm.

Visible: Horizon brightening is observed for all modelled cases. For both surface types, it is larger the larger the SZA. The maximum horizon brightening is observed at 800 nm with a factor of 15.5 for a VZA of 85° . At 695 nm and a VZA of 85° , horizon brightening for grass is slightly higher than for snow. At a SZA of 48° horizon brightening does not show a strong dependence on the type of surface.

To assess the effect of the different surface types, the ratio of the zenithal scans is calculated for a SZA of 82° and 48° (see Figure 6.7). Most of the ratios remain below unity, which means that the radiance is enhanced due to a highly reflective surface in comparison with a low albedo surface. This issue has already been discussed in Section 6.2.

To explain the spectral differences in the ratio of zenithal scans of radiance the UV and the visible wavelength ranges are considered separately:

UV: This enhancement due to a high surface albedo is more evident the shorter the wavelength. The reason is the strong wavelength dependence of Rayleigh scattering, which leads to more successive reflections between the surface and the atmosphere the shorter the wavelength. Atmospheric reflectance is maximal at 320 nm (LENOBLE, 1998). Therefore, it should be expected

6 Discussion

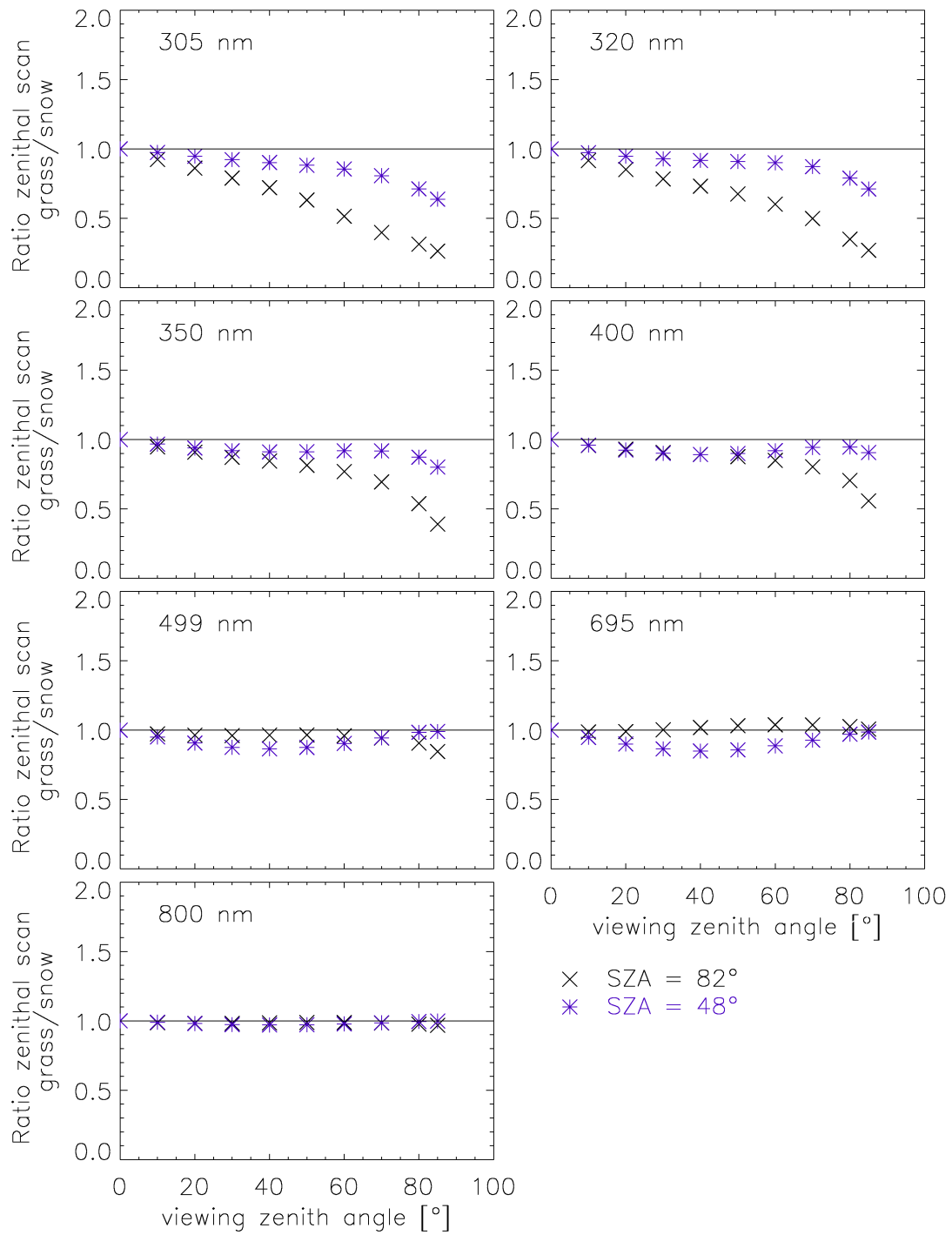


Figure 6.7: Modelled ratio of zenithal radiance scans for a SZA of 82° and 48° over a grass and snow surface. At an SZA of 48°, the ratio remains below unity for all wavelengths. This means that radiance over a highly reflective surface is enhanced compared to a surface with a lower albedo. For a SZA of 86°, the ratio is only below unity for 305 and 320 nm. For more details, see text.

6 Discussion

that the albedo effect decreases for decreasing wavelengths in the UVB, because of ozone absorption of the backscattered photons (SCHWANDER et al., 1999). However, the absence of tropospheric ozone leads to an increase of atmospheric reflectance for decreasing wavelength (LENOBLE, 1998). For an Antarctic site, tropospheric ozone can be expected to be well below the global average (PRATHER et al., 2001). Therefore, an increase in the albedo effect for decreasing wavelengths, even in the UVB as seen in Figure 6.7, is explained.

Visible: The deviation from unity is less than 20% for all VZA and wavelengths. At 800 nm both ratios deviate from unity by only less than 5% for all VZA. At 695 nm and an SZA of 82°, the ratio grass/snow is even larger than unity by about 5%. This indicates an enhanced horizon brightening for a grass surface. This is in contradiction with the results derived from the luminance measurements shown in Figure 6.4. The dependence of radiance on VZA is hardly influenced by different types of surface albedo. Another reason for the weak dependence of the albedo effect for visible wavelengths is that atmospheric scattering is negligible (LENOBLE, 1993).

To better compare the measured luminance and the modelled radiance zenithal scans for a grass and snow surface radiance zenithal scans are also modelled for 550 nm. This is the wavelength where luminance is most effective (see Figure 4.9). Figure 6.8 shows that especially for a SZA of 82°, horizon brightening is stronger for a grass surface. This can be seen in the upper panel, where the zenithal scans over grass and snow are displayed for solar zenith angles of 82° and 48° are depicted. The ratios of zenithal scans for each SZA in the lower panel underline the stronger horizon brightening for a grass surface at an SZA of 82°. This behaviour was not expected, as it contradicts the luminance measurements even more than the results for 695 nm discussed above. The discrepancy between measured luminance and modelled radiance zenithal scans may originate in the

- luminance measurements over grass at a VZA of 84° being affected by the obscured view of the horizon due to the Rocky Mountains (see Section 6.2.1). However, higher normalised radiance is also seen at lower VZA in Figure 6.8. Thus, the obscured horizon cannot be the (only) explanation.
- model not being validated for radiance and this spectral range.

More radiance measurements and model calculations need to be performed in order to solve this open question. Unfortunately, this was beyond the scope of this study. When investigating this problem, more extensively, it should also be focussed on the ratio of direct to diffuse irradiance in dependence of SZA

6 Discussion

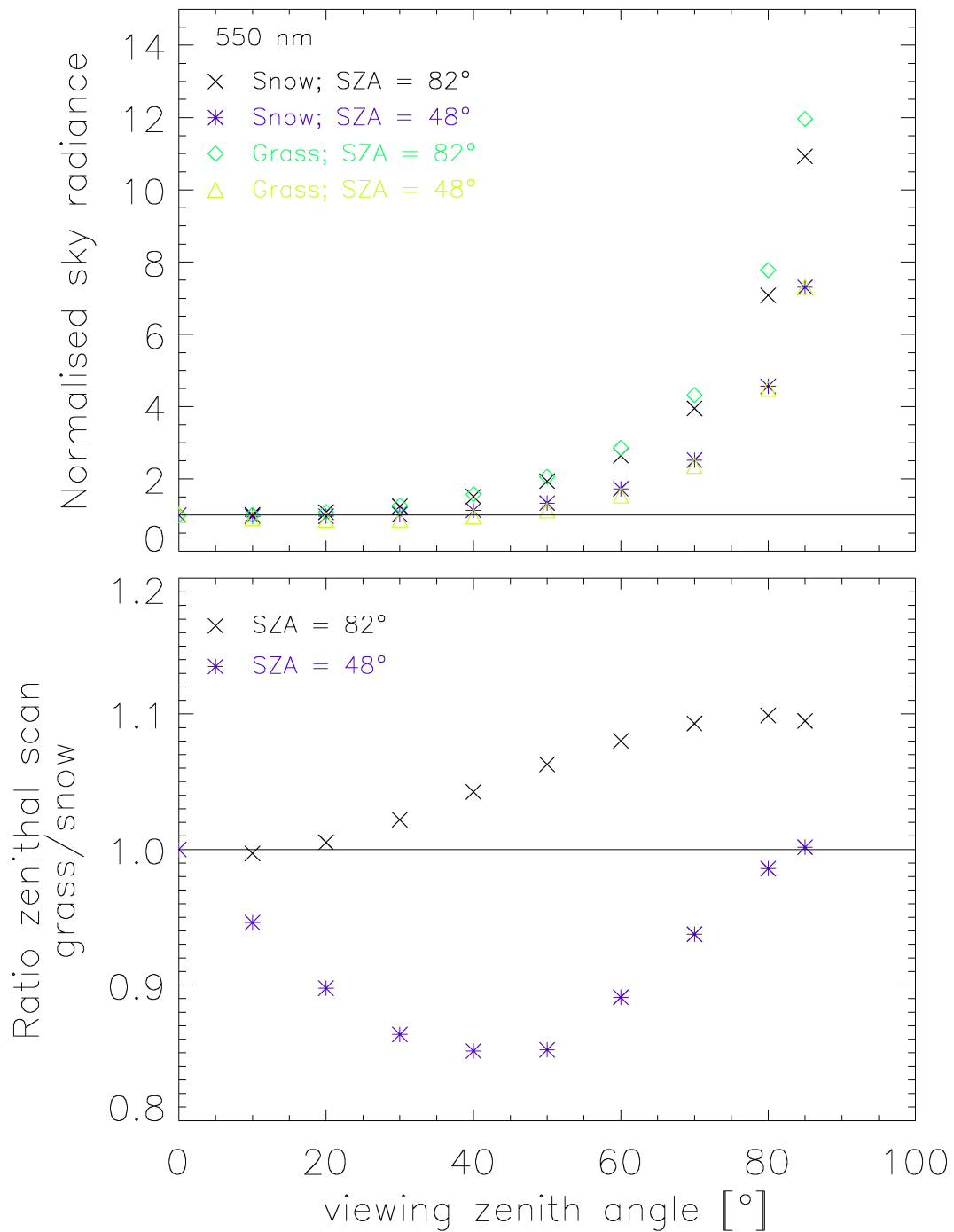


Figure 6.8: Upper Panel: Modelled ratio of zenithal radiance scans for a SZA of 82° and 48° over a grass and snow surface for 550 nm. Enhanced Horizon brightening is observed for grass at a SZA of 82°. Lower Panel: Ratio of the zenithal scans shown in the upper panel for each SZA. The enhancement in horizon brightening over grass amounts to 10% at a VZA of 80°. This behaviour is discussed in the text.

and wavelength. This ancillary information may deliver the necessary hints to understand the effect of horizon brightening over different types of surfaces.

The only investigations on radiance over a snow covered surface reported in the scientific literature have been conducted by HUBER et al. (2004). They compared radiance measurements over an inhomogeneously snow covered surface (albedo = 0.4) with model results corresponding to a situation with homogeneously snow covered ground (albedo = 0.8). For a SZA of 45° , they observe an enhancement in radiance of 40% at a VZA of 80° due to the snow covered surface at 310 and 350 nm. The corresponding enhancement shown in Figure 6.7 is only 12% (SZA = 48° , VZA = 80° , $\lambda = 350$ nm), even though the difference between grass and snow albedo equals 0.948 (see Table 6.1). A reason for this discrepancy has not been found so far. However, it shows the complexity of this problem and presents the need for additional experimental and modelling studies in order to investigate the effect of varying albedo on spectral radiance.

Another discrepancy arises from the modelling results of the zenithal radiance scans when compared to the experimentally determined zenithal luminance scans (see Section 6.2). The result of the zenithal luminance scans was that horizon brightening is increased due to the highly reflective snow surface. This cannot be observed for all of the visible wavelengths in Figures 6.6 and 6.7. It would have been favourable to have also modelled a zenithal radiance scan for 550 nm. However, as the three zenithal radiance scans in the visible wavelengths do not behave much differently from each other, it is not expected to see a completely different behaviour for a modelled radiance scan at 550 nm. The albedo of grass is 0.089, thus not much different from the albedo at 499 or 695 nm (see Table 6.1). In the next section, the relation of modelled to measured radiance is discussed. An extensive discrepancy between model and measurement is seen for the visible, so that the model performance for these wavelengths is questionable and should be viewed with care.

6.3.3 Measured Compared to Modelled Radiance

Measured radiance during cloud free conditions has been compared to modelled radiance for various wavelengths (see Figure 5.16). The deviation between model and measurement depends on wavelength as well as on SZA. The various sources for these deviations are found in both, the measured absolute spectral radiance and the model calculations.

Absolute radiance calibration

The absolute calibration of radiance as described in Section 4.5.2 involves uncertainties, that can partly be eliminated by improving the calibration procedure in

future. The main shortcoming is that no calibrated reflectance plaque had been available. By measuring the calibration lamp directly only part of the input optic is illuminated by the lamp. In case of an inhomogeneous optical fibre bundle the entrance slit of the monochromator is not evenly illuminated. This can be achieved by a diffuse radiation source such as a calibrated reflectance plaque. Radiance calibrations employing such a reflectance reference are described by MUELLER et al. (2003) or MEISTER et al. (2003). Diffuse illumination of the entrance optic for radiance measurements is important as the sky light also illuminates the entrance optic in a diffuse way.

Performance of input tubus

It is assumed that incident light originating from about 70° to 80° from the 0° -direction is reflected inside the tubus and thus reflected. This malfunction is supported by various factors.

Design of the input optic: Reflections of light inside the input tubus are possible because it is not black inside. Further, it is comparably short (10 cm) and has a wide FOV (4.4°). In contrast, the input tubus deployed by BLUMTHALER et al. (1996) and shortciteNhuber2004 is 30 cm long and has a FOV of only 1.5° .

FOV measurement: In Figure 3.3, local maxima at $\pm 70^\circ$ are seen. These are by one order of magnitude larger than the values at angles of about 10° to 60° from the centre and by four orders of magnitude lower than the maximum at 0° . Diffuse sky radiance is typically four to five orders of magnitude below the direct irradiance of the sun (GRÖBNER, 1996). Thus, the depression of reflected light may not be sufficient.

Diurnal cycle of zenith radiance: The diurnal cycle of zenith radiance (see Figure 5.12) shows local maxima at 6:00 as well as 18:30 UTC for wavelengths larger than 499 nm. A detector based problem can be excluded as at 499 nm the PMT is active, whereas the silica diode is addressed for wavelengths longer than 500 nm. So both detectors show these local maxima. The SZA at 6:00 and at 18:30 UTC is 70.5° and 68.6° , respectively, which would support the assumption of detecting reflected direct sun light inside the tubus.

Comparison with diurnal cycle of luminance: The diurnal cycle of luminance (see Figure 5.10) does not show these local maxima at SZA of about 70° . Therefore, these maxima have to be based on a malfunction of the tubus input optic.

For these reasons the maximum deviations between measurement and model are observed, when the angle between the position of the input tubus and the sun is about 70° to 75° . As most radiance measurements are performed for the zenith, the SZA describes this angle of difference. Thus, the maximal deviations in Figure 5.16 are observed at a SZA of 75° . Since not all radiance measurements have been performed for the zenith direction, a few ratios between model and measurement remain at 1.2 to 1.4 independent of SZA. This feature is stronger the longer the wavelength because the direct component of the incident irradiance is larger the longer the wavelength (SECKMEYER, 1997).

Accuracy of input parameters

Total ozone column: The deviation between measured and modelled radiance at 305 nm is larger compared to the longer wavelengths in the UV. This is due to the total ozone column not adequately known. TOMS data were used as input parameter. However, TOMS is known to overestimate total column ozone for Antarctic sites by 4 to 10% (BERNHARD et al., 2002), see also Section 6.4. Thus too much radiation is absorbed leading to lower radiance values. Decreasing the ozone column would lead to a reduction in the modelled radiance, and thus in a smaller deviation between model and measurement at 305 nm. Especially for SZA larger than 80° the TOMS data should be used carefully according to MCPETERS and LABOW (1996). Despite these concerns, TOMS data have been used because they provide a complete data set for the days that have been modelled. It could be argued to use the Microtops total ozone column from the second channel. This issue will be discussed in more detail in Section 6.4.

Aerosols: Aerosols have not been included in the model as aerosol information was not available. However, the assumption of zero aerosols is justified as the Antarctic atmosphere is known to be very clean (PIEL, 2004).

Polarisation: Polarisation has also not been accounted for. Radiance is not evenly polarised across the sky (HUBER et al., 2004; SECKMEYER et al., 2004; LIU and VOSS, 1997). When neglecting polarisation in radiative transfer calculations the error varies approximately between -8% and +8%. The error is negative on the side of the sun (neglecting polarisation underestimates the radiance), and positive (overestimation) on the opposite side (SECKMEYER et al., 2004). However, the error decreases with increasing surface albedo (MISHCHENKO et al., 1994). As radiance has mostly been measured opposite the sun, the modelled radiance overestimates the true value. Including polarisation would decrease the model result leading to a better agreement between measured and modelled radiance.

The response of the IMUK spectroradiometer with the input tubus as entrance optics is not dependent on the polarisation of the incoming radiation. This was tested in the IMUK radiation laboratory by placing a linear polarising filter between the entrance optic and a 100 W calibration lamp. The filter was turned in steps of 45° . The response of the IMUK spectroradiometer only changed within $\pm 1\%$ for all wavelengths between 250 and 1000 nm, which is the achievable accuracy when repeating measurements of a 100 W calibration lamp. Thus, the measured absolute radiance is not dependent on the degree of polarisation of the sky radiance. Only the model results convey an uncertainty based on polarisation.

Atmospheric profiles: The atmospheric profiles used to model radiance have been provided in the libRadtran package. They refer to a subarctic summer situation. Antarctic profiles have not been used because they are not contained in the standard version of libRadtran. BERNHARD et al. (2002) remark that especially the ozone and temperature profiles used in the model have an important influence on its performance, particularly for large SZA.

Model performance

Up to date, UVSPEC has not been validated for radiance in the complete wavelength range. However, the comparison between UVSPEC and results from a successive orders of scattering (SOS) radiative transfer code, kindly provided by Prof. Jacqueline Lenoble, Université Joseph-Fourier, Grenoble, France, indicates that the performance of both models seems to be satisfactory in the UV (see Figure 6.9). Both models have been evaluated in a model intercomparison for spectral irradiance performed by VAN WEELE et al. (2000). The deviation of up to 20% seen at 305 nm may be due to mid latitude atmospheric profiles used in the SOS code. However, these few model ratios of zenith radiance are too sparse to draw a final conclusion.

Additionally, the visible and near infrared up to 1050 nm is the spectral region with the largest deviations between model and measurement. For wavelengths larger than 500 nm, molecular absorption in the atmosphere has to be considered. In this study, the absorption parameterisation according to RICCHIAZZI et al. (1998) has been employed. This parameterisation is certainly not as accurate as, for example, line-by-line calculations (EDWARDS, 1992).

For a proper validation of the model, the input parameters would have to be known with a better accuracy. Furthermore, a wide range of atmospheric conditions needs to be considered to test the model with the largest possible combination of input parameters. Only this way, statistically significant results can be obtained.

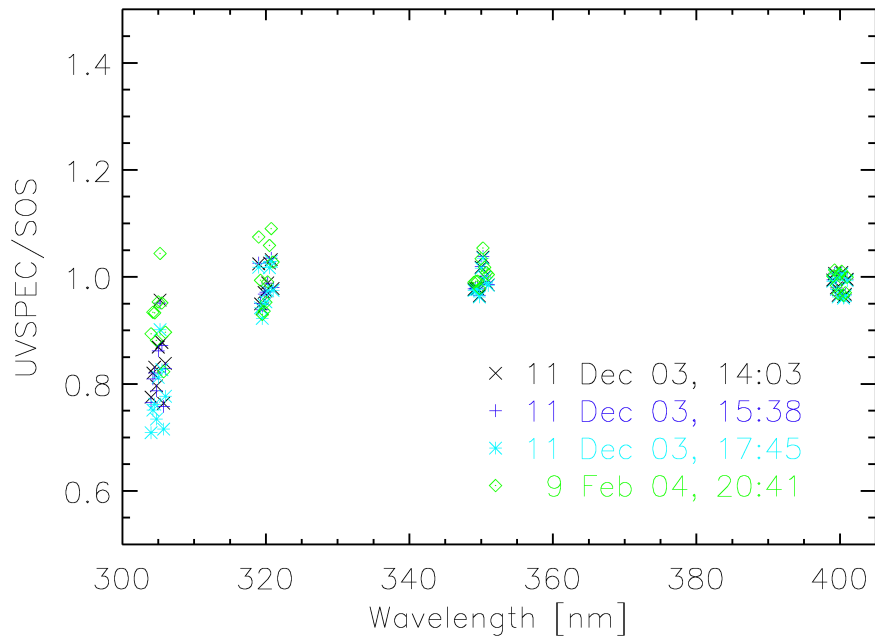


Figure 6.9: Ratios of zenith radiance modelled with UVSPEC and a successive orders of scattering code for selected situations.

6.4 Spectral Irradiance

The spectral irradiance measurements have mainly been performed to provide a connection between the radiation measurements performed at Neumayer and the NSF stations. Further, the spectral irradiance measurements for cloud free situations have been compared to model calculations.

6.4.1 Measured Compared to Modelled Irradiance

The comparison of modelled to measured irradiance shows a dependency on SZA for wavelengths larger than 500 nm (see Figure 5.17). This behaviour is due to the non-ideal cosine response of the irradiance input optics. The larger the wavelength the larger the portion of the direct relative to the diffuse irradiance (BERNHARD et al., 2002). Radiation at short wavelengths is scattered much more according to the inverse wavelength dependence of Rayleigh scattering (LENOBLE, 1993). Further, the larger the SZA the more pronounced is the deviation of the input optics from the ideal cosine response, even though the diffuser is already shaped. This is also supported by Figure 3.2, which already indicates that the cosine response at short wavelengths and low SZA shows a lower deviation from unity.

The larger deviation between model and measurement at 305 nm is due to an inaccurate total ozone column. Originally, the Microtops total ozone column was intended to be used because previous investigation have shown an excellent performance of the Microtops ozone channel 2 for various locations (Labow, 2003, personal communication). It can be seen in Figure 5.19 that the Microtops channel 2 underestimates the total ozone column compared to TOMS by 8% on average. This is in accordance to results stated by BERNHARD et al. (2002) that the TOMS data overestimate the total ozone column by 4 to 10%. Despite all these arguments in favour of Microtops data, TOMS total ozone has been used. If a lower ozone column had been used as an input into UVSPEC the deviation between measurement and model would be lower.

6.4.2 Relation to other Measuring Sites

The time series of the UV integral in Figure 5.18 are only preliminary results to compare spectral irradiance from Neumayer with spectral irradiance from other Antarctic sites, in particular the NSF sites. A comparison of spectral irradiance should at least include a comparison of

- various daily doses (e. g. UVB, UVA, UV, DNA, CIE) to account for the different radiation parameters at each station;
- situations with similar atmospheric conditions to be able to find reasons for possible differences;
- factors influencing UV irradiance, such as ozone, clouds or aerosols.

Since the investigation of the directional radiation parameters and snow albedo have been emphasised, the comparison of spectral irradiance in relation to other measuring sites was beyond the scope of this study.

7 Conclusions

In this study, the new IMUK spectroradiometric system has been developed to measure spectral radiance and irradiance in a wavelength range from 280 to 1050 nm in adverse Antarctic conditions. It has been shown that the IMUK spectroradiometer complies with the NDSC standards for UV spectroradiometry when detecting spectral irradiance. It will be possible to use the IMUK spectroradiometer as a travelling standard on behalf of the NDSC. Furthermore there is now an instrument that is capable to measure solar irradiance and radiance in a wavelength range from 250 to 1050 nm. Thus, the spectral UV data of the IMUK instrument are of high quality and serve as a basis to achieve the objectives of this study.

7.1 Assessment of Objectives

Overall, the campaign at Neumayer to measure solar spectral irradiance and radiance, as well as luminance and albedo has been a success. The spectroradiometer worked reliably throughout the complete duration of the campaign. After all, technical support and availability of spare parts at Neumayer was much better than expected prior to the campaign. In the following sections, the most important results are summarised and each single objective are assessed.

7.1.1 Characterising Luminance and Spectral Radiance

Zenith luminance for overcast situations is larger by one order of magnitude compared to cloudless situations. The maximum luminance occurs during cloud free situations in the aureole. For cloudless situations, in contrast to overcast skies, horizon brightening is observed. Over a snow covered surface at a viewing zenith angle of 84° the luminance exceeds the zenith luminance by a factor of 8.2 and 7.6 for a solar zenith angle of 86° and 48° , respectively. Over a surface covered by grass this factor only amounts to 4.9 for a solar zenith angle of 86° . Horizon brightening over grass for a solar zenith angle of 48° is hardly noticeable, with the luminance at a viewing zenith angle of 84° being only 1.4 times larger than the zenith luminance. Under an overcast sky, horizon brightening is not observed at all. The reason for the horizon brightening can be explained by scattering processes in the

7 Conclusions

atmosphere as discussed in Chapter 6. Horizon brightening is enhanced over a snow covered surface (high albedo) compared to grass (low albedo). At a viewing zenith angle of 84° this enhancement amounts to 80% and 40% for solar zenith angles of 48° and 86° , respectively.

Spectral radiance measurements show the radiance distribution over the sky being less homogeneous the larger the wavelength. This is also confirmed by model results. At 305 nm, the radiance at the horizon is only about 80% of the zenith radiance. At 1000 nm, the measured radiance opposite the position of the sun exceeds the zenith radiance by a factor of 11.

Model calculations of spectral radiance show that an enhancement of horizon brightening due to a snow covered surface cannot be seen for 695 and 800 nm. Horizon brightening is more pronounced the shorter the wavelength. At a solar zenith angle of 82° , the enhancement in radiance close to the horizon due to a high compared to a low surface albedo is 73% and only 16% at 305 and 499 nm, respectively. The radiative transfer model has neither been validated for irradiance in the visible and infrared spectral region nor for spectral radiance from 280 to 1050 nm. Thus, these modelling results are contentious.

The luminance measurements complement the radiance measurements based on the difference in acquisition. The advantage of the luminance measurements is the fast coverage of the complete sky in about 40 seconds. Spectral information can only be obtained from radiance measurements. Thus, it is a favourable strategy to decide upon the direction and atmospheric situations of radiance measurements after the distribution of luminance has been observed.

In this Antarctic campaign, only limited atmospheric situations have been considered. The need for a comprehensive data set arises to completely characterise the directional pattern of sky radiance and luminance. However, a dependence of sky luminance and spectral radiance distribution on solar zenith angle and surface albedo has been identified.

7.1.2 Spectral Behaviour of Snow Albedo

Dependencies on parameters influencing the snow albedo, such as SZA or snow grain size, can only partly be seen. The decrease of albedo due to increasing snow grain size has been identified. In contrast, an increase in albedo with increasing SZA could not be detected. For one, this is due to the small range of SZA during albedo measurements. For another, the effect of changing snow conditions outweighs the effect of changing SZA.

To further improve the results of the measured spectral albedo, a thorough consideration of uncertainties in the measurements are vital. Especially because the albedo over Antarctic snow basically reaches unity in the UV and visible part of

7 Conclusions

the solar spectrum, small changes in albedo will lead to relatively large changes in the surface energy budget. A slight spectral dependence of the albedo in the UV has been observed. It could not be conclusively established whether this decrease in albedo in the UV is an artefact due to the shadowing effect of the equipment. However, it can be stated, that the spectral dependence of the albedo in the UV and visible is not very pronounced. Depending on the requirement of accuracy of albedo measurements based on individual applications spectral measurements of albedo in such a fine resolution are not always necessary. It may be sufficient to use broadband or filter radiometers. This finding is not trivial and was not shown before.

The spectral snow albedo measured on the cloud free afternoon of 4 January 2004 has been successfully used as input parameter for the radiative transfer calculations performed in this study. In general the spectral albedo obtained in this study could also be used in other radiative transfer models to simulate the radiative transfer in Antarctica.

7.1.3 Assessing the Effect of Albedo on Incident Radiation

The spectral albedo measurements performed at Neumayer during the summer campaign 2003/04 serve their purpose of determining the spectral albedo as a basis for the analysis of sky luminance distributions, spectral irradiance and radiance. The mean spectral albedo measured under a cloudless sky on 4 January 2004 has been successfully used as input parameter into the radiative transfer model UVSPEC. The high surface albedo enhances luminance, spectral radiance and irradiance compared to a low albedo surface. It also enhances the effect of horizon brightening (see Section 7.1.1), which has been shown for the first time.

7.1.4 Spectral Irradiance connected to UV Monitoring

Spectral irradiance has been collected in all types of atmospheric conditions occurring at Neumayer during the austral summer 2003/04. The first step in connecting the spectral radiance collected at Neumayer with data of the NSF Polar UV net has been undertaken at the intercomparison at Boulder, Colorado, in June 2003. However, it was not possible to compare Antarctic spectral irradiance measured at NSF stations and Neumayer. It was focussed on the characterisation of the directional radiation parameters, spectral radiance and sky luminance, as well as albedo instead.

7.1.5 Model Evaluation using Spectral Irradiance

Comparisons between measured and modelled irradiance in a wavelength range from 290 to 1050 nm for cloud free situations show an agreement to within $\pm 15\%$ between 320 and 500 nm. For accurately modelling irradiance in the UVB, the model input for total ozone column needs to be known with the best accuracy possible. TOMS ozone data lead to deviations up to 100% at 305 nm. At wavelengths longer than 500 nm, the non-ideal cosine response of the irradiance input optics prevented a closer agreement between measurement and model.

Modelled and measured radiance show the best agreement in the UVA. The deviation is systematic, with measured radiance exceeding the modelled radiance by 30% on average. At wavelengths equal to and larger than 499 nm, a strong dependence on SZA can be observed. This is most likely due to reflections inside the input tubus.

Providing the atmospheric parameters necessary for model input are known, the spectral irradiance data collected at Neumayer provide a basis for evaluating radiative transfer models. For wavelengths longer than 500 nm the application of a cosine correction is recommended before model evaluation or even validation. The absolute calibration of radiance should be revised before radiative transfer models can be validated with data acquired with the IMUK spectroradiometric system. This was not possible within the scope of this study, because a calibrated reflectance plaque to generate diffuse illumination of the entrance optics had not been available at IMUK.

The excessive deviations up to a factor of 50 encountered in the visible and up to 1050 nm between model and measurement also lead to the hypothesis that the radiative transfer model itself may need to be improved in this wavelength range. In general, more Antarctic data is necessary in order to comprehensively validate radiation transfer models.

7.2 Insights into Possible Future Work

New goals concerning the technical improvement of the IMUK spectroradiometric system as well as further research needs can be derived from the results of this study.

7.2.1 Technical Improvements

An extension of the spectral range up to 2500 nm is technically possible, but not yet realised. The third detector (see Figure 3.1) needs to be incorporated in the measuring routine to be able to detect spectral radiation up to 2500 nm. Also a

7 Conclusions

different optical fibre has to be used as quartz absorbs in some spectral regions between 1000 and 2500 nm.

The communication between the Skyscanner and the IMUK spectroradiometer needs to be improved. So far, the Skyscanner is pointed separately to the desired position in the sky. This is time consuming in two respects:

- unnecessary long breaks occur when recording spectral radiance distributions;
- the operator needs to be present during the complete period of radiance measurements, so that other tasks, for example quality control, cannot be accomplished simultaneously.

Both, the irradiance and the radiance input optics, have to be improved. The cosine response of the irradiance input optic needs to be determined for wavelengths larger than 500 nm. A method to correct for the non-ideal cosine response needs to be developed. BERNHARD et al. (2003) suggest such a method. The reflections occurring inside the radiance entrance tubus at incident angles around 70° must be suppressed. It may be sufficient to blacken the inside of the tubus.

For the calibration of absolute radiance a different technique should be employed. A reflection plaque needs to be acquired and incorporated in the calibration procedure. The advantage is the diffuse illumination of the input tubus.

7.2.2 Future Research Needs

Knowledge of radiation conditions in Antarctica is of particular importance in order to improve the understanding of the surface radiation budget of polar regions. This plays an important role in the context of global climate change (HOUGHTON et al., 2001). On the other hand especially the UV region is important. For one, it is still not known how the ozone hole will develop within the next years and decades (WMO, 2003). For another, biological systems are most sensible to a change in prevailing UV radiation conditions (LÜDER, 2003).

The period of only one summer campaign is not sufficient to comprehensively characterise the radiation environment at an Antarctic site. Based on the experience of this one summer campaign, suggestions for further Antarctic campaigns are presented. The overall goals of contributing to the understanding of the surface energy budget with respect to climate change and the provision of high quality spectral radiation data to scientific user communities still remain.

7 Conclusions

Spectral albedo measurements in Antarctica

Methodical improvements concerning the acquisition of spectral albedo in Antarctica shall be named:

- A longer optical fibre is desirable to minimise the shadowing influence of the equipment.
- The spectral reflectivity of the air conditioned box is to be determined.
- A second sensor is preferable to measure reflected and incident radiation simultaneously. The second advantage is the exclusion of levelling uncertainties, because rotating the sensor will be redundant.
- Snow grain size should be determined on the days of albedo measurements.

One aim of the albedo measurements is to improve the accuracy of input into current GCMs. Therefore, it would be necessary to measure the albedo in a longer wavelength range. This will be possible once the third detector of the IMUK spectroradiometer is operational.

To investigate the effect of an inhomogeneous surface albedo, albedo measurements close to the ice edge should be repeated when open water is prevailing in Atka Bay. It would be preferable to conduct these measurements with the spectroradiometer. However, this will be most difficult to realise. One simple reason is the lack of a power supply outside the station area. Further a fast set up and dismantling of the equipment is crucial due to possible fast changes in weather conditions. In contrast, albedo measurements with the SL501 and the pyranometer only require a battery as power supply. Both instruments are easy to set up, thus they are excellent for albedo studies away from the station.

Spectral radiance measurements

Once the communication between the Skyscanner and the spectroradiometer is realised and the input tubus is improved, radiance measurements will be performed more easily and reliably.

It should be aimed at receiving a more complete coverage of the sky. Different data collection protocols should be followed:

- Complete scans of the principal plane should be performed. These scans could start in the azimuth direction of the sun, passing through the zenith until the horizon opposite the sun's position is reached. Steps of 10° are sufficient for most viewing zenith angles. Above the horizon, the step width

7 Conclusions

of the viewing zenith angle should be reduced to at least steps of 5° due to the strong relative change in radiance in the vicinity of the horizon.

- Scans of the almucantar ($SZA = VZA$, variable VAA) should be conducted. This way, the azimuth dependence of radiance can be investigated. Horizon brightening could be investigated not only dependent on solar zenith angle, but also on the azimuth direction. BLUMTHALER et al. (1996) and HUBER et al. (2004) have already performed radiance measurements in the almucantar. Thus, the results would be comparable to previous studies.
- It should be aimed at scanning one hemisphere of the sky to map radiance distributions. Scanning only one sky hemisphere is sufficient during cloudless situations because, according to the model results (see Figure 6.5), the distribution of radiance is symmetric to the principal plane. These sky maps should be measured for various small wavelength intervals to minimise the measuring time for one particular direction.

To assure the quality of sky radiance data it is recommended to participate in an intercomparison of spectral radiance. Up to now, such a task has not been reported in the scientific literature. Since at least one European group at the University of Innsbruck, Austria, is capable of performing spectral radiance measurements an intercomparison could be organised.

In general, deploying an array spectroradiometer will accelerate the mapping of spectral sky radiance distributions. The advantages of an array spectroradiometer over a scanning instrument have been discussed in Section 2.2.2.

Spectral irradiance measurements in Antarctica

Before the IMUK spectroradiometer is to be deployed in Antarctica again, the wavelength range should be extended up to 2500 nm. Since it will take almost one hour to record a spectrum from 280 to 2500 nm, the detected wavelength range should be adapted to the aims.

During ozone hole conditions the UV region should be emphasised. During periods designated for model validation the measured spectral range should be adapted to the specific one- or three-dimensional radiative transfer model to be validated. Input parameters vital for the model calculations need to be acquired. Depending on the model, the input parameters comprise

aerosol information: At Neumayer, there is an air chemistry observatory. So in principle, aerosol information is available.

atmospheric profiles of temperature and pressure: Radio sonde data will help to acquire such profiles.

7 Conclusions

total ozone column: Total ozone column derived from the Microtops channel 2 should be used instead of TOMS ozone data.

cloud information: Cloud detection should be improved. This could be realised by operating a CCD cloud camera. Also, the development of algorithms to evaluate luminance distributions with respect to determine the cloud type would provide an improvement.

Radiative transfer models currently in use have neither been validated for visible and infrared irradiance nor for spectral radiance in the complete wavelength region (280 to 2500 nm). Radiative transfer models are an important tool for

- process studies of i.e. chemical reactions or the determination of photodissociation rates in the atmosphere (MAYER et al., 1998);
- the derivation of surface radiation parameters from space based methods (WUTTKE et al., 2003);
- the provision of accurate input into climate models (HOUGHTON et al., 2001)

These applications present the need for accurately modelling radiative transfer in the atmosphere. This can only be guaranteed after a thorough validation with high quality spectral radiation data.

Deploying the IMUK spectroradiometer on behalf of the NDSC

Concerning the deployment of the IMUK instrument as a NDSC travelling instrument an intercomparison between the IMUK and AWI spectroradiometer is planned. The AWI spectroradiometer does not comply with the NDSC standards so far. AWI operates one permanent spectroradiometer at Neumayer, and one at Ny Ålesund, Spitsbergen, Norway. This site is a primary NDSC station (<http://www.ndsc.ws/>), where AWI already operates a variety of instruments to measure atmospheric parameters. Thus, it would be favourable for the AWI spectroradiometers to become certified NDSC instruments. Since the AWI instruments contain array detectors it is necessary to develop routines for a meaningful intercomparison. Scanning and array spectroradiometers have been successfully intercompared before (LANTZ et al., 2002). However, the AWI array spectroradiometers still have some deficiencies over scanning instruments, which is discussed in Section 2.2.2.

Hemispheric intercomparisons

Spectral radiation data collected in Antarctica should be compared to Arctic measurements to investigate geographical differences in incident radiation regarding polar regions. This is one of the goals formulated in SECKMEYER et al. (2001). Spectral irradiance data from the northern and southern hemisphere have been compared by SECKMEYER et al. (1995) or MCKENZIE et al. (2001). Possible reasons for observed differences in radiation levels may be a difference in cloud cover and aerosol content. The snow may be contaminated with soot in the northern hemisphere preventing the albedo to be as high as in the southern hemisphere. In a polar environment the total ozone column as well as the tropospheric ozone content needs to be considered as a cause for possible hemispheric differences.

In both polar regions the same instrument should be deployed to improve the comparability of the data. The same parameters should be measured and the same data collection protocols should be applied. Favourable Arctic sites complementing the Antarctic measurements comprise

Summit: This research station is located in the middle of Greenland on an inland glacier providing a homogeneously snow covered surface in the surrounding similar to Antarctica. The NSF has recently set up a SUV-150B spectroradiometer at this site. Therefore, general infrastructure should be adequate.

Ny Ålesund: AWI already monitors various atmospheric parameters at this primary NDSC site. Infrastructure is provided. The disadvantage is the inhomogeneous landscape surrounding the research station.

Sodankylä: One of the longest time series of spectral irradiance is monitored at this station. However, trees prevent a homogeneous snow cover of the surrounding area.

Monitoring of spectral irradiance

Radiation measurements performed in this study only cover one Antarctic summer season. More measurements, especially in spring under ozone hole conditions, need to be performed to be able to rely on a more diverse data set of radiation parameters. A permanent monitoring station of spectral irradiance would provide long term information on the radiation environment at an Antarctic site. The collected data could be provided to international databases such as EUVDB or WOUDC. The Polar UV network of the NSF already provides valuable spectral UV irradiance measured at three Antarctic locations to user communities for more than 12 years. Radiation measurements at Neumayer should not only be aimed at monitoring. Even more, it should be concentrated on case studies to answer specific questions raised in the scientific community.

List of Symbols

Symbol	Physical Parameter	Unit
a	albedo	
a_K	albedo corrected for the shadowing effect	
a_λ	spectral measured albedo	
A	unit area	m^2
B	bandwidth	nm
E	irradiance	Wm^{-2}
$E_L(\lambda)$	spectral irradiance produced by calibration source	Wm^{-2}nm
E_M	measured irradiance	Wm^{-2}
E_{MES}	measured spectrum of downwelling irradiance	$\text{Wm}^{-2}\text{nm}^{-1}$
E_{MESK}	spectrum corrected for the SZA at the time of recording the following reflected spectrum	$\text{Wm}^{-2}\text{nm}^{-1}$
E_{MODE}	spectrum of irradiance modelled with SZA according to measured downwelling spectrum	$\text{Wm}^{-2}\text{nm}^{-1}$
E_{MODR}	spectrum modelled with SZA according to following measured reflected spectrum	$\text{Wm}^{-2}\text{nm}^{-1}$
E_λ	spectral irradiance	$\text{Wm}^{-2}\text{nm}^{-1}$
E_\odot	extraterrestrial irradiance	Wm^{-2}
H	radiant exposure	Jm^{-2}
I	radiant intensity	Wsr^{-1}
I_{ph}	luminous intensity	cd
K	correction factor for measured albedo	
L	radiance	$\text{Wm}^{-2}\text{sr}^{-1}$
L_λ	spectral radiance	$\text{Wm}^{-2}\text{sr}^{-1}\text{nm}^{-1}$
L_{ph}	luminance	cdm^{-2}
M	radiant exitance	Wm^{-2}
N_p	number of photons	
$r(\lambda)$	spectral responsivity	$\text{nAW}^{-1}\text{m}^2\text{nm}$
R_{MES}	reflected measured irradiance	$\text{Wm}^{-2}\text{nm}^{-1}$

List of Symbols

R_{MESK}	reflected measured irradiance corrected for the shadowing effect	$\text{Wm}^{-2}\text{nm}^{-1}$
$s(\lambda)$	response of the luminance sensor	
$S_M(\lambda)$	signal of the spectroradiometer	nA^{-1}
$S_L(\lambda)$	spectral signal of the spectroradiometer measuring a calibration source	nA^{-1}
t	time	s
$V(\lambda)$	response of the human eye	
W	radiative energy	J
\vec{x}	direction in Cartesian coordinates	
α	angle between normal of a surface and direction of luminance	$^\circ$
θ	solar zenith angle	$^\circ$
λ	wavelength	nm or μm
λ_0	centre wavelength of the slit function	nm
ν	frequency	s^{-1}
ϕ	solar azimuth angle	$^\circ$
Φ	radiant flux	W
Ω	unit solid angle	sr

Symbol	Physical Constant	Value
h	Planck's constant	$6.626 \cdot 10^{34} \text{ Js}$
S	solar constant	$1368 (\pm 2) \text{ Wm}^{-2}$

List of Acronyms

Acronym or Abbreviation	Meaning
AAO	Antarctic oscillation
AOT	Aerosol optical thickness
ASRC	Atmospheric Sciences Research Center at the State University of New York
ATI	Institute for Medical Physics, University of Innsbruck, Austria
AWI	Alfred Wegener Institute for Polar and Marine Research
BSI	Biospherical Instruments Inc.
BSRN	Baseline Surface Radiation Network
CASE	Characterisation of the specific solar radiation conditions in polar regions with respect to climate change and ozone depletion
CCD	Charge coupled device
CIE	Commission Internationale d'Eclairage
CUCF	Central UV Calibration Facility
DFG	Deutsche Forschungsgemeinschaft
DIN	German Industry Norm
DISORT	Discrete Ordinates method
DU	Dobson Units
EC	European Commission
ECUV	European reference Centre for Ultraviolet Radiation Measurements
EDUCE	European database for ultraviolet radiation characterization and evaluation
EPA	University of Georgia's National UV Monitoring Center
EUVDB	European ultraviolet database
FIJ	Finnish Meteorological Institute, Finland
FOV	Field of view
FWHM	Full width half maximum
GBM	Institute of Science and Technology, University of Manchester, Great Britain
GCM	Global circulation model

List of Acronyms

GRT	Laboratory of Atmospheric Physics, Aristotle University Thessaloniki, Greece
ICSU	International Council of Scientific Unions
IE	Ice edge
IMUK	Institute of Meteorology and Climatology
IR	Infrared
ISQ	Brewer spectroradiometer of ECUV
JRC	Joint Research Centre, Space Application Institute
LIDAR	Light detection and ranging
N	North
NASA	National Aeronautics and Space Administration
NDSC	Network for the Detection of Stratospheric Change
NIWA	National Institute for Water and Atmospheric Research of New Zealand
NLR	National Institute of Public Health and Environment, Bilthoven, Netherlands
NM	Neumayer Station
NOAA	National Oceanic and Atmospheric Administration
NSF	National Science Foundation
NSL	National standards laboratory
O	East
PAR	Photosynthetic active radiation
PMT	Photomultiplier
PTB	Physikalisch-Technische Bundesanstalt
QA	Quality assurance
QASUME	Quality Assurance of Spectral Ultraviolet Measurements in Europe through the developments of a transportable unit
QC	Quality control
RSS	Rotating shadowband spectroradiometer
S	South
SAA	Solar azimuth angle
SAM	Swing-away-mirror
SL501	Solar Light Model 501 Biometer
SOS	Successive orders of scattering
SSC	Scientific Steering Committee
SUV	Spectral ultraviolet
SZA	Solar zenith angle
TOMS	Total Ozone Mapping Spectrometer
USDA	United States Department of Agriculture
UTC	Universal Time Coordinated
UV	Ultraviolet
VIS	Visual spectral range
VZA	Viewing zenith angle

List of Acronyms

W	West
WCRP	World Climate Research Programme
WMO	World Meteorological Organization
WOUDC	World Ozone and Ultraviolet Radiation Data Centre

List of Figures

3.1	Schematic diagram of the Bentham DTM300 double monochromator	26
3.2	Cosine response for irradiance input optics	28
3.3	Logarithmic FOV in steps of 5°	30
3.4	FOV in steps of 0.5°	30
3.5	Logarithmic FOV in steps of 0.5°	31
3.6	Slit function	32
3.7	Wavelength shift at different ambient temperatures	34
3.8	Field Calibrator	36
3.9	Ratio of spectral irradiance on 8 May 2002	39
3.10	Time series of ratio JRC/IMUK	39
3.11	Ratio of erythral irradiance in Boulder	43
3.12	Ratio of erythral irradiance in Boulder	43
3.13	Ratio BSI/IMUK and NIWA/IMUK at three different times	45
3.14	Diurnal cycle of ratios at different wavelengths on 22 June 2003	46
3.15	Logarithmic Slit Function	49
4.1	Neumayer’s location in Antarctica	52
4.2	Photograph of Neumayer Station	53
4.3	Schematic set-up of the IMUK spectroradiometric system	55
4.4	Stability of the spectroradiometric system over time, diffuser	56
4.5	Wavelength shift on 8 Dec 03 and 13 Jan 04	58
4.6	Wavelength shift on 20 Feb 04 and mean shift	59
4.7	Albedo measurements at the ice edge	61
4.8	Ratios of albedo correction factors	64
4.9	Response of the luminance sensor	65
4.10	Ratio $s(\lambda)/V(\lambda)$	65
4.11	Skyscanner set up to measure Sky Radiance	68
4.12	Stability of the spectroradiometer over time, tubus	69
5.1	Mean spectral albedo	73
5.2	Mean spectral albedo for limited wavelengths	73
5.3	Diurnal albedo cycle on 4 January 2004	75
5.4	Diurnal albedo cycle on 2 January 2004	76

List of Figures

5.5	All albedo values derived from SL501	76
5.6	Sky luminance distribution, cloudless	77
5.7	Sky luminance distribution, cloud cover	78
5.8	Cloudless and cloudy zenithal luminance scans	79
5.9	Zenithal luminance scans measured at Neumayer and Boulder	80
5.10	Diurnal cycle of luminance	81
5.11	Cloudless radiance spectra	82
5.12	Diurnal cycle of radiance from 10 to 13 December 2003.	83
5.13	Cloudy and cloud free spectrum of zenith radiance	85
5.14	Radiance spectra of a zenithal scan.	86
5.15	Measured and modelled zenithal radiance scans.	87
5.16	Ratio of measured to modelled radiance as a function of SZA.	89
5.17	Ratio of modelled to measured irradiance in dependence of SZA	91
5.18	Time series of wavelength integrated UV irradiance.	92
5.19	Comparison Microtops/TOMS	94
5.20	Height of cloud base and sunshine duration (BSRN data)	95
6.1	Ratios of modelled snow albedo	99
6.2	Albedo spectra measured at Neumayer	100
6.3	Ratios of Snow Albedo with different grain sizes	102
6.4	Ratios of zenithal luminance scans (Boulder/Neumayer)	104
6.5	Modelled sky radiance distributions	108
6.6	Modelled zenithal scans for varying SZA and surface albedo	109
6.7	Ratio of zenithal radiance scans for varying SZA and albedo	111
6.8	Ratio of zenithal radiance scans at 550 nm	113
6.9	UVSPEC vs. SOS code	118

List of Tables

3.1	NDSC specifications	48
4.1	Summary of Antarctic measurements	56
5.1	Summary of conditions of albedo measurements	72
6.1	Albedo of grass and snow for different wavelengths	110

Bibliography

Bais, A. F., B. G. Gardiner, et al., 2001: The SUSPEN intercomparison of ultraviolet spectroradiometers. — *J. Geophys. Res.*, **106**, 12509–12526.

Bernhard, G., C. Booth, J. Ehramjian, 2002: Comparison of measured and modeled spectral ultraviolet irradiance at Antarctic stations used to determine biases in total ozone data from various sources. — In: *Ultraviolet Ground and Space-Based Measurements, Models and Effects*, J. Slusser, J. Herman, W. Gao, Ed., Bellingham, Washington, D.C., Vol. 4482 of *Proceedings of SPIE*, 115–126.

Bernhard, G., C. Booth, J. Ehramjian, 2003: The quality of data from the National Science Foundation's UV Monitoring Network for Polar Regions. — In: *Ultraviolet Ground and Space-Based Measurements, Models and Effects II*, W. Gao, J. Herman, G. Shi, K. Shibasaki, J. Slusser, Ed., Vol. 4896 of *Proceedings of SPIE*, 79–93.

Bernhard, G., C. R. Booth, J. C. Ehramjian, 2004: Version 2 data of the National Science Foundation's Ultraviolet Radiation Monitoring Network: South Pole. — *J. Geophys. Res.*, **in press**.

Bernhard, G., G. Seckmeyer, 1997: New Entrance Optics for Solar Spectral UV Measurements. — *Photochem. Photobiol.*, **65**, 923–930.

Bernhard, G., G. Seckmeyer, 1999: Uncertainty of measurements of spectral solar UV irradiance. — *J. Geophys. Res.*, **104**, D12, 14321–14345.

Bigelow, D. S., J. R. Slusser, A. F. Beaubien, J. H. Gibson, 1998: The USDA Ultraviolet Radiation Monitoring Program. — *Bull. Am. Met. Soc.*, **79**, 4, 601–615.

Blumthaler, M., W. Ambach, 1988: Solar UVB-Albedo of various Surfaces. — *Photochem. Photobiol.*, **48**, 1, 85–88.

Blumthaler, M., J. Gröbner, M. Huber, W. Ambach, 1996: Measuring spectral and spatial variations of UVA and UVB sky irradiance. — *Geophys. Res. Lett.*, **23**, 5, 547–550.

Bibliography

- Borowski, D., 2003:** *The Antarctic Circumpolar Current: Dynamics of a circumpolar channel with blocked geostrophic contours.* — Reports on Polar and Marine Research 453, Alfred Wegener Institute for Polar and Marine Research, Bremerhaven, Germany.
- Cede, A., E. Luccini, L. Nunez, R. D. Piacentini, M. Blumthaler, 2002a:** Calibration and uncertainty estimation of erythemal radiometers in the Argentine Ultraviolet Monitoring Network. — *Appl. Opt.*, **41**, **30**, 6341–6350.
- Cede, A., E. Luccini, L. Nunez, R. D. Piacentini, M. Blumthaler, 2002b:** Monitoring of erythemal irradiance in the Argentine ultraviolet network. — *J. Geophys. Res.*, **107**, **D13**, 10.1029/2001JD001206.
- Cosimo, J. C., 2000:** Variability and trends in Antarctic surface temperatures from in situ and satellite infrared measurements. — *J. Climate*, **13**, 1674–1696.
- Degünther, M., R. Meerkötter, A. Albold, G. Seckmeyer, 1998:** Case study on the influence of inhomogeneous surface albedo on UV irradiance. — *Geophys. Res. Lett.*, **98**, 3587–3590.
- DIN 5031, 1982:** Strahlungsphysik im optischen Bereich und Lichttechnik. — Beuth Verlag GmbH, 8 .
- DIN 5036, 1979:** Strahlungsphysikalische und lichttechnische Eigenschaften von Materialien. — Beuth Verlag GmbH, 8 .
- Dirmhirn, I., F. Eaton, 1975:** Some Characteristics of the Albedo of Snow. — *J. Appl. Meteor.*, **14**, 375–379.
- Edwards, D. P., 1992:** *GENLN2: A general line-by-line atmospheric transmittance and radiance model: Version 3.0 description and users guide.* — Tech. Rep. NCAR/TN-367+STR, National Center for Atmospheric Research (NCAR), Boulder, Colorado.
- Fabian, P., 1992:** *Atmosphäre und Umwelt.* — Springer Verlag, Berlin, Germany, fourth Ed., 144 .
- Farman, J., B. G. Gardiner, J. Shanklin, 1985:** Large losses of total ozone in Antarctica reveal seasonal ClO_x/NO_x interaction. — *Nature*, **315**, 207–210.
- Feister, U., R. Grewe, 1995:** Spectral Albedo Measurements in the UV and visible region over different types of surfaces. — *Photochem. Photobiol.*, **62**, **4**, 736–744.
- Gay, M., M. Fily, C. Genthon, M. Frezzotti, H. Oerter, J.-G. Winther, 2002:** Snow grain-size measurements in Antarctica. — *J. Glaciol.*, **48**, **163**, 527–535.

Bibliography

- Gillett, N. P., D. W. J. Thompson, 2003:** Simulation of Recent Southern Hemisphere Climate Change. — *Science*, **302**, 273–275.
- Giorgi, F., H. B., J. Christensen, H. M., P. von Storch, P. Whetton, R. Jones, L. Mearns, C. Fu, 2001:** *Regional Climate Information - Evaluation and Projections*, Cambridge University Press, Cambridge, United Kingdom and New York, NY, USA, Chap. 10. — Climate Change 2001: The Scientific Basis. Contribution of Working Group I to the Third Assessment Report of the Intergovernmental Panel on Climate Change, 583–638.
- Grant, R., G. Heisler, 1997:** Obscured Overcast Sky Radiance Distributions for Ultraviolet and Photosynthetically Active Radiation. — *J. Appl. Meteor.*, **36**, 1337–1345.
- Grant, R., G. Heisler, W. Gao, 1997a:** Clear Sky Radiance Distributions in Ultraviolet Wavelength Bands. — *Theor. Appl. Climatol.*, **56**, 123–135.
- Grant, R., G. Heisler, W. Gao, 1997b:** Ultraviolet Sky Radiance Distributions of Translucent Overcast Skies. — *Theor. Appl. Climatol.*, **58**, 129–139.
- Grenfell, T., S. Warren, P. Mullen, 1994:** Reflection of solar radiation by the Antarctic snow surface at ultraviolet, visible and near-infrared wavelengths. — *J. Geophys. Res.*, **99**, D9, 18669–18694.
- Gröbner, J., 1996:** *Ultraviolet solar radiation measurements using a high precision spectroradiometer*. — Dissertation, Naturwissenschaftliche Fakultät der Leopold-Franzens-Universität Innsbruck, Innsbruck, Austria, 101 .
- Gröbner, J., A. Albold, et al., 2000:** The Variability of spectral solar ultraviolet Irradiance in an Alpine Environment. — *J. Geophys. Res.*, **105**, D22, 26991–27003.
- Gröbner, J., A. Bais, et al., 2004:** *A travelling unit for routine quality assurance of spectral solar ultraviolet irradiance measurements*. — report, Optical Society of America.
- Hanken, T., H. Tüg, 2002:** Development of a Multichannel UV-Spectroradiometer for Field Measurement. — *Environ. Sci. Pollut. Res*, **Special Issue 4**, 35–39.
- Hansen, J., L. Nazarenko, 2004:** Soot climate forcing via snow and ice albedos. — In: *Proc. Natl. Acad. Sci.*, Vol. 101, 423–428.
- Herman, J. R., R. L. McKenzie, S. B. Diaz, J. B. Kerr, S. Madronich, G. Seckmeyer, 1999:** *Ultraviolet Radiation at the Earth's Surface*, World Meteorological Organization, Geneva, Chap. 9. — Scientific Assessment of Ozone Depletion: 1998, 9.1–9.46.

Bibliography

- Houghton, J., Y. Ding, D. Griggs, M. Noguer, P. van der Linden, D. X., K. Maskell, C. Johnson, Ed., 2001:** *Climate Change 2001: The Scientific Basis. Contribution of Working Group I to the Third Assessment Report on Climate Change*. — Cambridge University Press, Cambridge, United Kingdom, 881 .
- Huber, M., M. Blumthaler, J. Schreder, B. Schallhart, J. Lenoble, 2004:** Effect of inhomogeneous surface albedo on diffuse UV sky radiance at a high-altitude site. — *J. Geophys. Res.*, **109**, D08107, doi:10.1029/2003JD004013.
- Igawa, N., H. Nakamura, K. Matsuura, 1999:** Sky luminance distribution model for simulation of daylight environment. — In: *Proceedings of Building Simulation '99*, Kyoto, Japan, Vol. 2 of *IBPSA conference*, 269–275.
- Ineichen, P., 1996:** *Use of Meteosat data to produce sky luminance maps*. — Report of the satellight project, GAP - Energy / University of Geneva, Switzerland.
- Iqbal, M., 1983:** *An Introduction to Solar Radiation*. — Academic Press, Toronto, Canada, 390 .
- Jacka, T. H., W. F. Budd, 1998:** Detection of temperature and sea-ice-extent changes in the Antarctic and Southern Ocean. — *Ann. Glaciol.*, **27**, 553–559.
- Johnson, B., O. Mikkelsen, M. Hannevik, L. T. Nilsen, G. Sævi, K. G. Blaasaas, 2002:** *The Norwegian UV monitoring program. Period 1995/96 to 2001*. — StralevernRapport 4, Norwegian Radiation Protection Authority, Oslo, Norway.
- Karsten, U., K. Bischof, D. Hanelt, D. Wiencke, 1999:** The effect of ultraviolet radiation on photosynthesis and ultraviolet-absorbing substances in the endemic Arctic macroalga *Devaleraea ramentacea* (Rhodophyta). — *Physiologia Plantarum*, **105**, 58–66.
- Kerr, J., G. Seckmeyer, et al., 2003:** *Surface Ultraviolet Radiation: Past and Future*, World Meteorological Organization, Geneva, Chap. 5. — Scientific Assessment of Ozone Depletion: 2002.
- Kerr, R. A., 2002:** A Single Climate Mover for Antarctica. — *Science*, **296**, 825–826.
- Kiedron, P., J. Michalsky, J. Berndt, H. L.C., 1999:** Comparison of spectral irradiance standards used to calibrate shortwave radiometers and spectroradiometers. — *Appl. Opt.*, **38**, 2432–2439.

Bibliography

- Kondratyev, K., A. Cracknell, 1998:** *Observing Global Climate Change*. — Tayler & Francis Ltd, London, UK, 562 .
- König, H., A. Aden, 1999:** *UV reflectance and measurement device*. — report 2, University of Technology, Helsinki, Finland.
- König-Langlo, G., A. Herber, 1996:** *The Meteorological Data of the Neumayer Station (Antarctica) for 1992, 1993, and 1994*. — Reports on Polar Research 187, Alfred Wegener Institute for Polar and Marine Research, Bremerhaven, Germany.
- Kylling, A., A. Dahlback, B. Mayer, 2000:** The Effect of Clouds and Surface Albedo on UV Irradiances at a High Latitude Site. — *Geophys. Res. Lett.*, **27**, **9**, 1411–1414.
- Lantz, K., P. Disterhoft, et al., 2002:** The 1997 North American interagency intercomparison of ultraviolet spectroradiometers including narrowband filter radiometers. — *J. Res. Natl. Inst. Stand. Technol.*, **107**, 19–62.
- Lefebvre, J., H. Gallee, J.-P. van Ypersele, W. Greuell, 2003:** Modelling of snow and ice melt at ETH camp (West Greenland): a study of surface albedo. — *J. Geophys. Res.*, **108**, **D8**, doi:10.1029/2001JD001160.
- Lenoble, J., 1993:** *Atmospheric Radiative Transfer*. — A. Deepak Publishing, Hampton, VA, 532 .
- Lenoble, J., 1998:** Modelling of the influence of snow reflectance on ultraviolet irradiance for cloudless sky. — *Appl. Opt.*, **37**, **12**, 2441–2447.
- Li, S., X. Zhou, 2003:** Assessment of the accuracy of snow surface direct beam spectral albedo under a variety of overcast skies derived by a reciprocal approach through radiative transfer simulation. — *Appl. Opt.*, **42**, 5427–5441.
- Liou, K. N., 1980:** *An Introduction to Atmospheric Radiation*, Vol. 26 of *International Geophysics Series*. — Academic Press, Orlando, 392 .
- Liu, Y., K. Voss, 1997:** Polarized radiance distribution measurement of skylight. II. Experiment and data. — *Appl. Opt.*, **36**, **33**, 8753–8764.
- Lüder, U. H., 2003:** *Acclimation of the photosynthetic apparatus of the endemic Antarctic red macroalga *Palmaria decipiens* to seasonally changing light conditions*. — Reports on Polar and Marine Research 469, Alfred Wegener Institute for Polar and Marine Research, Bremerhaven, Germany.
- Mayer, B., M. Degünther, 2000:** Comment on “Measurements of Erythral Irradiance near Davis Station, Antarctica: Effect of inhomogeneous Surface Albedo. — *Geophys. Res. Lett.*, **27**, **21**, 3489–3490.

Bibliography

- Mayer, B., C. A. Fischer, S. Madronich, 1998:** Estimation of Surface Actinic Flux from Satellite (TOMS) Ozone and Cloud Reflectivity Measurements. — *Geophys. Res. Lett.*, **25**, **23**, 4321–4324.
- Mayer, B., G. Seckmeyer, A. Kylling, 1997:** Systematic long-term comparison of spectral UV measurements and UVSPEC modeling results. — *J. Geophys. Res.*, **102**, **D7**, 8755–8767.
- McArthur, L. J. B., 1998:** *Baseline Surface Radiation Network (BSRN)*. — Operations Manual WMO/TD-No. 879, WCRP/WMO.
- McKenzie, R., P. Johnston, G. Seckmeyer, 1997:** UV spectroradiometry in the network for the detection of stratospheric change (NDSC). — In: *Solar Ultraviolet Radiation. Modelling, Measurements and Effects*, C. Zerefos, A. Bais, Ed., Springer, Berlin, 279–287.
- McKenzie, R., K. Paulin, S. Madronich, 1998:** Effects of snow cover on UV irradiance and surface albedo: A case study. — *J. Geophys. Res.*, **103**, **D22**, 28785–28792.
- McKenzie, R., G. Seckmeyer, A. F. Bais, J. B. Kerr, S. Madronich, 2001:** Satellite-retrievals of erythemal UV dose compared with ground-based measurements at Northern and Southern mid-latitudes. — *J. Geophys. Res.*, **106**, **D20**, 24051–24062.
- McKinlay, A. F., B. L. Diffey, 1987:** A reference action spectrum for ultraviolet induced erythema in human skin. — *CIE J.*, **6**, **1**, 17–22.
- McPeters, R. D., G. J. Labow, 1996:** An assessment of the accuracy of 14.5 years of Nimbus 7 TOMS Version 7 ozone data by comparison with the Dobson network. — *Geophys. Res. Lett.*, **23**, **25**, 3695–3698.
- Meister, G., P. Abel, et al., 2003:** *The Second SIMBIOS Radiometric Intercomparison (SIMRIC-2), March–November 2002*. — report NASA/TM-2003, Goddard Space Flight Center, Greenbelt, Maryland, USA.
- Meyers Lexikon, 1989:** *Wie funktioniert das? Wetter und Klima*. — Meyers Lexikonverlag, Mannheim, 304 .
- Mishchenko, M. I., A. A. Lacis, T. L. D., 1994:** Errors induced by the neglect of polarization in radiance calculations for Rayleigh-scattering atmospheres. — *J. Quant. Spectrosc. Radiat. Transfer*, **51**, 491–510.
- Mueller, J., C. Pietras, S. Hooker, R. Austin, M. Miller, K. Knobelspiesse, R. Frouin, B. Holben, K. Voss, 2003:** *Instrument Specifications, Characterization and Calibration*. — Ocean Optics Protocols For Satellite Ocean

Bibliography

Color Sensor Validation Revision 4, Volume II, Goddard Space Flight Center, Greenbelt, Maryland, USA.

Newman, P. A., J. A. Pyle, et al., 2003: *Polar Stratospheric Ozone: Past and Future*, World Meteorological Organization, Geneva, Chap. 3. — Scientific Assessment of Ozone Depletion: 2002.

Nichol, S., G. Pfister, G. Bodeker, R. McKenzie, S. Wood, G. Bernhard, 2003: Moderation of Cloud Reduction of UV in the Antarctic Due to High Surface Albedo. — *J. Appl. Meteor.*, **42**, 1174–1183.

Piel, C., 2004: *Variability of chemical and physical parameters of aerosol in the Antarctic troposphere*. — Reports on Polar and Marine Research 476, Alfred Wegener Institute for Polar and Marine Research, Bremerhaven, Germany.

Prather, M., D. Ehhalt, et al., 2001: *Atmospheric Chemistry and Greenhouse Gases*, Cambridge University Press, Cambridge, United Kingdom and New York, NY, USA, Chap. 4. — Climate Change 2001: The Scientific Basis. Contribution of Working Group I to the Third Assessment Report of the Intergovernmental Panel on Climate Change, 239–287.

Ricchiazzi, P., C. Gautier, 1998: Investigation of the effect of surface heterogeneity and topography on the radiation environment of Palmer Station, Antarctica, with hybrid 3-D radiative transfer model. — *J. Geophys. Res.*, **103**, D6, 6161–6176.

Ricchiazzi, P., S. Young, C. Gautier, D. Sowle, 1998: A research and teaching software tool for plane-parallel radiative transfer in the Earth's atmosphere. — *Bull. Am. Meteorol. Soc.*, **79**, 2101–2114.

Sansonetti, C., M. Salit, J. Reader, 1996: Wavelengths of spectral lines in mercury oencil lamps. — *Appl. Opt.*, **35**, 74–77.

Schmidt, T., G. König-Langlo, 1994: *Radiation Measurements at the German Antarctic Station Neumayer 1982-1992*. — Reports on Polar Research 146, Alfred Wegener Institute for Polar and Marine Research, Bremerhaven, Germany.

Schwander, H., B. Mayer, A. Ruggaber, A. Albold, G. Seckmeyer, P. Köpcke, 1999: Method to determine snow albedo values in the UV for radiative transfer modelling. — *Appl. Opt.*, **38**, **18**, 3869–3875.

Seckmeyer, G., 1997: *Die genaue Messung und Simulation der solaren UV-Strahlung*. — Habilitationsschrift, Technische Universität Ilmenau, 116 .

Bibliography

- Seckmeyer, G., A. Bais, G. Bernhard, M. Blumthaler, P. Eriksen, R. L. McKenzie, C. Roy, M. Miyauchi, 2001: Instruments to measure solar ultraviolet radiation, part I: spectral instruments. — WOM-GAW report, 30 .
- Seckmeyer, G., T. Martin, T. Ali, 2004: *European Database for UV Climatology and Evaluation*. — Final report to the commission of the european communities, Contract No. EVK2-CT-1999-00028.
- Seckmeyer, G., B. Mayer, et al., 1995: Geographical Differences in the UV measured by Intercompared Spectroradiometers. — *Geophys. Res. Lett.*, **22**, 1889–1892.
- Slaper, H., H. A. J. M. Reinen, M. Blumthaler, M. Huber, F. Kuik, 1995: Comparing ground-level spectrally resolved solar UV measurements using various instruments: A technique resolving effects of wavelength shift and slit width. — *Geophys. Res. Lett.*, **20**, 2721–2724.
- Smolskaia, I., M. Nunez, K. Michael, 1999: Measurements of Erythema Irradiance near Davis Station, Antarctic: Effect of Inhomogeneous Surface Albedo. — *Geophys. Res. Lett.*, **26**, 10, 1381–1384.
- Stamnes, K., S. C. Tsay, W. Wiscombe, K. Jayaweera, 1988: A numerically stable algorithm for discrete-ordinate-method radiative transfer in multiple scattering and emitting layered media. — *Appl. Opt.*, **27**, 2502–2509.
- Takao, T., M. Aono, T. Kishi, K. Sakurai, O. Ijima, M. Takakwa, O. Narita, M. Shitamichi, 1999: Ultraviolet Spectral Irradiance Observations at Syowa Station, Antarctica 1991-1996. — *The Geophysical Magazine Series 2*, **3**, 3, 95–107.
- Thompson, D. W., S. Solomon, 2002: Interpretation of recent Southern Hemisphere climate change. — *Science*, **296**, 5569, 895–899.
- Tregenza, P., 1987: Subdivision of the Sky Hemisphere for Luminance Measurements. — *Lightning Research and Technologies*, **19**, 13–14.
- Vaughan, D. G., G. J. Marshall, W. M. Connolley, J. C. King, R. Mulvaney, 2001: Devil in the Detail. — *Science*, **293**, 5536, 1777–1779.
- Vida, J., I. Foyo-Moreno, L. Alados-Arboledas, 1999: The European Community Cloudless Sky Radiance Model. An Evaluation by Means of the Skyscan'834 Data Set. — *Theor. Appl. Climatol.*, **63**, 141–147.
- Walkenhorst, O., J. Luther, C. Reinhart, J. Timmer, 2002: Dynamic annual daylight simulations based on one-hour and one-minute means of irradiance data. — *Solar Energy*, **72**, 5, 385–395.

Bibliography

- Warren, S., R. E. Brandt, P. O’Rawe Hinton, 1998:** Effect of surface roughness on bi-directional reflectance of Antarctic snow. — *J. Geophys. Res.*, **103**, E11, 25789–25807.
- Webb, A. R., 2000:** Guidelines for Site Quality Control of UV monitoring. — WMO-GAW report.
- van Weele, M., T. J. Martin, et al., 2000:** From model intercomparison toward benchmark UV spectra for six real atmospheric cases. — *J. Geophys. Res.*, **105**, D4, 4915–4925.
- Weih, P., J. Lenoble, et al., 2001:** Modeling the effect of an inhomogeneous surface albedo on incident UV radiation in mountainous terrain: determination of an effective surface albedo. — *Geophys. Res. Lett.*, **28**, 16, 3111–3114.
- Weih, P., A. Webb, S. Hutchinson, G. Middleton, 2000:** Measurements of the diffuse UV sky radiance during broken cloud conditions. — *J. Geophys. Res.*, **105**, D4, 4937–4944.
- Wiscombe, W., S. Warren, 1980:** A Model for the Spectral Albedo of Snow. I: Pure Snow. — *J. Atmos. Sci.*, **37**, 2712–2733.
- WMO, 2003:** *Scientific Assessment of Ozone Depletion: 2002*. — Global Research and Monitoring Project - Report No. 47, Geneva, 498 .
- Wuttke, S., G. Bernhard, J. Ehranjian, R. McKenzie, P. Johnston, M. O’Neill, G. Seckmeyer, 2004:** New spectroradiometers complying with the NDSC standards. — *Photochem. Photobiol.*, submitted.
- Wuttke, S., J. Verdebout, G. Seckmeyer, 2003:** An improved Algorithm for Satellite-derived UV Radiation. — *Photochem. Photobiol.*, **77**, 1, 52–57.
- Zhou, X., S. Li, K. Morris, 2001:** Measurement of all-wave and spectral albedos of snow-covered summer sea ice in the Ross Sea, Antarctica. — *Ann. Glaciol.*, **33**, 267–274.

Acknowledgements

Many people have supported me during the past three years. Time has come to express my thankfulness.

First of all I would like to thank my supervisor Prof. Dr. Gunther Seckmeyer for his support throughout my PhD work. Numerous discussions improved my understanding of the scientific world. Working with him, I have experienced both, fruitful advice and the necessary freedom to work independently.

Without the support of Dipl.-Ing. Anton Gugg-Helminger from Gigahertz-Optik it would have taken ages to learn how to operate the spectroradiometer and to spot malfunctions.

During the first two intercomparisons, Dipl.-Met. Holger Studemund was a strong help. For the opportunity to participate in the NDSC intercomparison, I want to express my thankfulness to Dr. James Slusser who invited us and covered all the costs. For the success Dr. Kathy O. Lantz, Dr. Patrick Disterhoft, Dr. Germar Bernhard, and Dr. Paul Johnston need to be thanked most. For the technical support at IMUK, in particular prior the Antarctic campaign, Ulrich Meyer, Dipl.-Met Sonja Fabig, and Dr. Notker Fechner is thanked.

The excellent preparation of the Antarctic campaign thanks to the AWI Logistics department, represented by Jürgen Janneck and Dr. Hartwig Gernandt, was the basis to conduct successful measurements at Neumayer. On station I received more support than previously expected. Thanks go to Dr. Johannes Käßbohrer (solving problems with the input optics), Dr. Gert König-Langlo (providing supporting frame for albedo measurements), Ulf Müller (providing UPS, helping with radiance and albedo measurements), and Dipl.-Ing. Felix Riess (fixing the Skyscanner).

Further, I would like to thank Dipl.-Met. Merle Glandorf for sharing office with me throughout the duration of my thesis, which is not as easy as it may seem. Thanks for all the important discussions and spotting lots of mistakes in my thesis. For proofreading, I also thank Dr. Ulrich Finke, Dipl.-Met. Wiebke Deierling, and Ulf Müller.

Finally, I do not want to forget to thank my parents and close friends for providing continuous support, throughout the past years and in particular during the last stages of working for the PhD.

Danksagung

Viele Menschen haben mich während der letzten drei Jahre begleitet. Die Zeit ist gekommen, mich zu bedanken.

Zuerst möchte ich meinem Betreuer Prof. Dr. Gunther Seckmeyer für seine Unterstützung danken. Viele Diskussionen mit ihm haben mein Verständnis für die Welt der Wissenschaft verbessert. Während unserer Zusammenarbeit habe ich sowohl wertvolle Anregungen erhalten als auch die Freiheit genossen, selbständig zu arbeiten.

Ohne die Unterstützung von Dipl.-Ing. Anton Gugg-Helminger von der Firma Gigahertz-Optik hätte ein so schneller Einsatz des Spektralradiometers viel länger gedauert. Das Betreiben des Spektralradiometers und das Finden von Fehlern geschah gerade anfangs viel mit seiner Hilfe.

Während der ersten beiden Messgerätevergleiche war Dipl.-Met. Holger Studemund eine große Hilfe. Unsere Teilnahme am NDSC Messgerätevergleich wurde durch die Einladung und Finanzierung von Dr. James Slusser ermöglicht. Für den Erfolg danke ich vor allem Dr. Kathy O. Lantz, Dr. Patrick Disterhoft (both NOAA), Dr. Germar Bernhard (BSI), und Dr. Paul Johnston (NIWA). Für die technische Unterstützung am IMUK bedanke ich mich besonders bei Ulrich Meyer, Dipl.-Met. Sonja Fabig und Dr. Notker Fechner.

Die vorzügliche Vorbereitung der Meßkampagne in der Antarktis ist der Logistik-Abteilung des AWI zu verdanken. Stellvertretend seien hier Jürgen Janneck und Dr. Hartwig Gernandt genannt, welche die Grundlage für erfolgreiche Messungen auf Neumayer ermöglichten. Auf der Station selbst wurde ich mehr unterstützt als zuvor angenommen. Gedankt sei vor allem: Dr. Johannes Käßbohrer (Lösen von Problemen mit der Eingangsoptik), Dr. Gert König-Langlo (Bereitstellung des Gestells für Albedomessungen), Ulf Müller (Bereitstellung einer USV, Hilfe bei Albedo- und Strahldichtemessungen), and Dipl.-Ing. Felix Riess (Reparatur des Skyscanners).

Desweiteren möchte ich mich bei Dipl.-Met. Merle Glandorf bedanken, die die ganze Zeit ein Zimmer mit mir geteilt hat. Das mag einfacher erscheinen, als es tatsächlich ist. Danke für die wichtigen Diskussionen und für die vielen gefundenen Fehler in meiner Dissertation. Für das Korrekturlesen möchte ich mich

Bibliography

außerdem bei Dr. Ulrich Finke, Dipl.-Met. Wiebke Deierling, und Ulf Müller bedanken.

Zum Schlußdanke ich meinen Eltern und engen Freunden für die fortwährende Unterstützung in vielerlei Hinsicht, besonders während der letzten Phase meiner Doktorandenzeit.

Curriculum Vitae

Personal Details

Education and Employment

August 1990 to May 1995	Goetheschule Hannover, Gymnasium, Hannover, Germany
August 1992 to July 1993	Exchange Student at Sprague High School, Salem, USA; American High School Diploma
May 1995	Abitur at Goetheschule Hannover
October 1995 to June 2001	Studies in Meteorology, University of Hannover; Degree: Diplom-Meteorologin; Title of the thesis: Validating and Developing an Algorithm for Satellite-derived UV Radiation
February to December 1999	Exchange student at the Institute for Antarctic and Southern Ocean Studies, University of Tasmania, Hobart, Australia; Degree: Graduate Diploma of Science with Honours; Title of the thesis: Skin-Bulk Temperatures in the Southern Ocean: Analysis of Meteorological Effects
September 2001 to October 2004	Research assistant at the Institute of Meteorology and Climatology, University of Hannover, Germany